Medical imaging with Synchrotron Radiation

Giuliana Tromba

SYnchrotron **R**adiation for **ME**dical **P**hysics (SYRMEP) beamline

Elettra - Sincrotrone Trieste

XIV School on Synchrotron Radiation:
Fundamentals, Methods and Applications
Muggia, Italy / 18-29 September 2017

Outline

- ✓Advantages of using SR for medical applications
- ✓SR X-rays imaging techniques

  Absorption, K-edge imaging

  Phase sensitive techniques:

  Free Propagation Imaging (FPI)
  Analizer Based Imaging (ABI)
  X-ray interferometry with crystals
  Grating interferometric imaging (GI)
  Grating non-interferometric imaging (Edge Illumination(EI))

- ✓Some applications at ESRF, Spring8, PSI, Melbourne, Elettra

  Bronchography
  Mammography
  Studies of bones, joints and cartilages
  Lungs imaging
  Brain studies
  Imaging of atherosclerotic plaques
  and others…..

- ✓Quantitative analysis

Advantages of SR for biomedical imaging

Monochromaticity allows for:

- *optimization* of X-ray energy according to the specific case under study (dose reduction)
- quantitative CT evaluations
- no beam hardening
- convenient use of contrast agent (K-edge and L-edge imaging)

Spatial coherence enables the applications of ***phase sensitive imaging*** **techniques**

- Phase contrast overcomes the limitation of conventional radiology
- It brings to a dose reduction
- Improved contrast resolution, edges enhancement
- Use of phase retrieval algorithms

High fluxes

- Short exposure time
- Dynamic studies….

Collimation

- parallel beams, scatter reduction
- beam shaping (micro-beams)

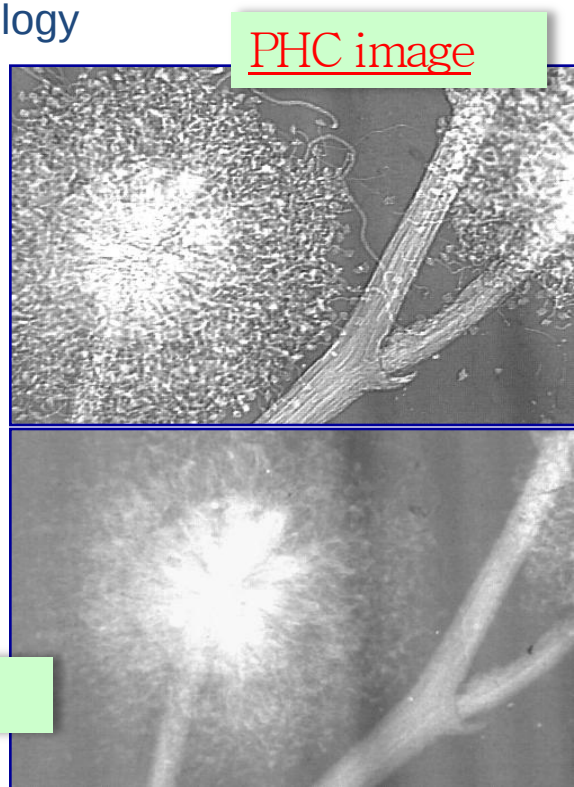

Different imaging approaches

- Clinical: applications to patients
  (es. mammography, angiography, ecc.)
  *Need to **limit** radiation dose. Find best compromise between dose and image quality*

- Imaging of small animals: applied for different purposes in the development of ***animal models***
  (es. Cell tracking, Osteoporosis, genetic diseases,..)
  Research protocols, control of dose.

- "In vitro" imaging: it concerns the study of biological samples. (es. micro-tomography applied on bone samples, scaffolds, cartilages, etc.)
  Requirements of high resolution and high sensitivity

Increase of dose and spatial resolution

SR X-rays imaging techniques

1) K-edge subtraction imaging

Exploiting the monochromaticity of SR…

K-edge Subtraction Imaging

1. Contrast agent: Iodine, or Gadolinium, etc.
2. Two Images are acquired : Above (A) and Below (B) the K-edge
3. Image processing : Iodine and Tissue images

$$x_i = \frac{\mu_{Bi}\ln(A) - \mu_{Ai}\ln(B)}{\mu_{Bi}\mu_{At} - \mu_{Ai}\mu_{Bt}}$$

$$x_t = \frac{\mu_{Bi}\ln(A) - \mu_{Ai}\ln(B)}{\mu_{Bi}\mu_{At} + \mu_{Ai}\mu_{Bt}}$$

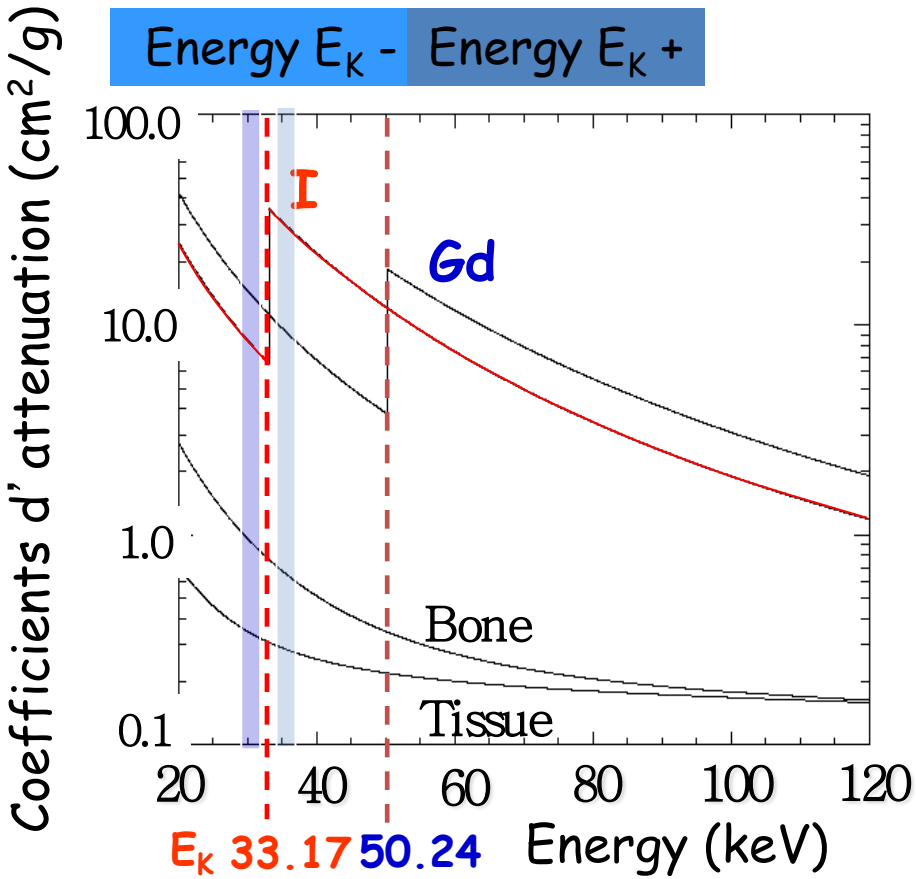

Below Above K-edge

Iodine Image

Courtesy of A.Bravin (ESRF)

K-Edge absorption imaging: application

- Bronchography (pre-clinical – animal model)

Bronchography - Tomographic imaging at ESRF

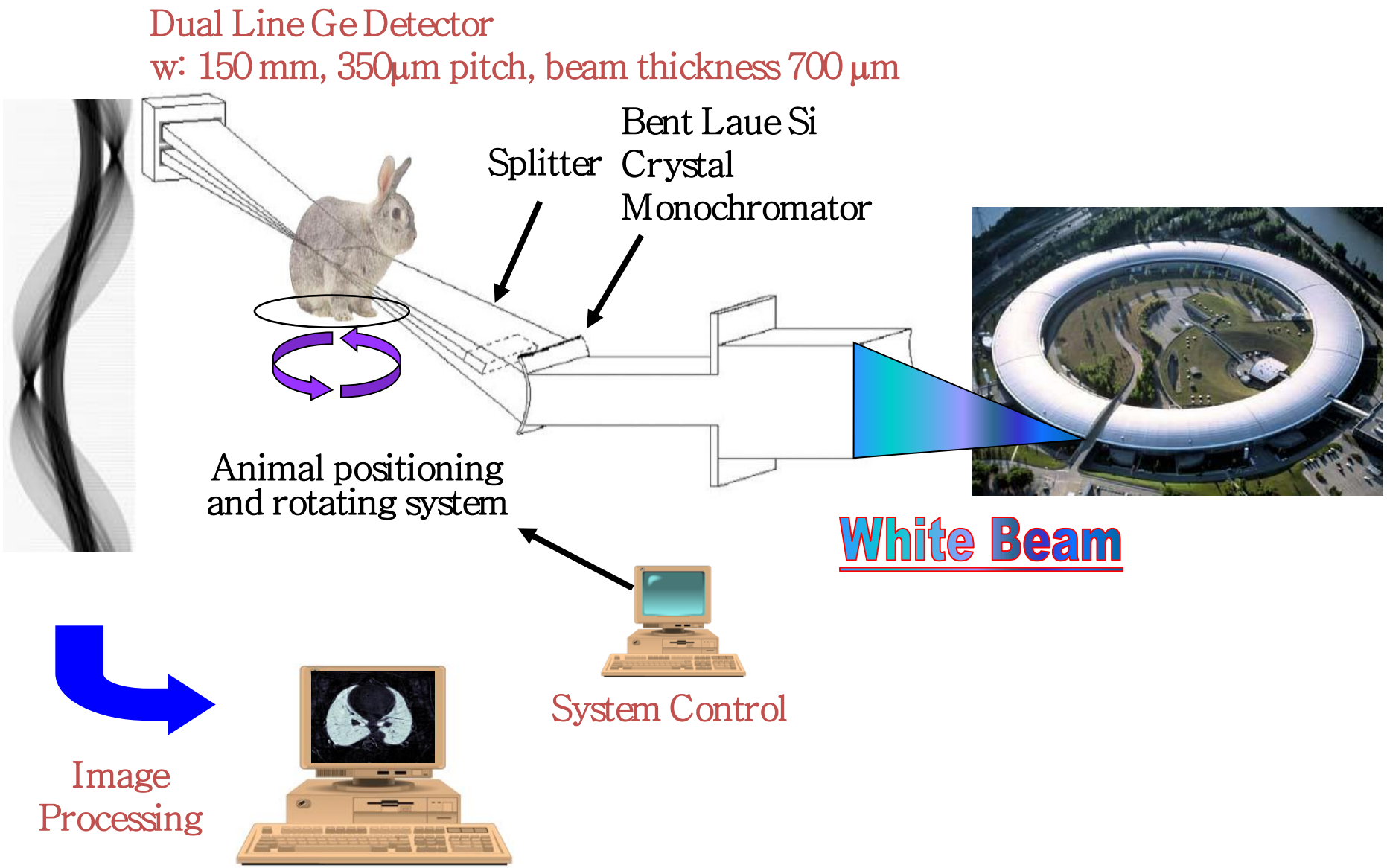

Courtesy of A.Bravin (ESRF)

K-edge Subtraction - Lung Tomography

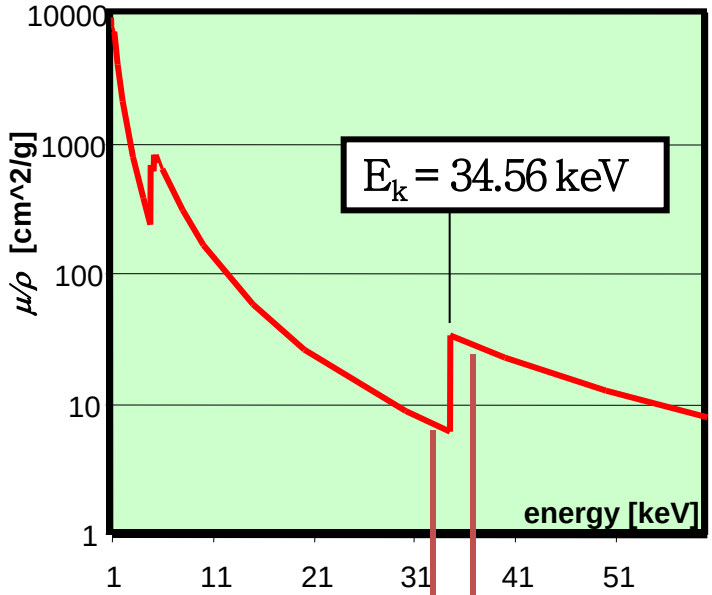

$E < E_k$

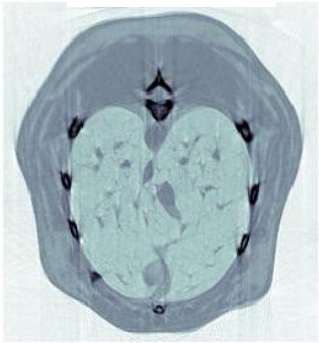

$E > E_k$

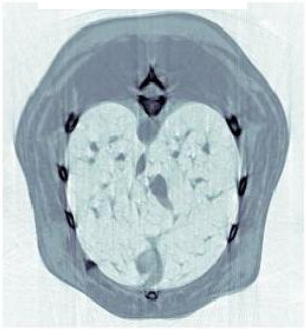

$$(\rho t)_I = \frac{\ln(\frac{I}{I_0})^+ - \ln(\frac{I}{I_0})^-}{(\frac{\mu}{\rho})_I^+ - (\frac{\mu}{\rho})_I^-}$$

Subtraction

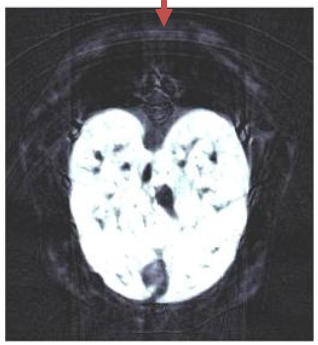

Courtesy of A.Bravin (ESRF)

Experimental Set-up

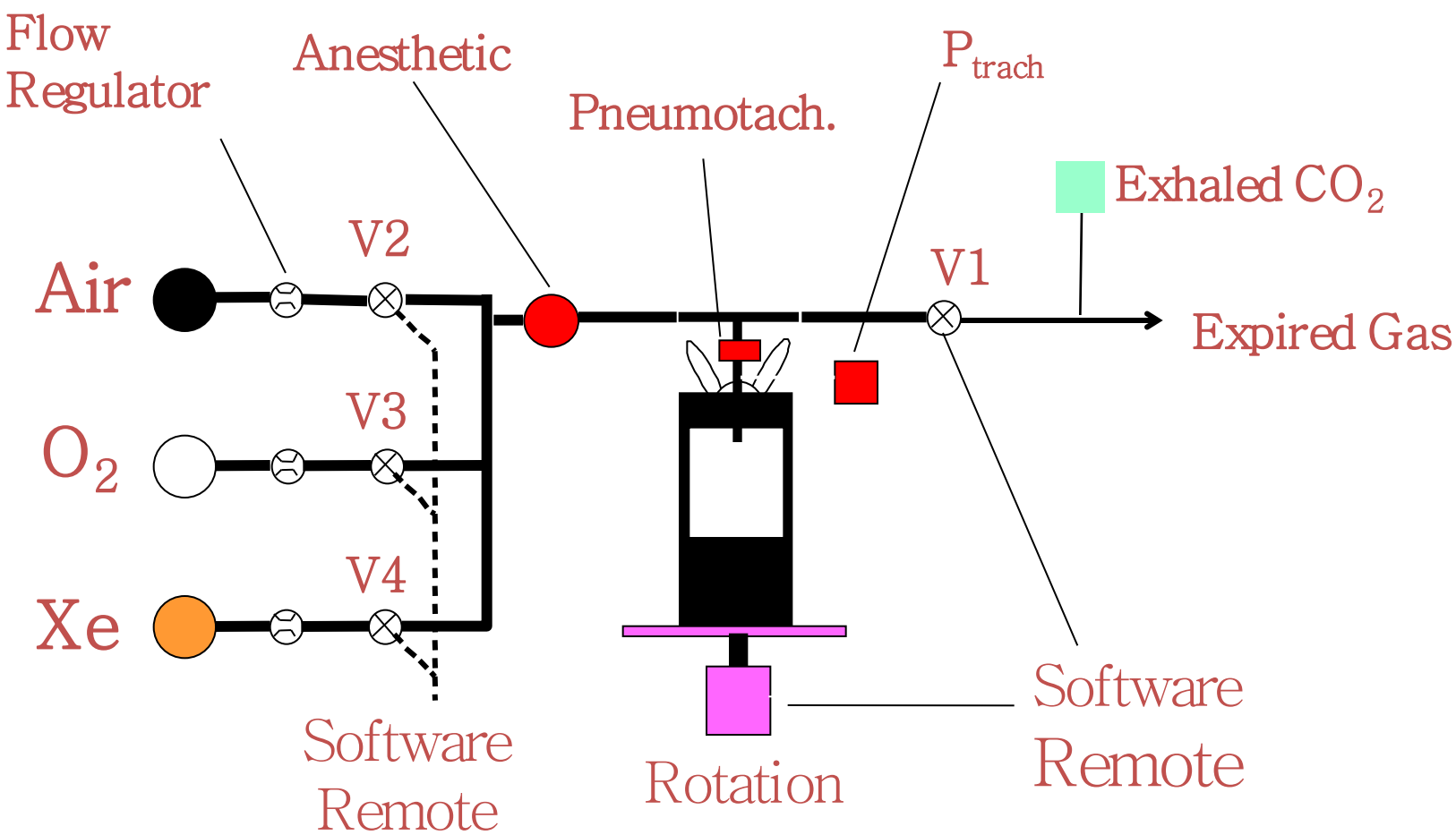

Courtesy of A.Bravin (ESRF)

Imaging Sequence

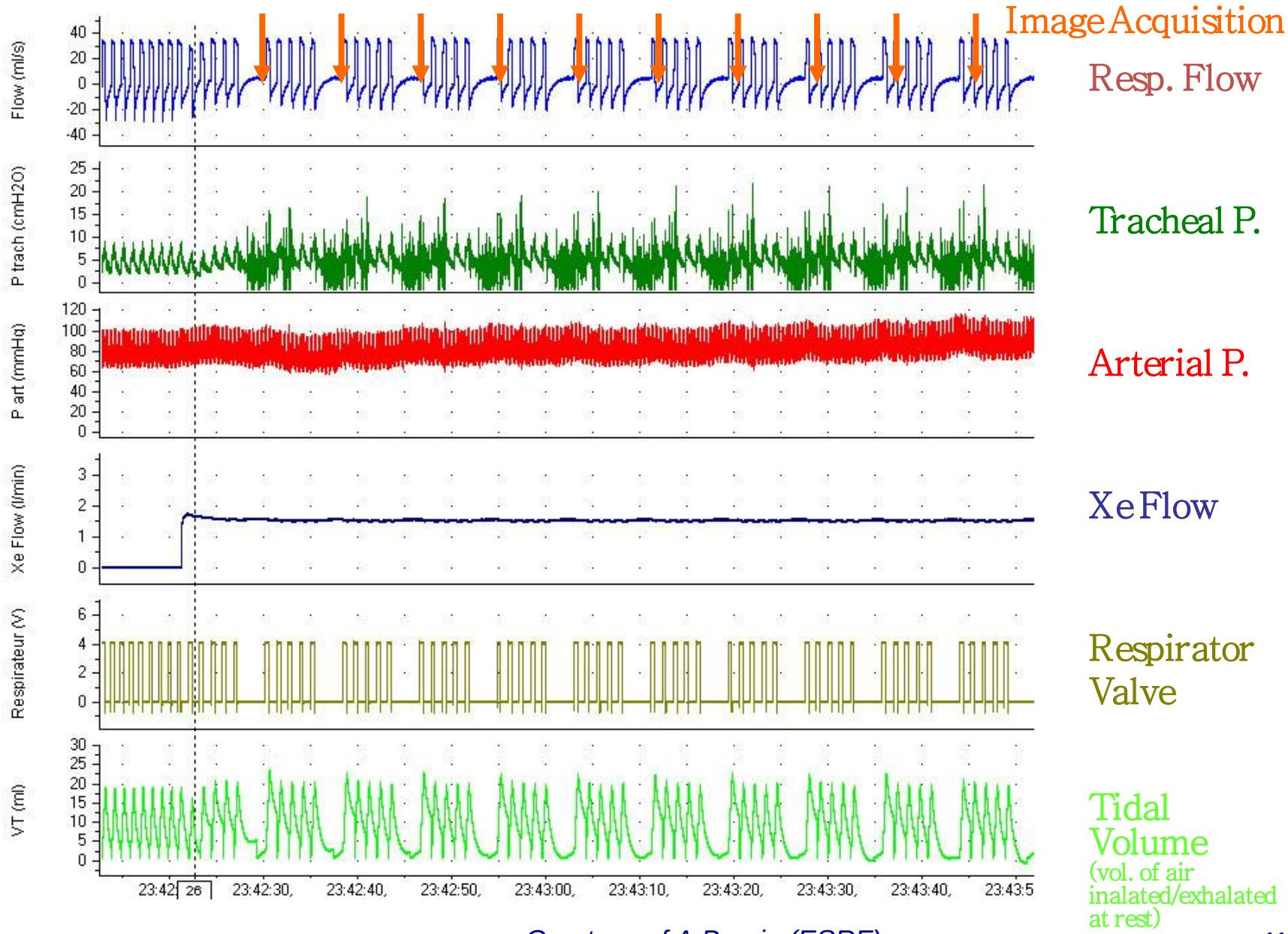

Courtesy of A.Bravin (ESRF)

Projection Images
In Vivo Rabbit Lung
Xenon K-edge Imaging

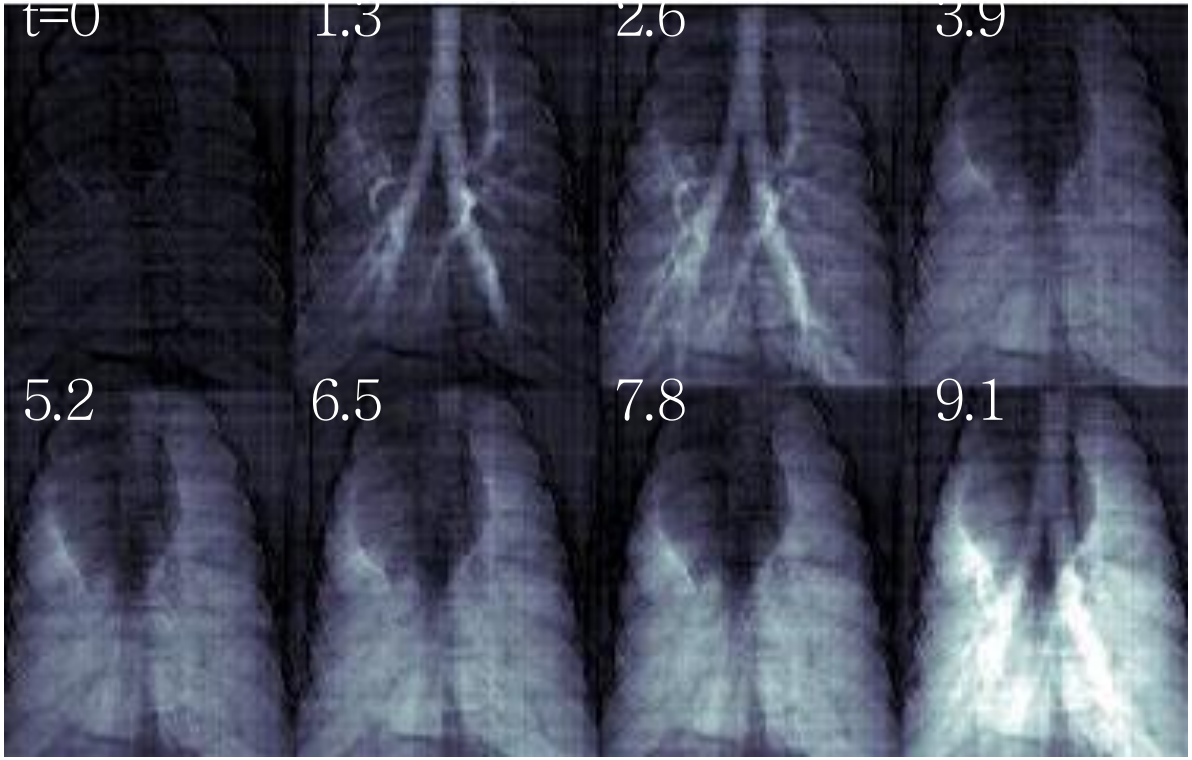

Time between images = 1.3 sec

Courtesy of A.Bravin (ESRF)

Effects on lungs ventilation induced by different treatments on healthy or asthmatic animals.

Experimental asthma studies have been carried out to study allergic reactions by using **ovalbumine-sensitized rabbit model**. Allergic reactions were compared with asthma reactions caused by **non-specific drug provocation** (**Methacholine, Mch**). Mch caused airway narrowing mainly on the central large airways, while allergen (ovalbumine) induces a predominantly peripheral and heterogeneous lung response.

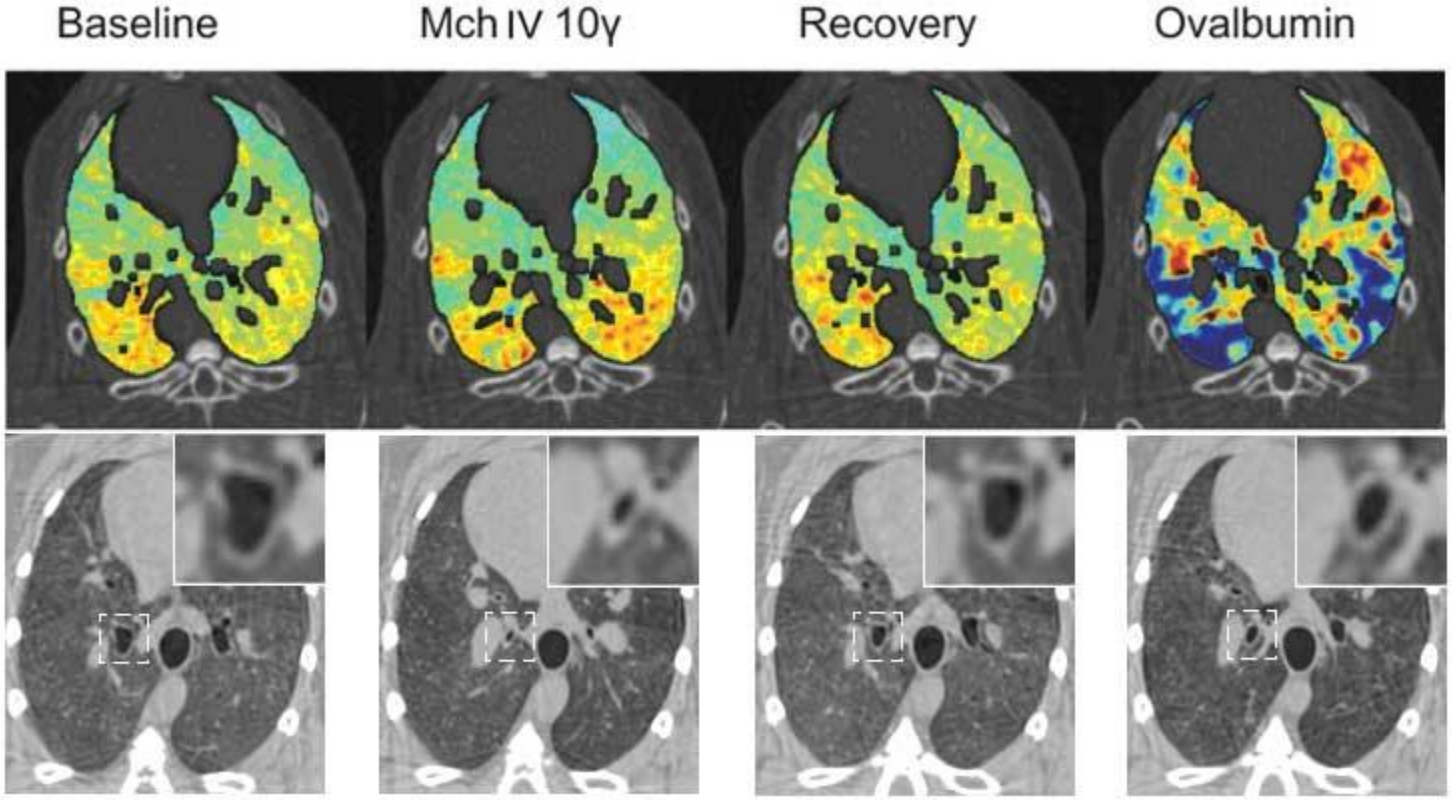

Upper part: images of specific ventilation in one sensitized rabbit at baseline, during Mch infusion, upon recovery and after Ovalbumine allergen provocation. Lower part: Absorption CT slices showing changes in the central airway cross-sectional area at the different experimental stages in one representative animal. Magnifications of the indicated square areas are shown in the right-upper corners.

Bayat S. et al:, Am J Respir Crit Care Med. Aug 15;180(4):296-303 (2009).

2 - *Phase – contrast* imaging techniques: main cathegories

- ✓ Propagation-based Imaging (PBI)
- ✓ Analizer-Based Imaging (ABI)
- ✓ X-ray interferometry with crystals
- ✓ Grating interferometric imaging (GI)
- ✓ Grating non-interferometric imaging

Exploiting the spatial coherence of SR…

PHase contrast vs. conventional imaging

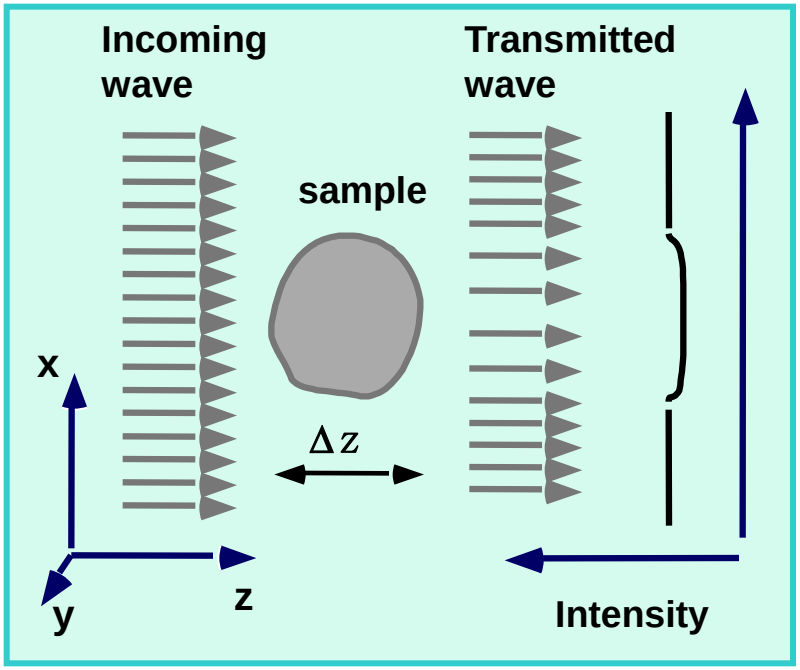

Conventional radiology

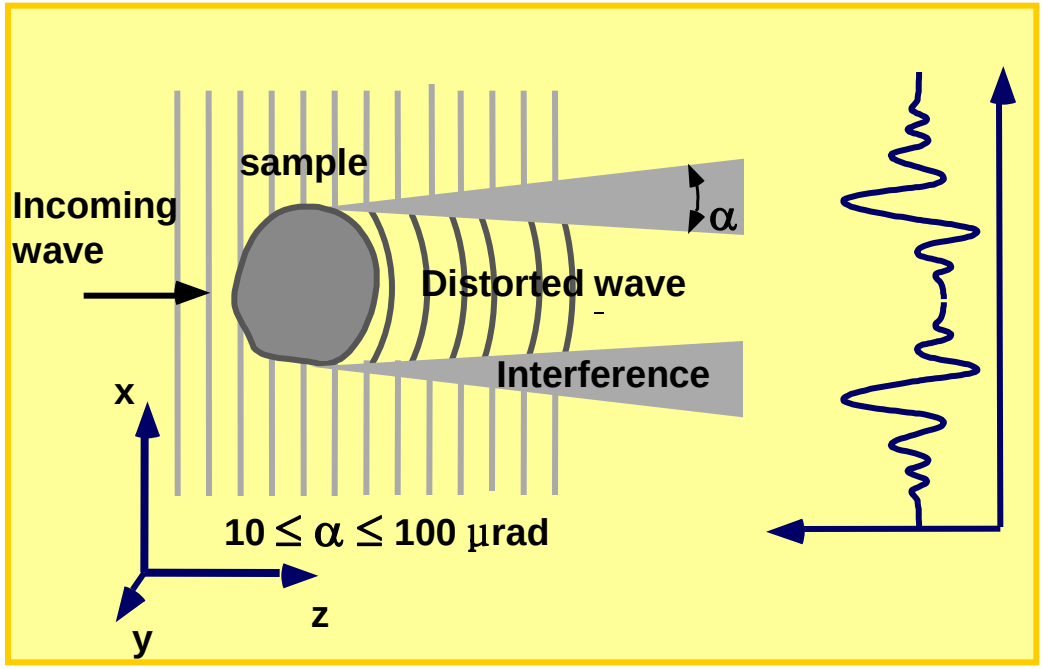

PHC

In conventional radiology image formation is based on differences in X-ray absorption properties of the samples. The image contrast is generated by density, composition or thickness variation of the sample. Main limitation: poor contrast in soft tissue differentiation. ***Phase contrast* techniques** are based on the observation of the *phase shifts* produced by the object on the incoming wave. Contrast arises from interference among parts of the wave front differently deviated (or phase shifted) by the sample. Edge enhancement effects.

Refraction index for hard X-rays : $n = 1 - \delta + i\beta$, β = absorption term, δ = phase shift term

for soft tissue@17 keV: $\beta \sim 10^{-10}$; $\delta \sim 10^{-6}$, $\delta \propto \lambda^2$, $\beta \propto \lambda^3$

Absorption radiology -> contrast is generated by differences in the x-ray absorption ($C_{abs} \sim x\,\Delta\beta$),

Phase Radiology –> contrast is generated by phase shifts ($C_{\phi} \sim x\ \Delta\delta$)

x = object size // to beam direction

$\delta >> \beta$ ➔ phase shifts effects >> absorption

Propagation based imaging (PBI)

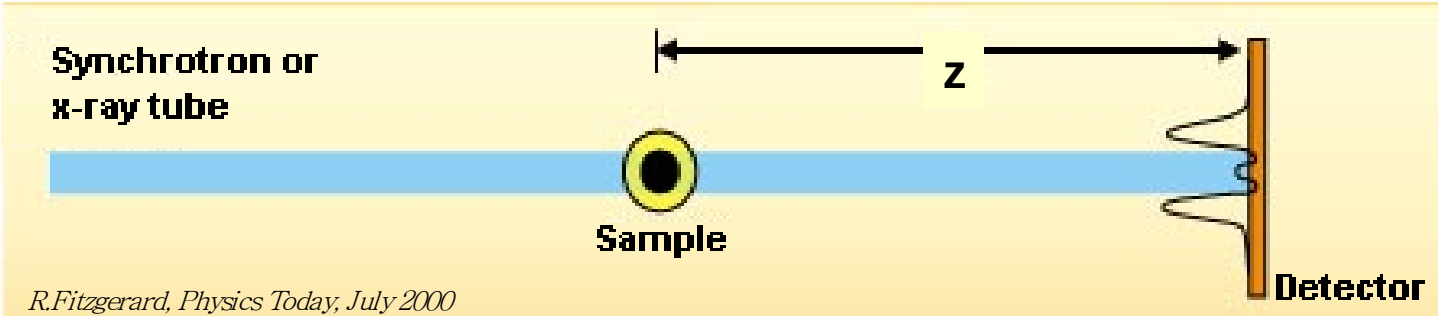

- The technique exploits the high spatial coherence of the X-ray source.
- z =0 -> absorption image
- For z > 0 -> interference between diffracted and un-diffracted wave produces edge and contrast enhancement. A variation of δ is detected
- Measure of $\nabla^2\Phi(x,y)$
- The technique requires a high spatial coherence source, monochromaticity is not needed

Regimes

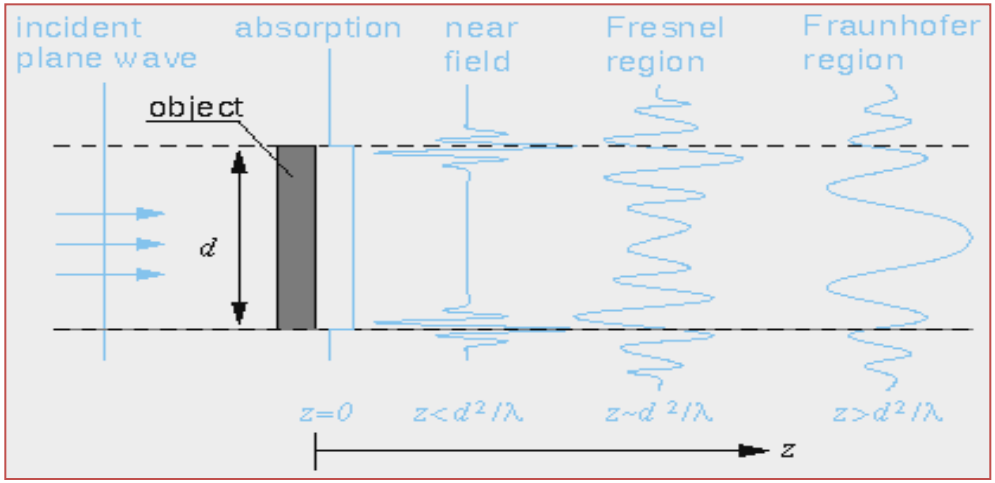

Snigirev A. et al., Rev. Sci. Instrum. 66, 1995
Wilkins S. W. et al., Nature 384, 1996
Cloetens P. et al., J. Phys D: Appl. Phys. 29, 1996
Arfelli F et al., Phys. Med. Biol. 43,1998

Images of a Mimosa flower

10 keV

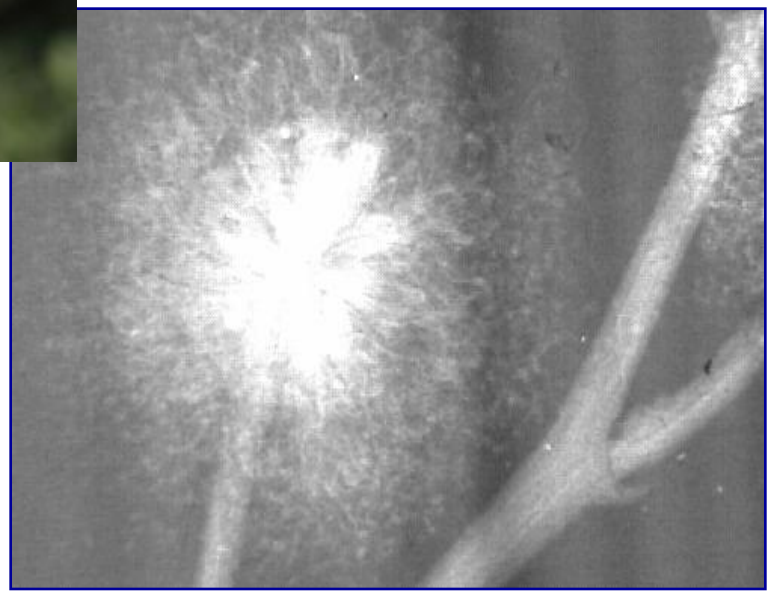

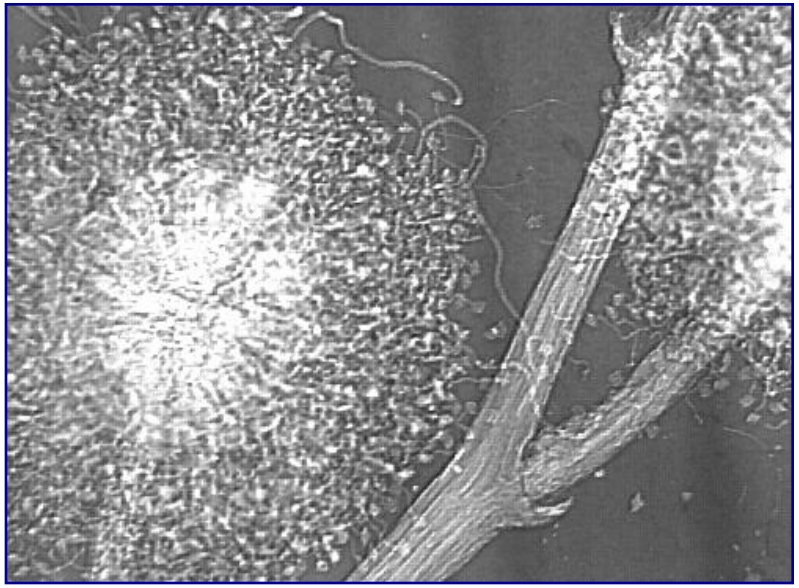

Absorption **PBI**

25 keV

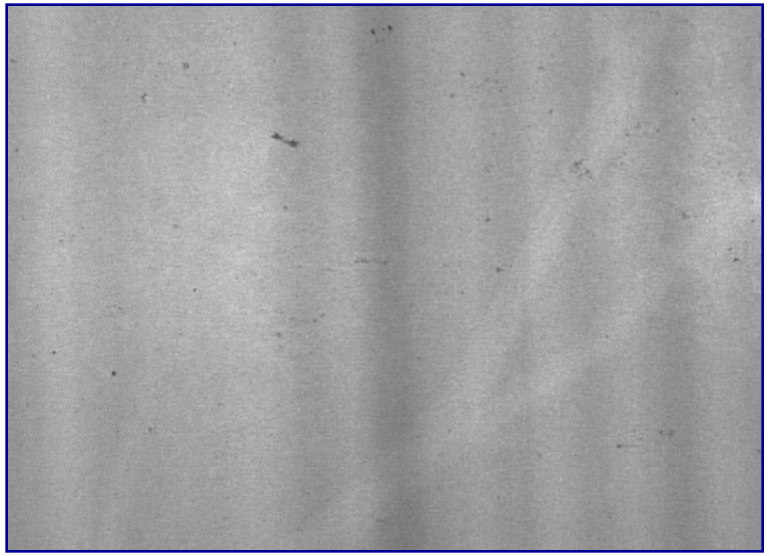

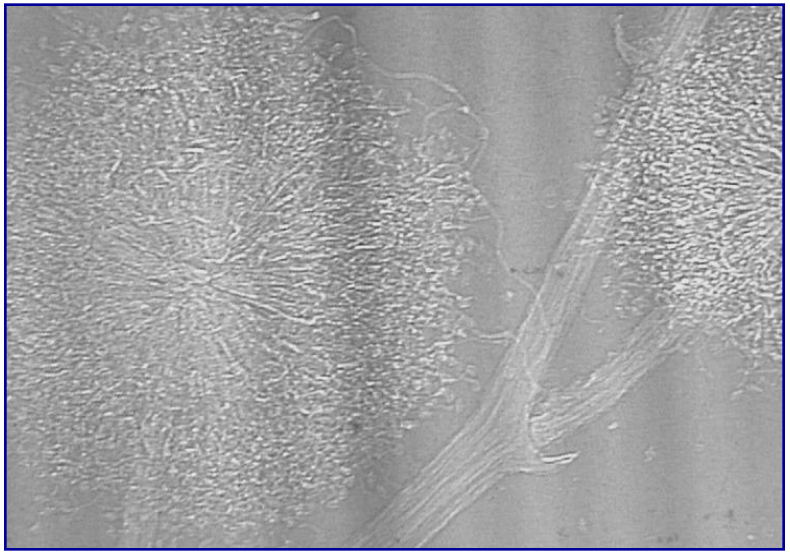

Analyzer Based Imaging (ABI)

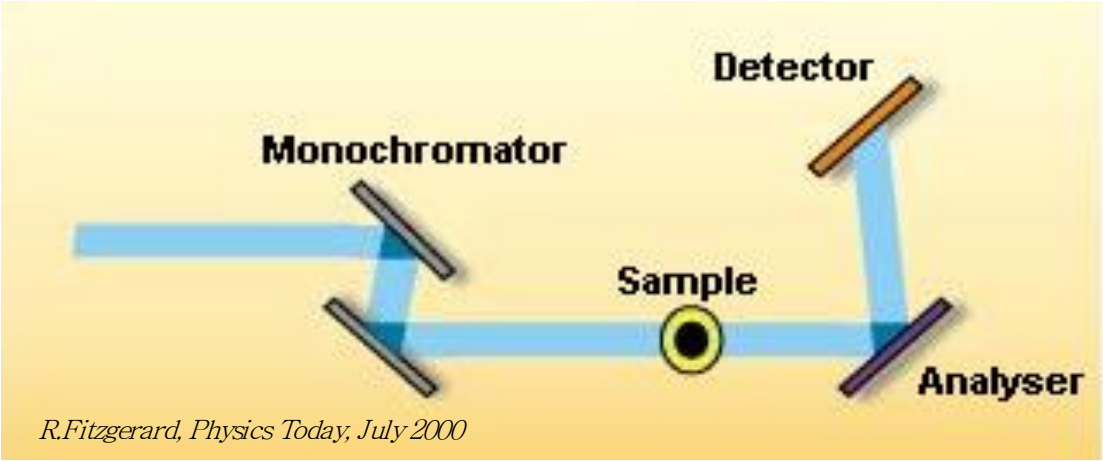

- A perfect crystal is used as an angular filter to select angular emission of X-rays. The filtering function is the rocking curve (FWHM: 1-20 μrad)
- Image formation with ABI is sensitive to a variation of δ in the sample. Indeed, **refraction angle is roughly proportional to the gradient of δ**
- Analyzer and monochromator aligned -> X-ray scattered by more than some tens μrad are rejected
- Small misalignments -> investigation of phase shift effects
- With greater misalignments the primary beam is almost totally rejected and pure refraction images are obtained
- Sensitive to $\nabla\Phi(x,y)$
- The technique requires the beam monochromaticity.

Podurets K. M. et al., Sov. Phys. Tech. Phys. 34(6), 1989
V. N. Ingal and E. A. Beliaevskaya, J. Phys. D: Appl. Phys. 28, 1995
Chapman D et al., Phys. Med. Biol. 42, 1997

ABI image manipulation (original algorithm)

I_L

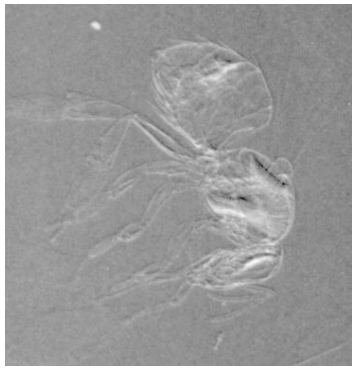

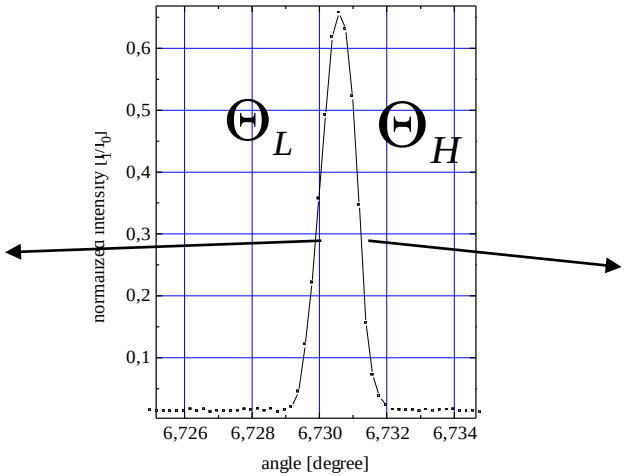

I_H

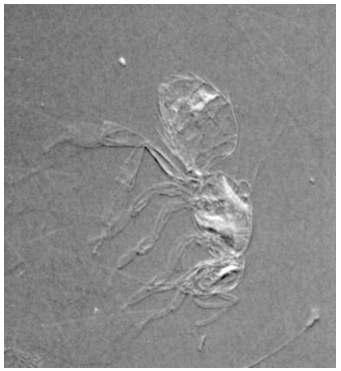

Linear approximation of rocking curve at half values (I_R and I_L)

$$I_L = I_R\left(R(\Theta_L) + \frac{\partial R}{\partial \Theta}(\Theta_L)\Delta\Theta_z\right)$$

$$I_H = I_R\left(R(\Theta_H) + \frac{\partial R}{\partial \Theta}(\Theta_H)\Delta\Theta_z\right)$$

Θ_Z = refraction Image

I_R = apparent absorption image (absorption+extinction)

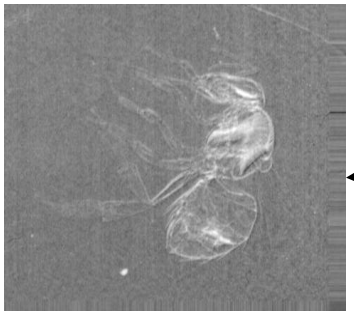

Apparent Absorption Image

$$I_R = \frac{I_L \cdot \left.\frac{dR}{d\Theta}\right|_{\Theta_H} - I_H \cdot \left.\frac{dR}{d\Theta}\right|_{\Theta_L}}{R(\Theta_L)\cdot \left.\frac{dR}{d\Theta}\right|_{\Theta_H} - R(\Theta_H)\cdot \left.\frac{dR}{d\Theta}\right|_{\Theta_L}}$$

$$\Theta_Z = \frac{I_H \cdot R(\Theta_L) - I_L \cdot R(\Theta_H)}{I_L \cdot \left.\frac{dR}{d\Theta}\right|_{\Theta_H} - I_H \cdot \left.\frac{dR}{d\Theta}\right|_{\Theta_L}}$$

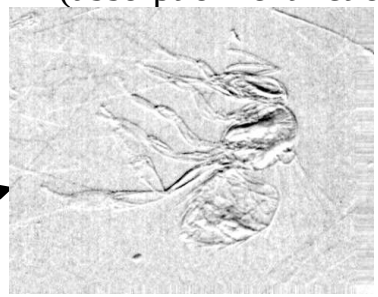

Refraction Image

Ref: Chapman et al, Phys.Med.Biol, 42,1997

Limitations and Requirements

PBI

- It is the simplest method as it requires the detector to be set at a certain distance from the sample. It does not require monochromaticity.
- Requirements:
  - a high spatial coherence of the beam
  - adequate spatial resolution of the detector to detect interference fringes (edge-enhancement)
- Exposure time related to beam intensity
- The recorded signal is proportional to the second derivative of the phase term ($\nabla^2\Phi(x,y)$)
- Adequate to study samples with important variations of refractive index

ABI

- It requires the implementation and control of at least one crystal
- Requirements:
  - high monochromaticity
  - parallel beam
- Sensitive to beam instabilities
- The recorded signal is proportional to the first derivative of the phase term ($\nabla\Phi(x,y)$)
- Adequate to study cartilages, joints, samples with wide variation of refractive intex

Interferometry: from phase shift to image contrast

- Interferometry is a family of techniques in which waves are superimposed in order to extract information.
  - Widely used in optics (visible light)
  - It can be used in X-ray phase contrast imaging to transform the phase shift introduced by the object into image contrast
- Two different interferometric approaches:
  - Crystal interferometry (Bonse and Hart, 1965)
  - Grating interferometry (David et al, 2002; Momose et al., 2003)

Bonse, U. and Hart, M. (1965). Appl. Phys. Lett. ***6****, 155–156.*
David, C., Nöhammer, B. et al. (2002). Appl. Phys. Lett. 81, 3287–3289
Momose, A. et al. (2003). Japan J. Appl. Phys.: 2 Lett. 42, L866– L868

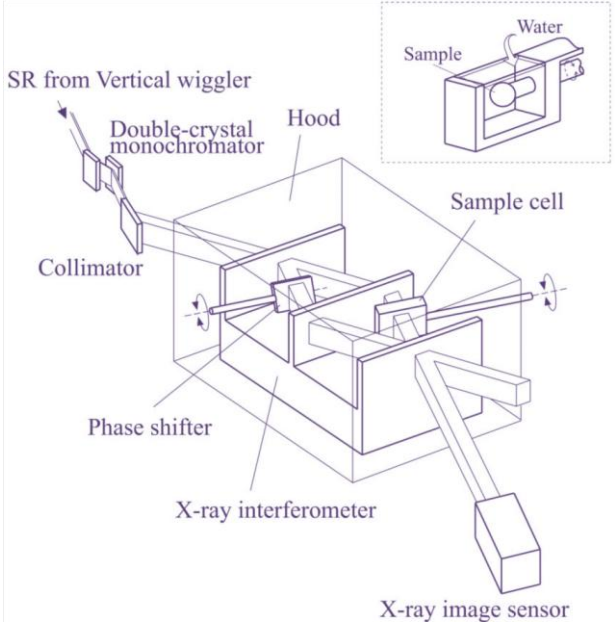

X-ray interferometry with crystals

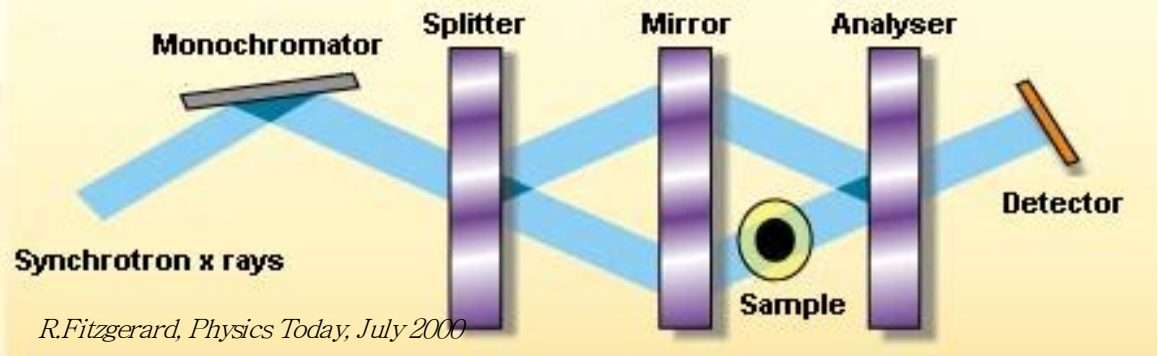

- The method has been pioneered by U.Bonse and M.Hart. A.Momose, T.Takeda et al. have refined the technique for medical applications.
- the I crystal splits the monochromatic beam into two beams with the same phase, the II crystal acts as a mirror, the III crystal recombines the two beams
- A phase shift on the probe beam is produced by the presence of the sample
- The beams re-combinated at the analyzer position generate an interference pattern registered by the detector
- Direct access to $\Phi(x,y)$
- Using monolithic Si crystal the limitation of the technique concerns the maximum size of samples to be studied. Interferometers based on double crystal systems are very sensitive to vibrations and require very accurate alignment systems: this limits their applications for imaging purposes.

Refs.: U.Bonse, M.Hart, Appl.Phys.Lett. 6,1965; A.Momose et al:, NIMA 352, 1995, A.Momose et al.: Opt. Express 11 2003, A. Momose et al., Japan J. Appl. Phys. 44, 2005

Grating interferometric imaging (GI)

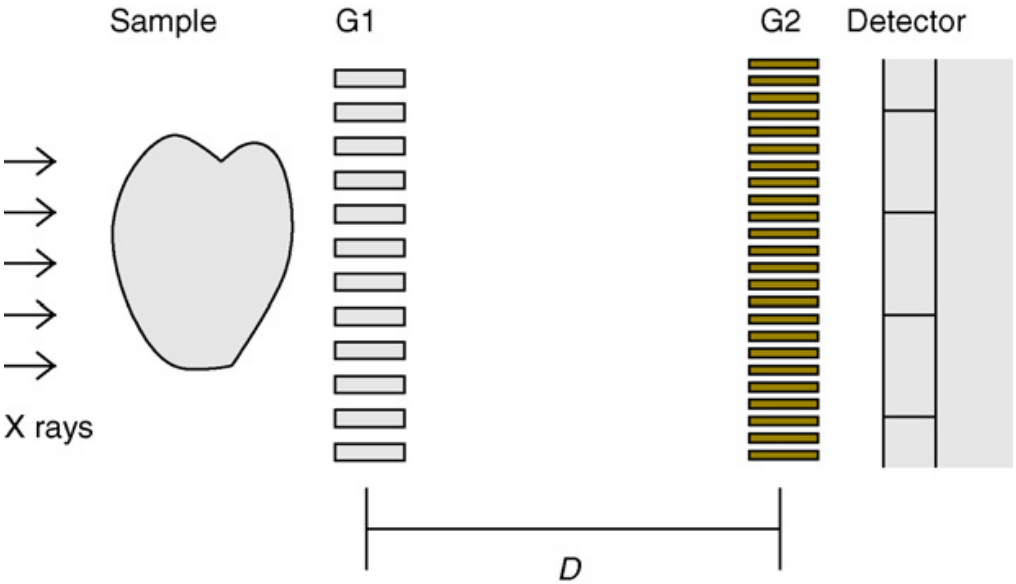

Based on an optical phenomenon discovered by Talbot (1936) and explained by Rayleigh (1881).

With a coherent radiation, the image of the grating is repeated at regular distances behind the grating, $D = 2d^2/\lambda$ (d=grating period, λ=wavelength).

The beam is split and analyzed by means of two gratings, introduced between the object and the detector:

The X-ray wavefront transmitted by the sample go through a **linear diffraction grating G1** (*beam splitter*). Downstream G1, a pattern of interference fringes is formed. The local distortions of the fringe pattern from its ideal regular shape contain information on the sample structure.

Since the fringes are too closely spaced to be resolved by the pixel detector, **an additional absorption grid** (**G2**, called *analyzer*) in front of the detector is needed to transform fringe-position information into intensity values on the detector.

A modified set-up can be applied to polychromatic spectrum from an X-ray tube.

T. J. Davis et al., Phys. Rev. Lett. 74, (1995), A.Momose et al.: Opt. Express 11, 2003, Weitkamp, T., et al., Opt. Express, 13(16), 2005, Weitkamp T et al, Eur. J. Radiol. 68, 2008

Grating Interferometry- Limitations

- Demanding mechanical requirements (precision ~ 20-30 nm)
  - Field of view must be increased to clinical size
  - At the moment 5 cm x 5 cm
- Limited exploitation of X-ray output
  - 20% - 30% due to source grating
  - grating silicon substrates (~ 300 μm)
- Long exposure time and high delivered dose

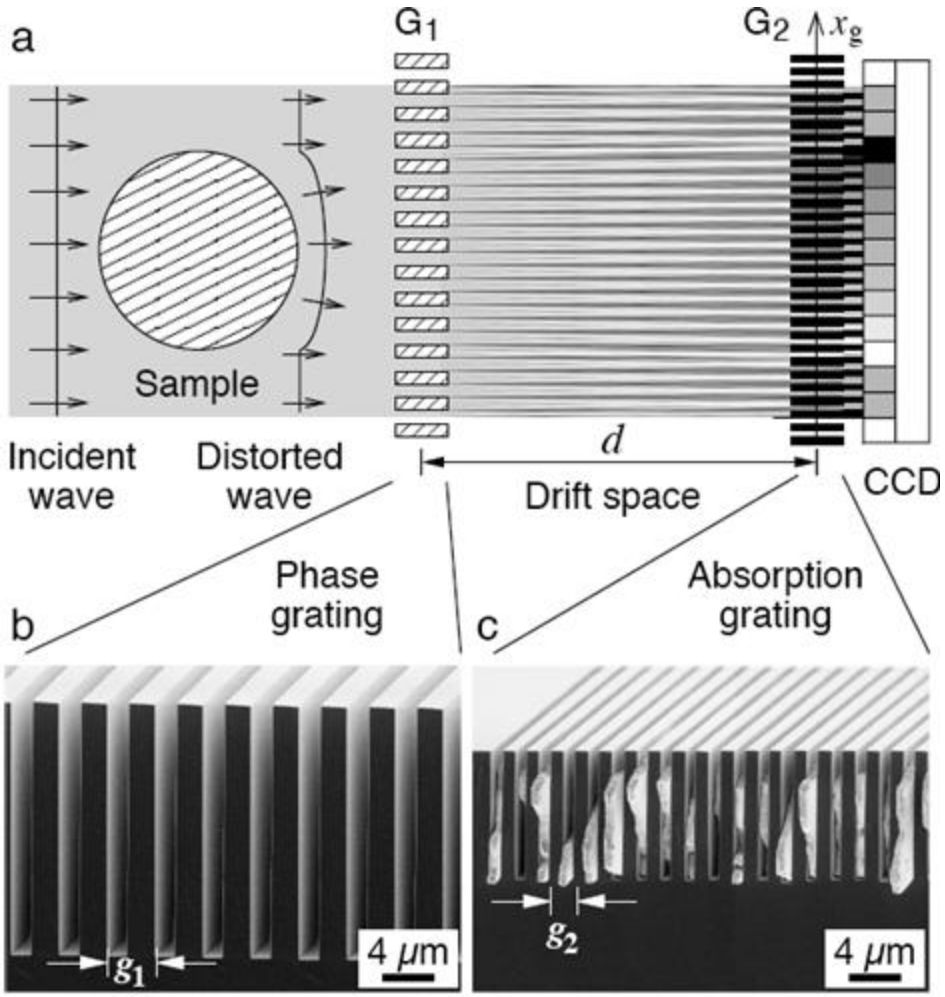

Grating non-interferometric imaging: Edge Illumination (EI)

Working Principle -------

- Similarly to ABI, EI method is based on the detection of the refraction angles suffered by photons crossing the sample
- Instead of a crystal two masks (or slits) are used (sample and detector masks)
- Sample mask creates a collimated beam, second mask is aligned with one pixels row of detector
- There is a slight misalignment between these two slits, so the beam exiting from the first slit, reaches the edge of the detector and is partially stopped by the second slit (partial illumination condition).

With the sample in, the beam is refracted, thus the beam falling on the detector slit is shifted by the quantity $\Delta y = d \tan(\Delta\theta)$, where d = sample- to-detector slit dist. , $\Delta\theta$ is the component of the refraction angle in the direction orthogonal to the slits. For small refraction angles, with d = 1 m, $\Delta y \approx$ a few micrometers.

If the beam is shifted towards the aperture, the counts on the detector will increase, viceversa, if the deviation goes towards the slits, the counts on the detector will be less. In this way, the refraction angle caused by the object is translated into a modulation of the intensity on the detector.

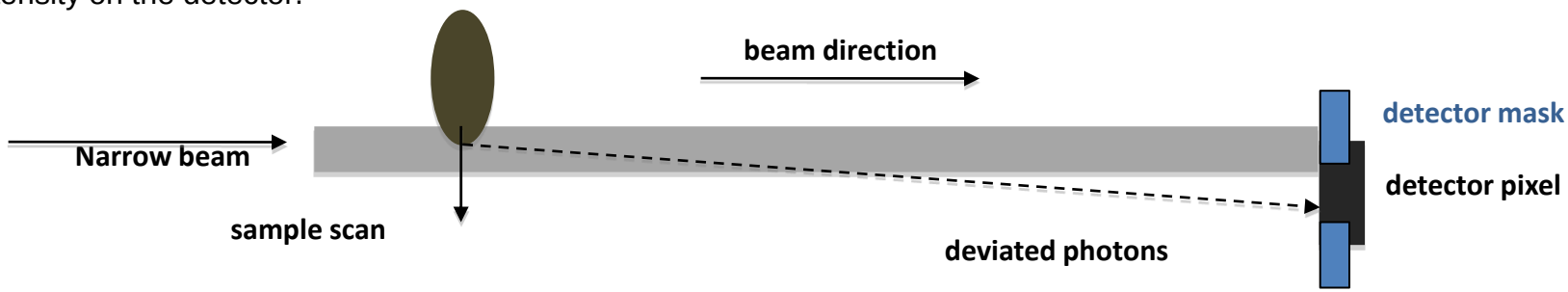

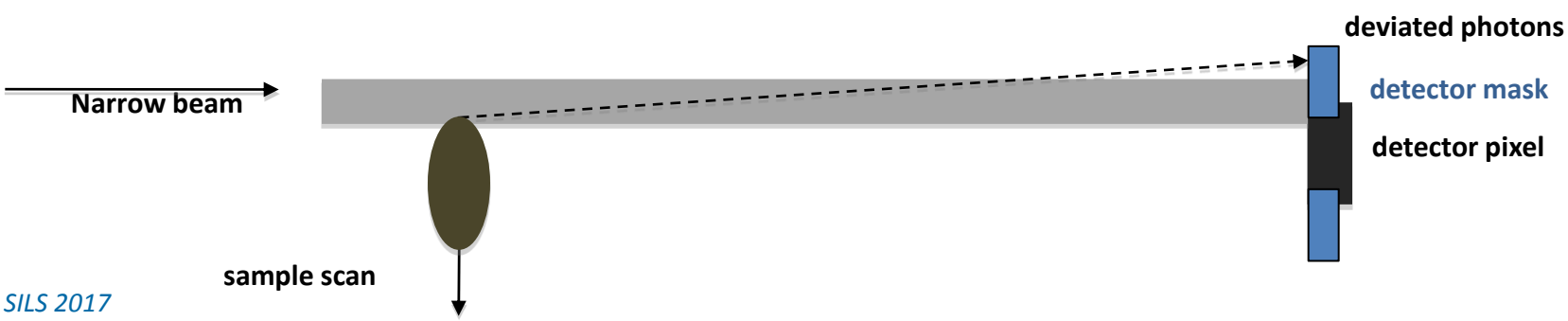

Edge Illumination - Implementation

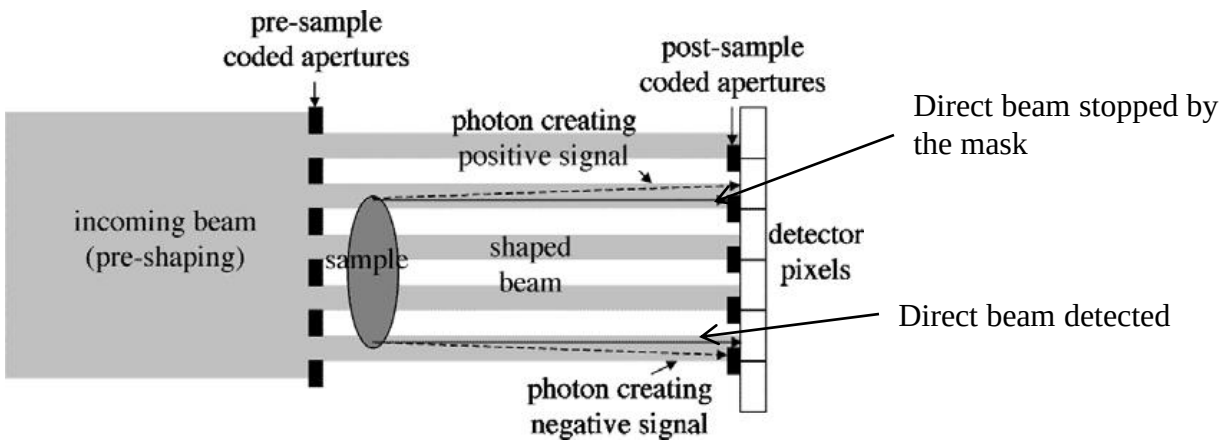

- ✓ The detector is divided by a mask ('detector mask') into a pattern of sensitive and insensitive regions between adjacent pixels
- ✓ A pre-sample mask creates the same pattern of beams that impinges on the boundaries of sensitive and insensitive regions.
- ✓ The beams are deviated by refraction in the sample, resulting in intensity variation at the detector.
- ✓ With the sample in the beam, photons previously incident on the edge can be deviated onto the detector pixels (increasing the detected signal), or the opposite can happen (decreasing the detected signal), according to the direction of refraction. The sample image is obtained by scanning the sample through the beam in the direction orthogonal to the edge.
- ✓ It can be applied to polychromatic radiation from an X-ray tube

Olivo A et al., Med. Phys. ***28****, 2001, Olivo A and Speller R, Appl. Phys. Lett. 91, 2007*

ABI setup – Bragg configuration – single crystal layout

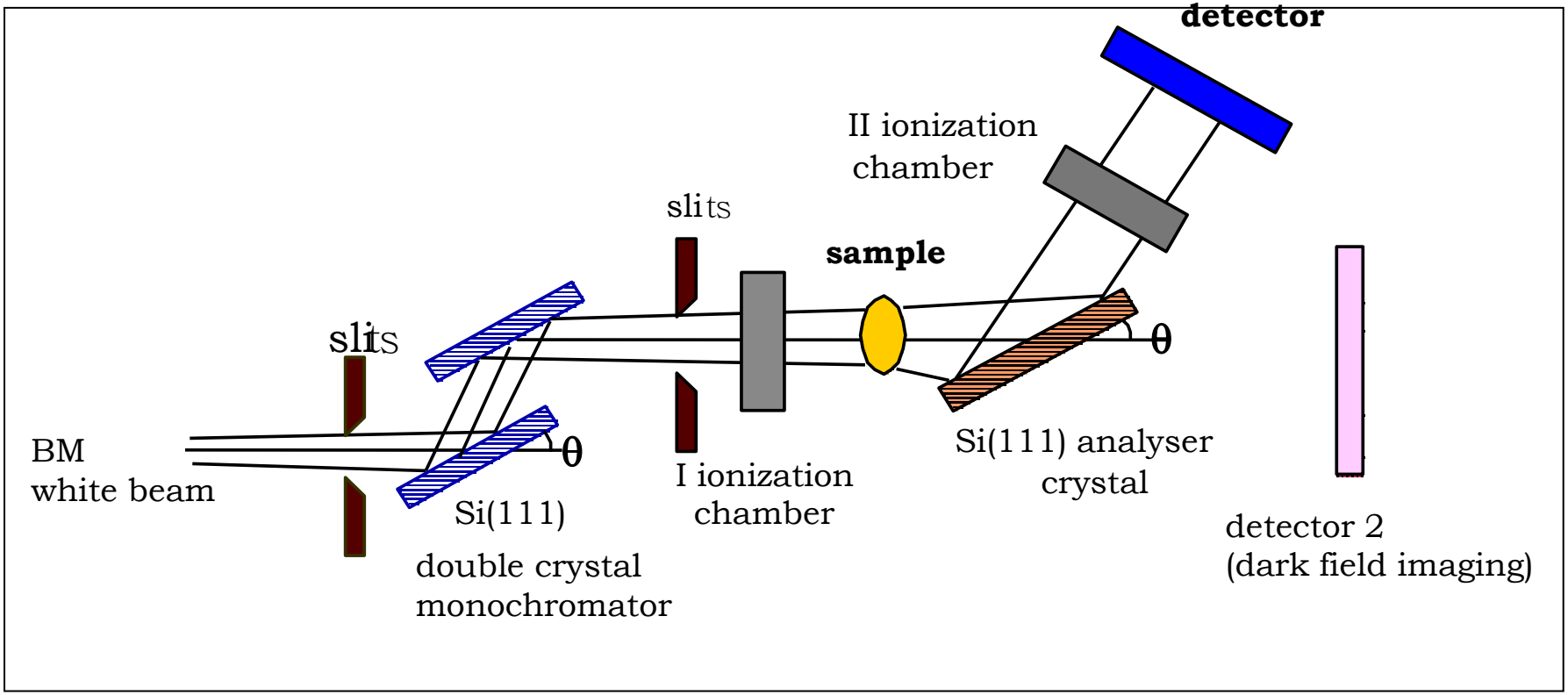

ABI setup – Bragg configuration – double crystal layout

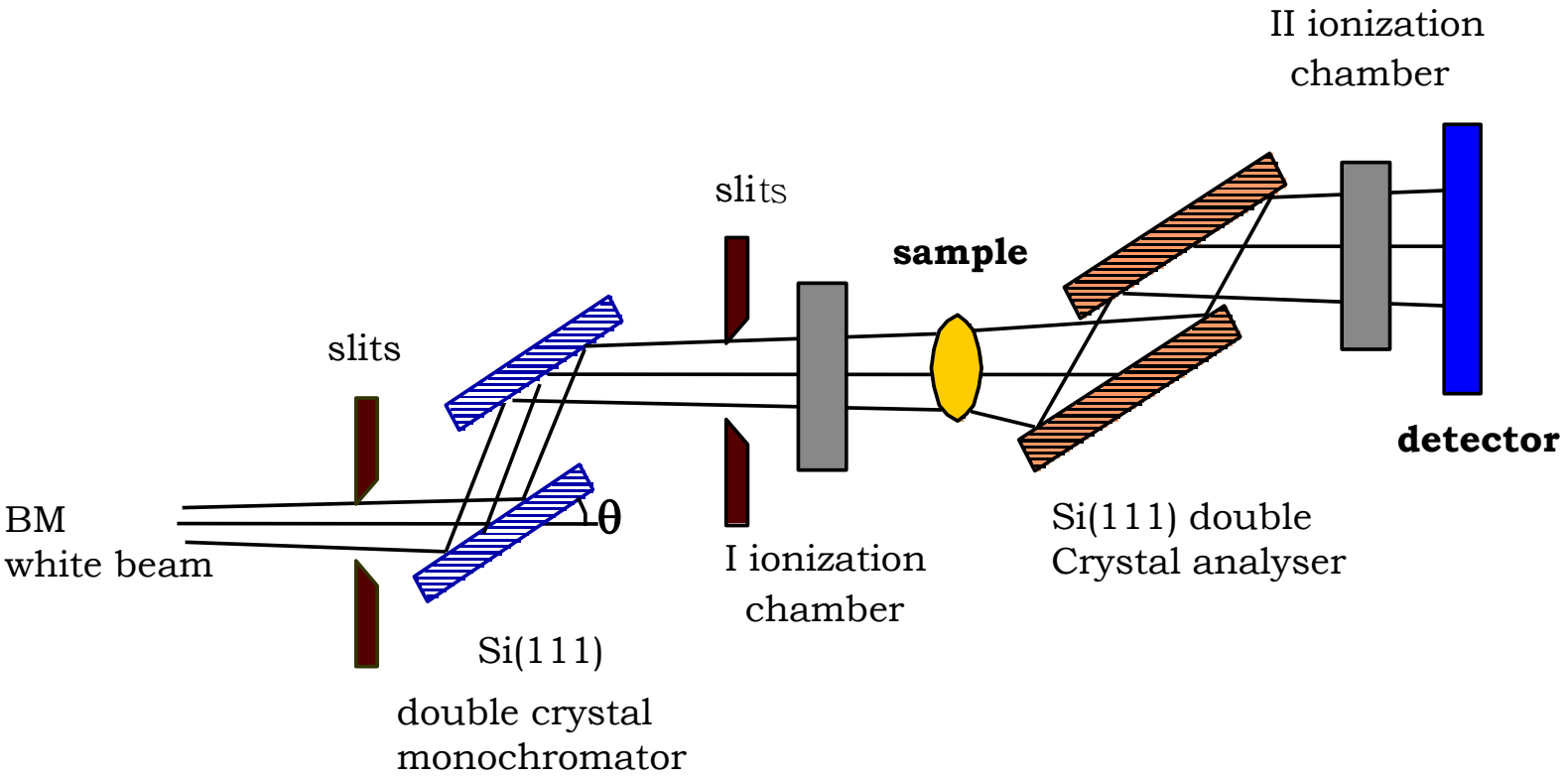

Mouse

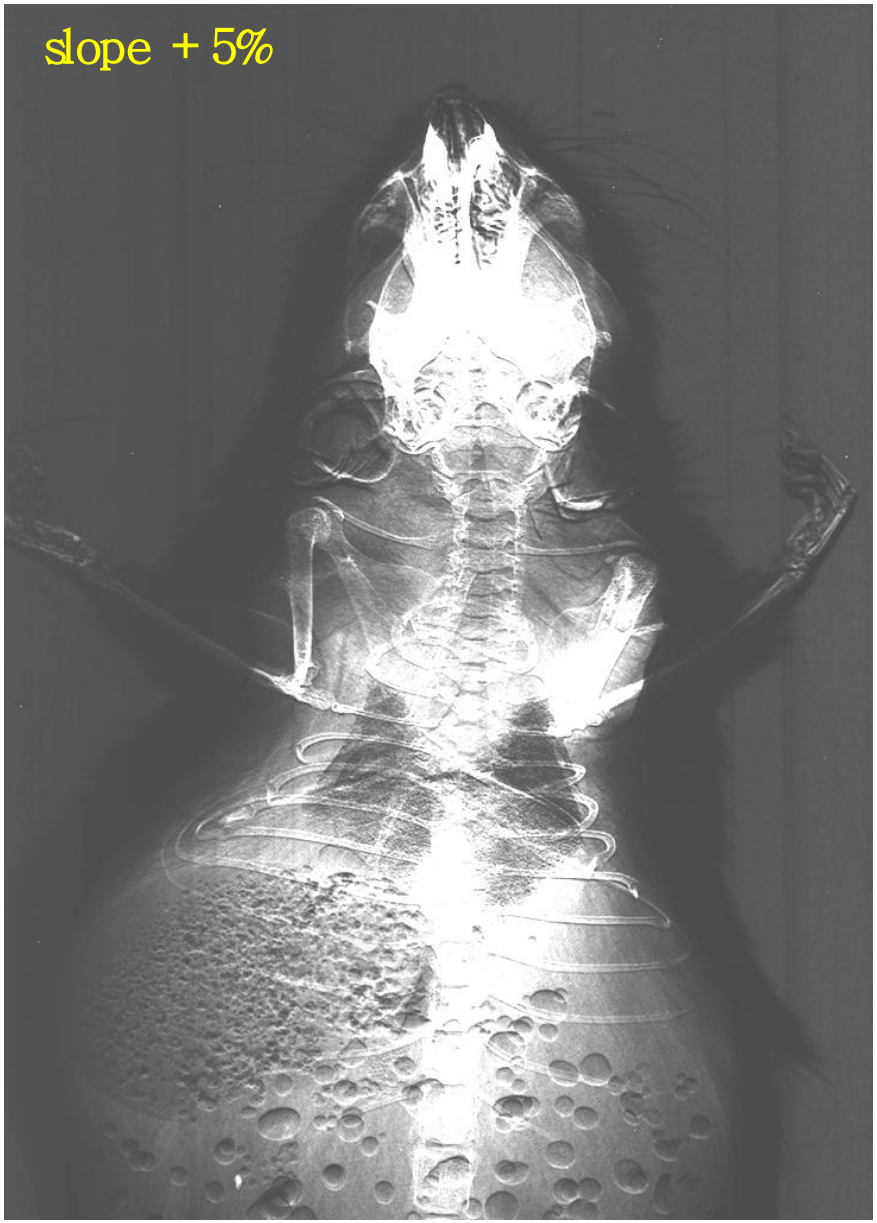

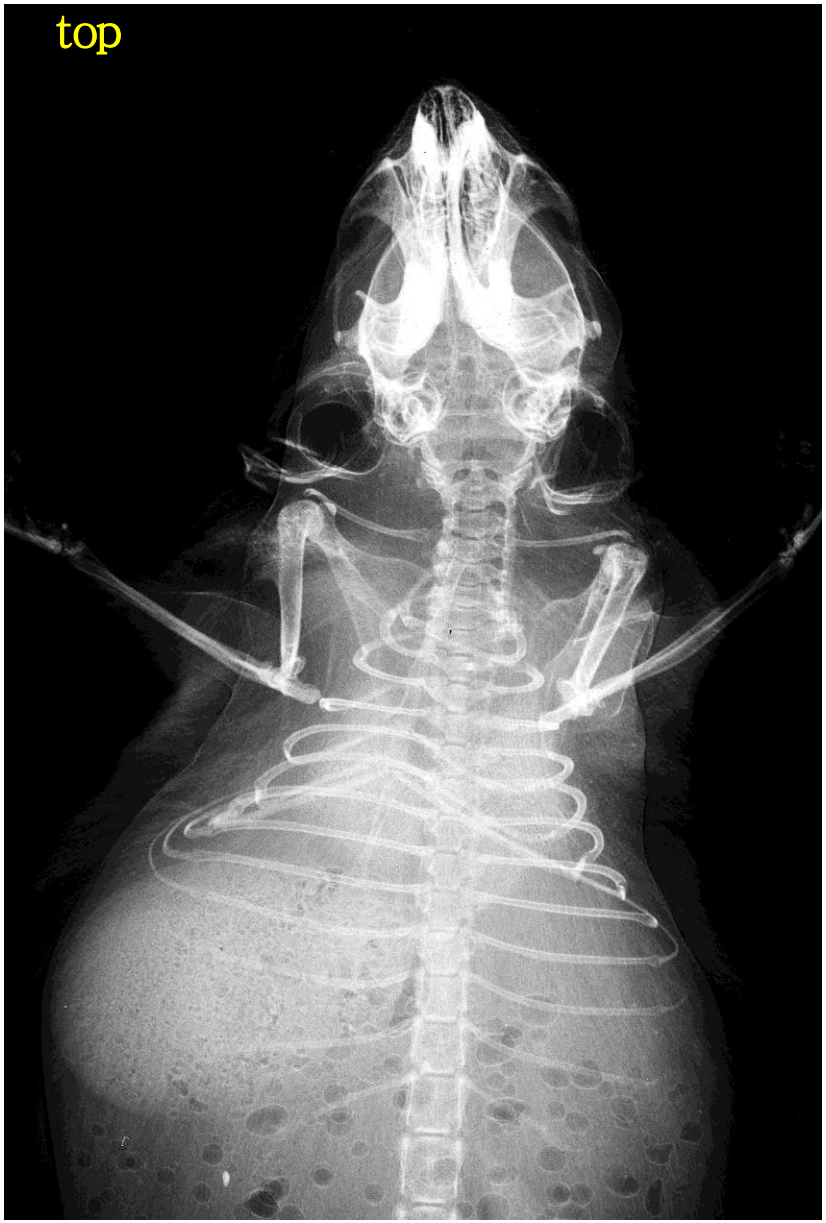

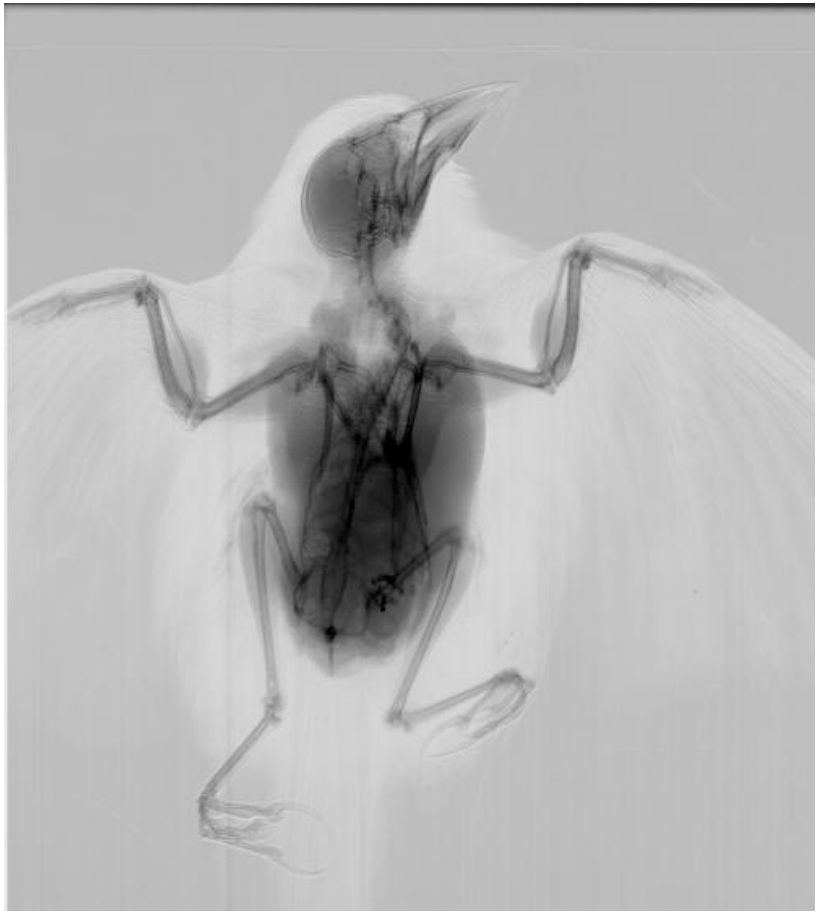

Apparent absorption

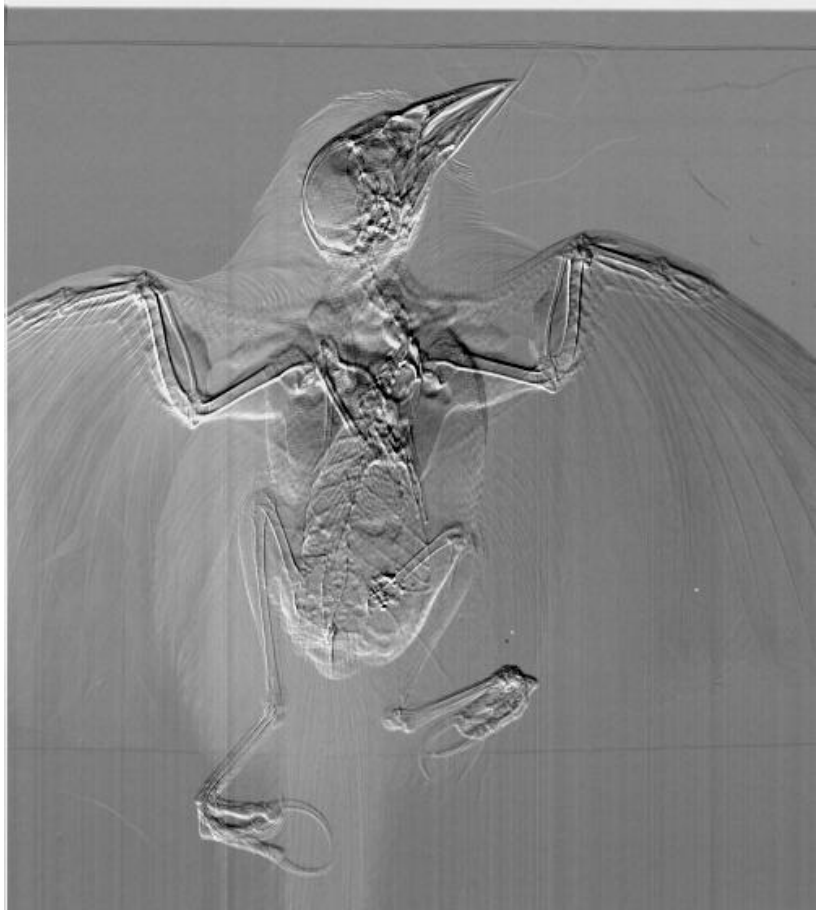

Refraction image

ABI – Laue set-up (Spring 8)

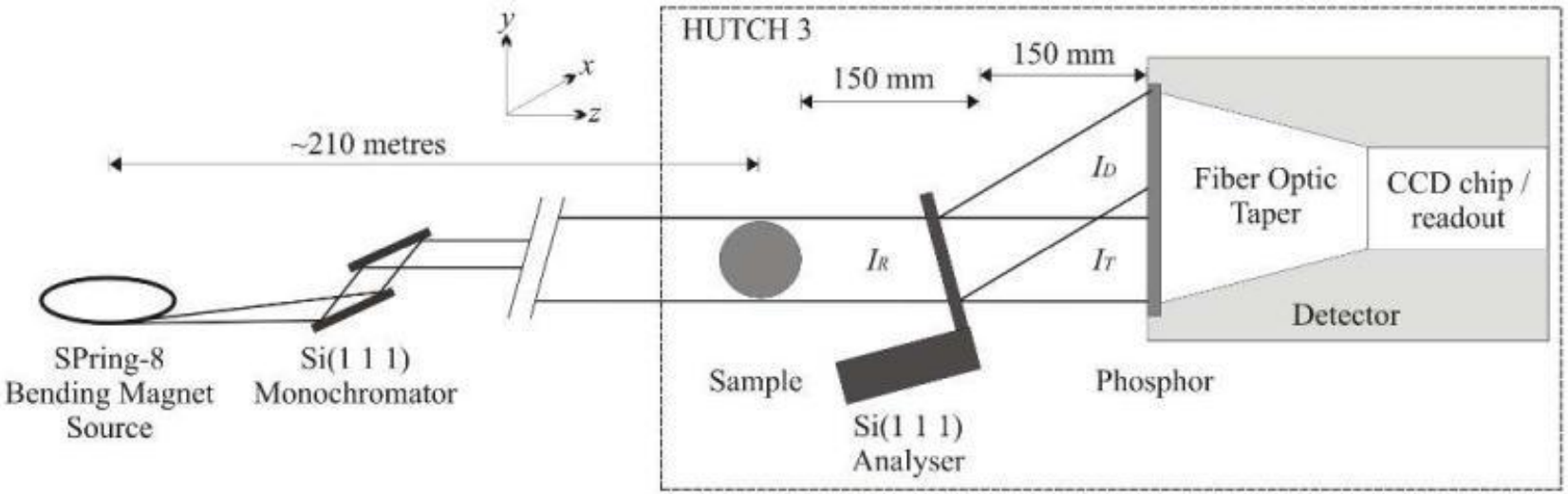

Using an analyzer crystal working in Laue configuration two images from diffracted and transmitted beams can be acquired simultaneusly providing different phase contrast information about the sample

M. Kitchen et al, Eur. J. of Radiology 68S, 2008
M. Kitchen et al., Optics Express, Vol. 18, No. 19, 2010

Computed μ-Tomography (μ -CT)

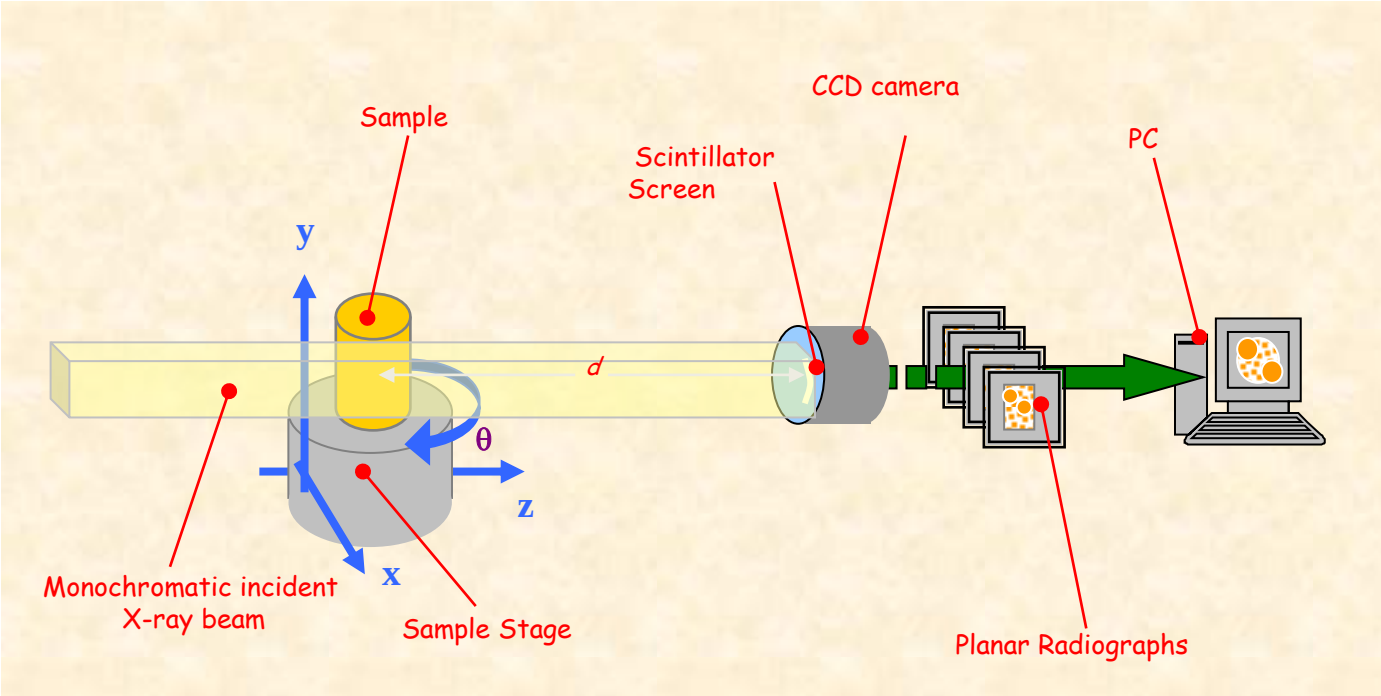

- *not destructive tool* to study the ***internal structure*** of any kind of sample
- no sample preparation
- it gives access to quantitative information on the *density maps* of the irradiated volumes
- suited for *in vivo* imaging of small animals

Breast imaging

Techniques: PHC, planar imaging for patients protocol

DEI, planar and CT for *in-vitro* imaging

Mammography

- Breast cancer is the most common cancer amongst women (incidence: 8%)
- The success of treatment depends on early detection (asynthomatic women)
- Screening programs for large population area above 50 years old
- Sensitivity of conventional mammography: 85-90%, Specificity: 90%
- False positive/true positive ≈ 5 -10%
- High number of doubtful cases makes frequent the need of biopsies
- Conventional mammography is **not enough effective** for dense breasts

Radiographs of breasts with increasing density: mainly adipose breast (left) up to high fibro-glandularity breast (right)

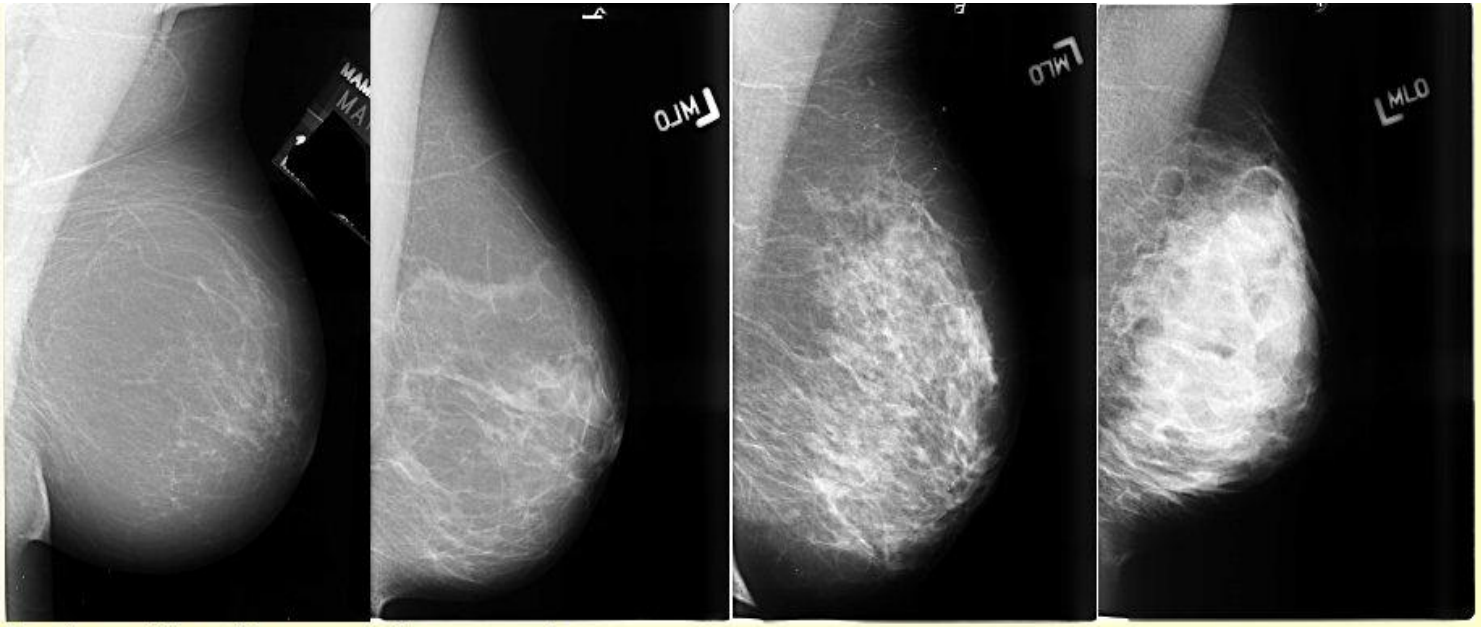

Breast composition and its mammographic appearance.[1]

Breast imaging – first protocol with patients at Elettra

Agreement among the Public Hospital of Trieste, the University of Trieste and Elettra

Aim: Explore the potential of phase contrast imaging on selected cases

Target: Patients whose conventional diagnosis gave uncertain results.

Modality:
I) PHC radiography with film systems
II) PHC imaging with digital detectors
III) Tomo-mammography
(X-ray energy: 32-40 keV)

Projection imaging
X-ray energy: 17– 22 keV

Outcomes from the first protocol (I, II)

SR exams have:
- higher specificity,
- better agreement with the golden standard (biopsy),
- improved image quality,
- strong reduction of delivered doses.

E.Castelli et al.: Radiology, vol 259 (2011), R.Longo et al., Phil. Trans. R. Soc. A 372 (2014)

The SYRMA beamline

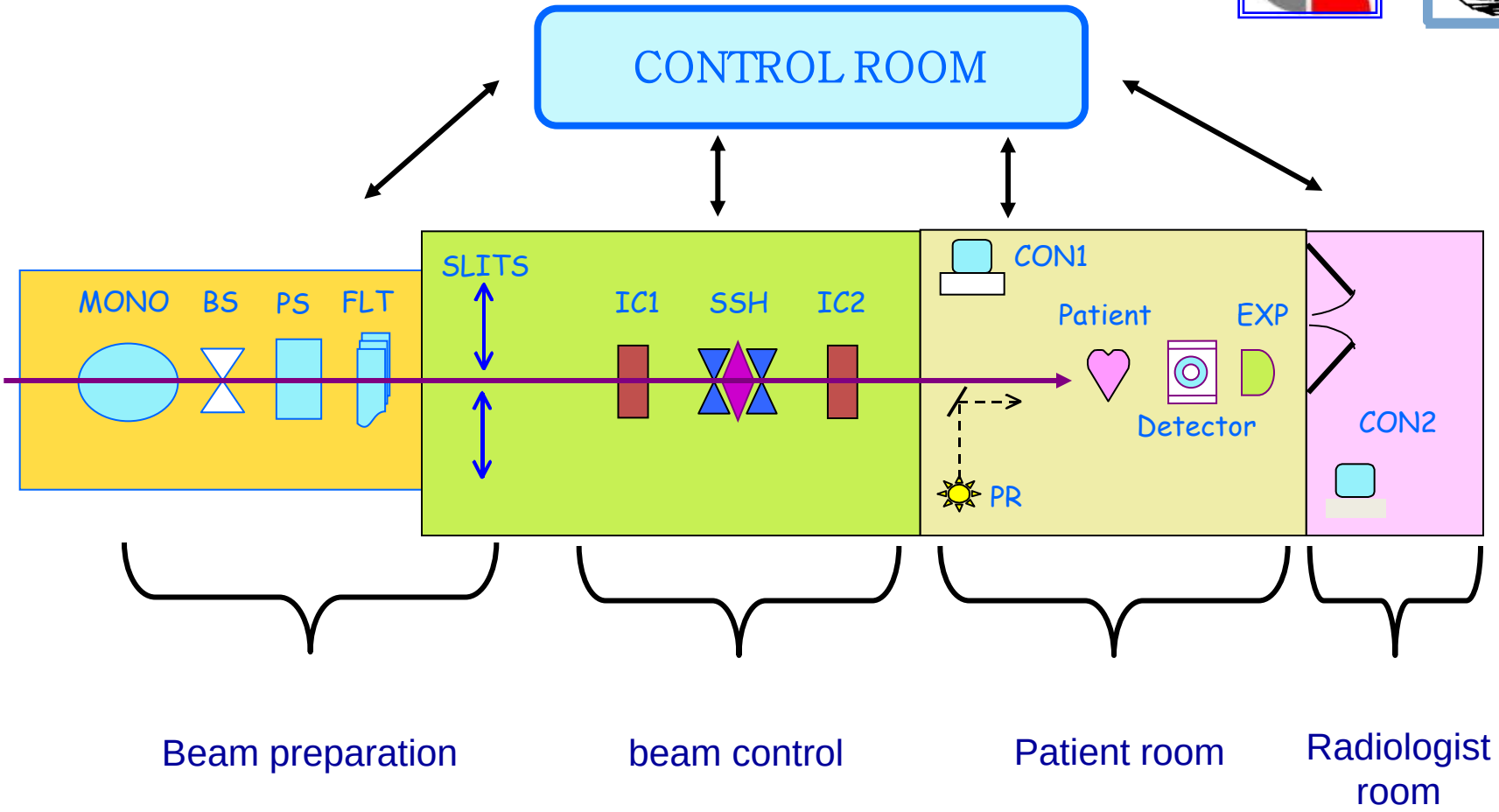

Safety systems:

- Beamline access control system (for personnel)
- Dose control system (for patient)

Dose monitoring, safety and imaging shutters

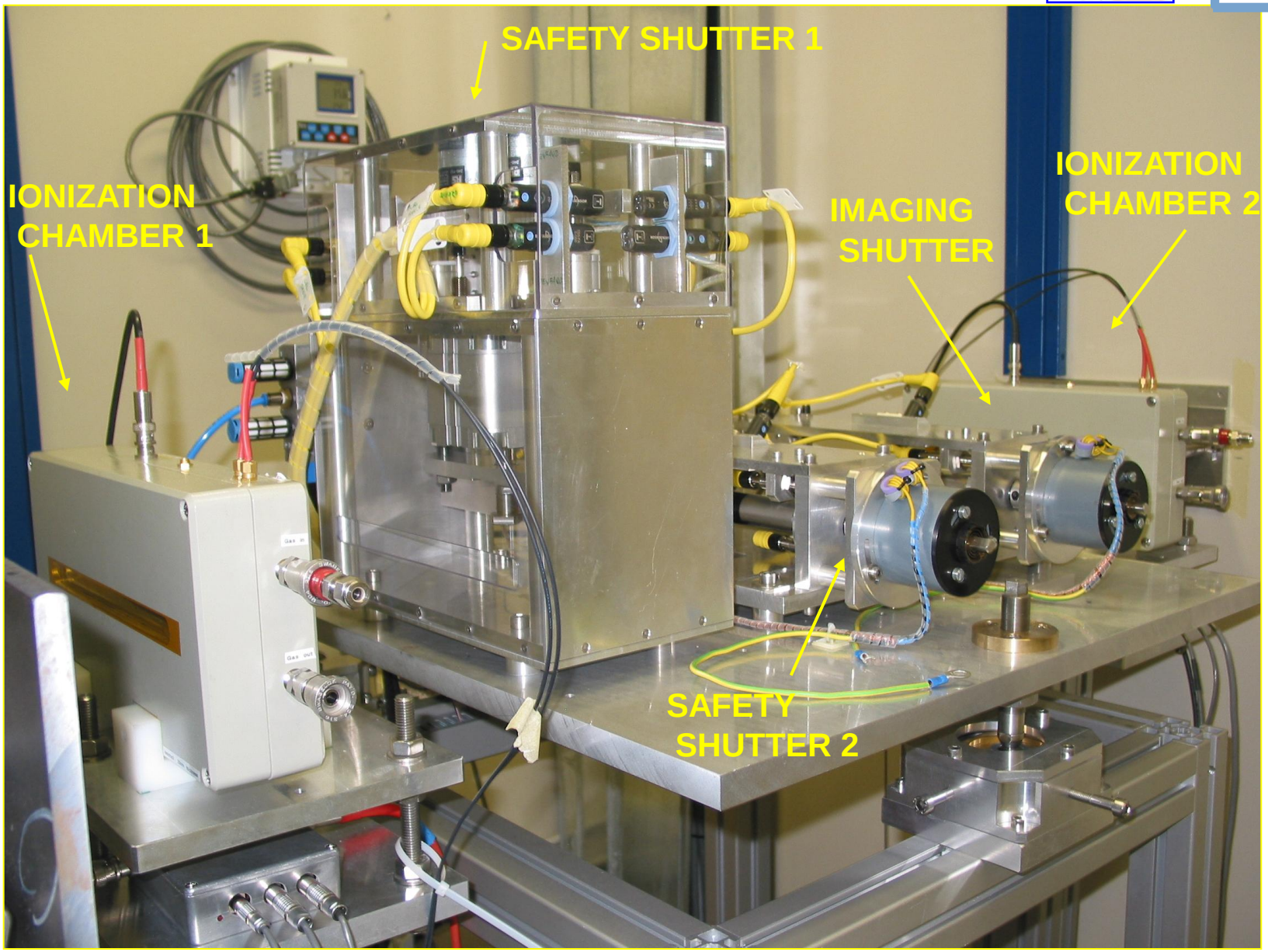

Patient support

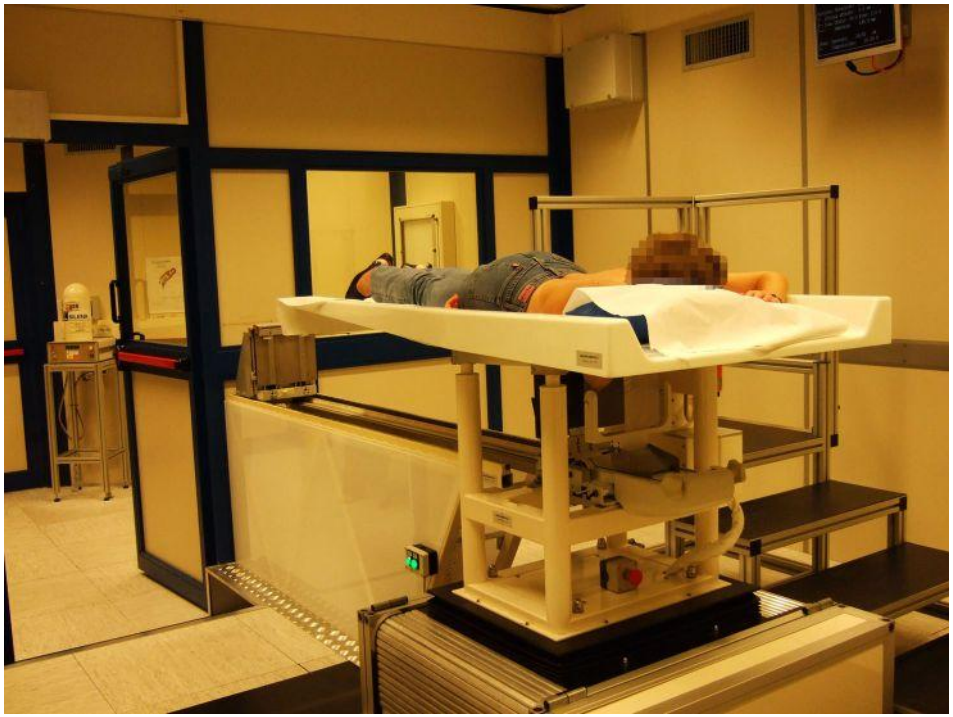

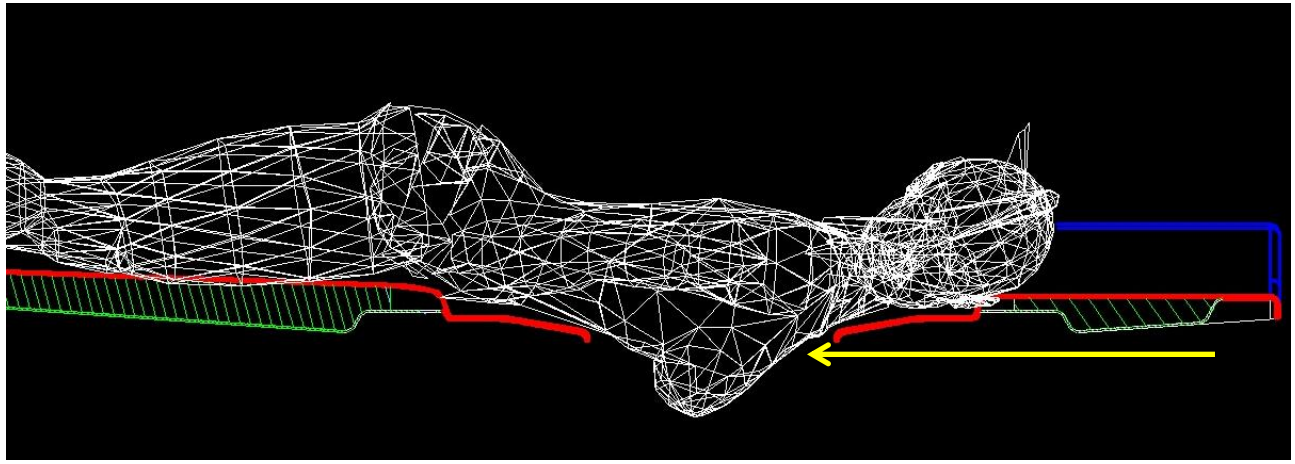

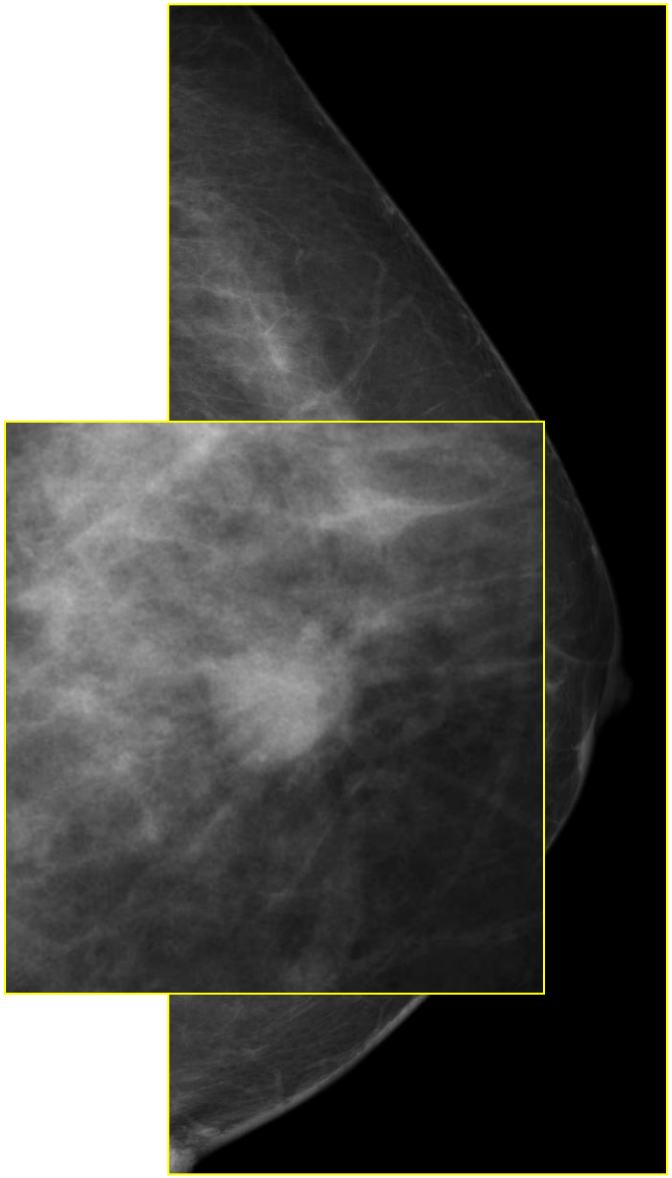

CONVENTIONAL unit

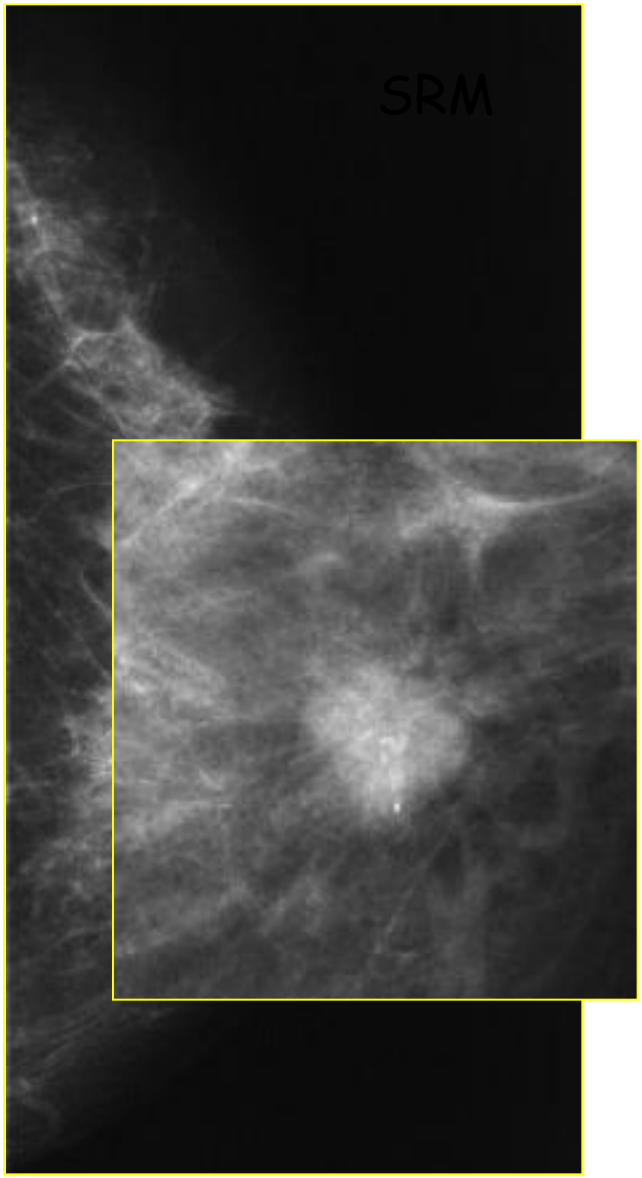

Synchrotron Radiation

Comparison: Synchrotron (SR) versus Conventional (CONV) images

Scores of **lesion** relative visibility

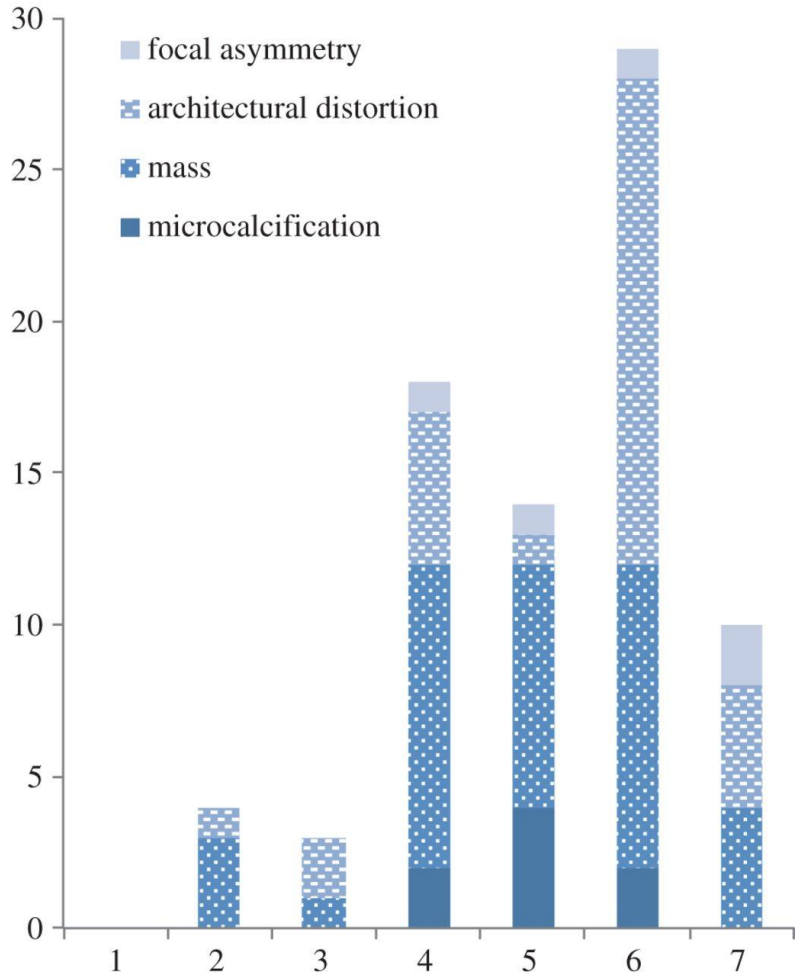

Scores of **glandular structure** relative visibility

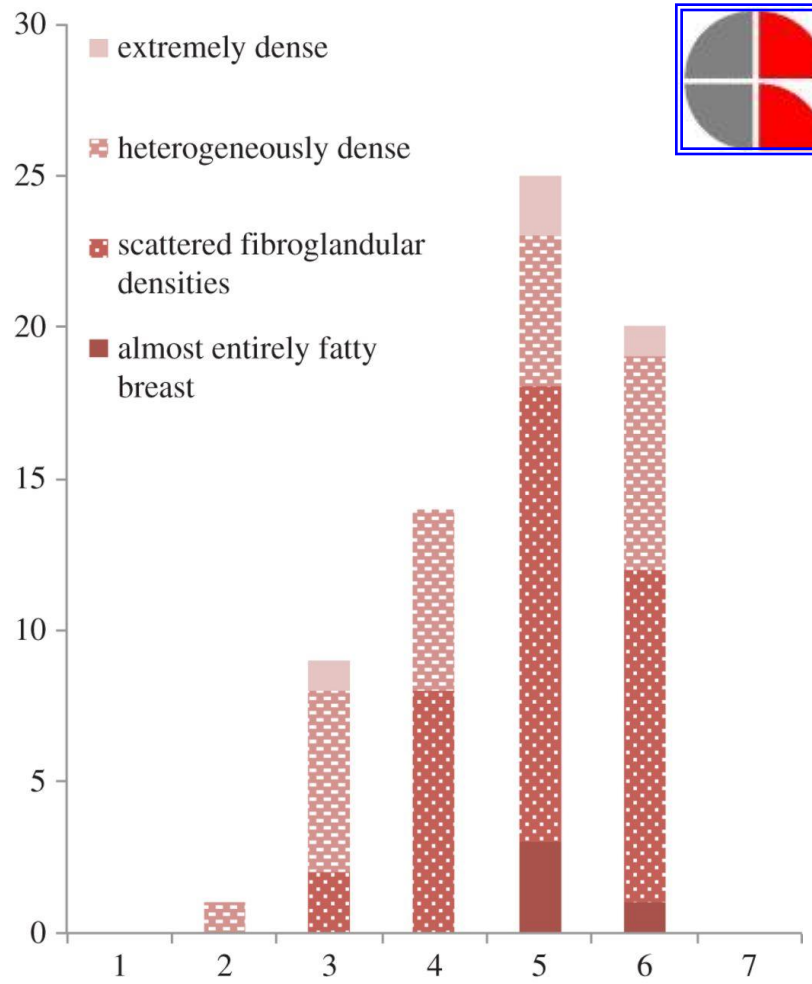

Score ranged from 1 to 7, where:

7 → excellent visualization with SR and poor visualization with CONV
4 → same visualization
1 → excellent visualization with CONV and poor visualization with SR

Breast tissue with ABI at ESRF

Ductal Ca 19 mm

1. Siemens Mammomat 3000, 23 kV, 8 mAs, MGD=0.6 mGy
2. DEI image, top, 25 keV, MGD= 0.6 mGy
3. DEI image, plus 0.7, 25 keV, MGD= 0.6 mGy
4. Histology

50 % more micro-calcifications have been scored in DEI images vs. conventional

S.Fiedler et al., Physics in Medicine and Biology 49, 175-188 (2004)

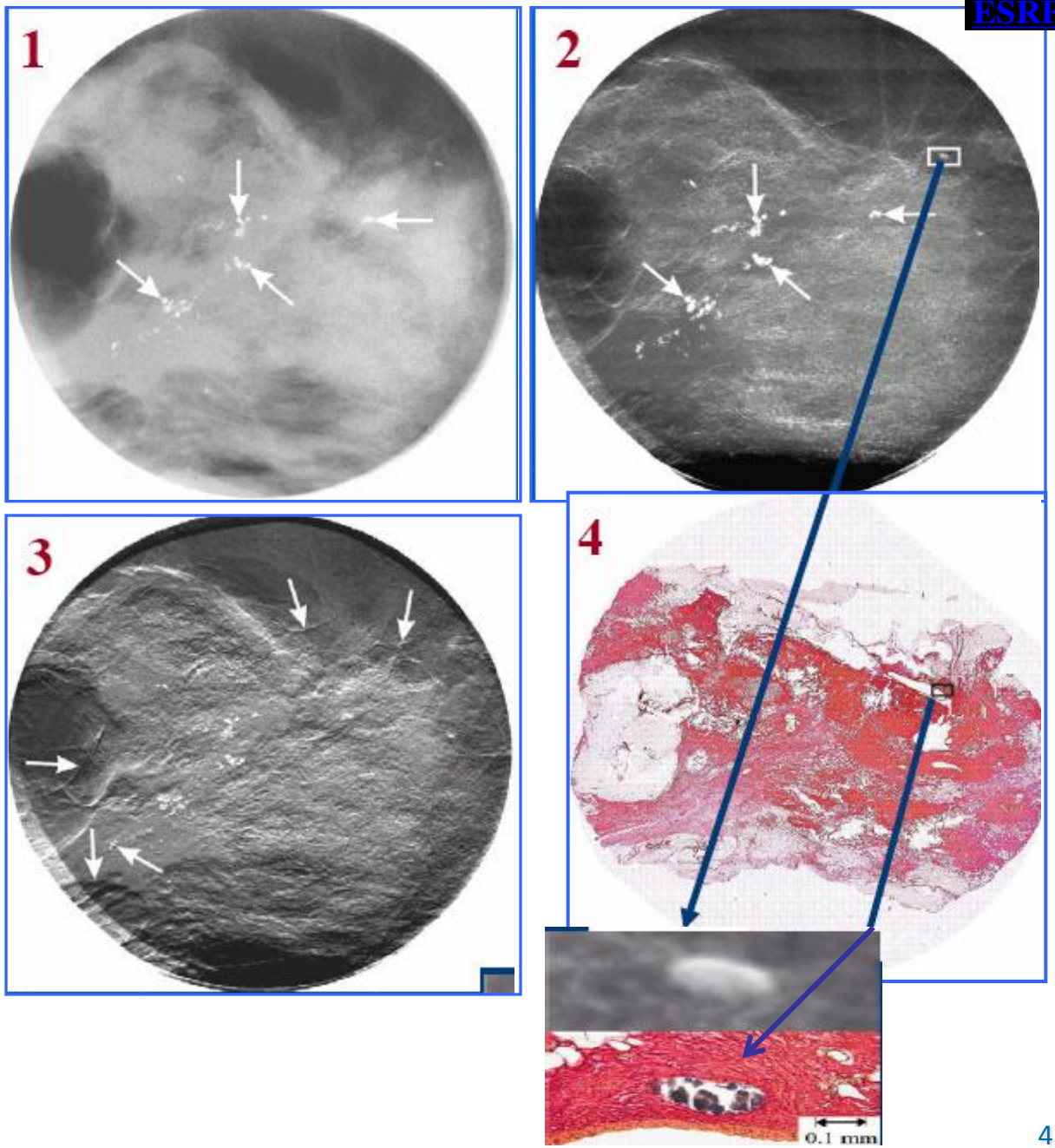

Lobular Breast carcinoma - ABI CT

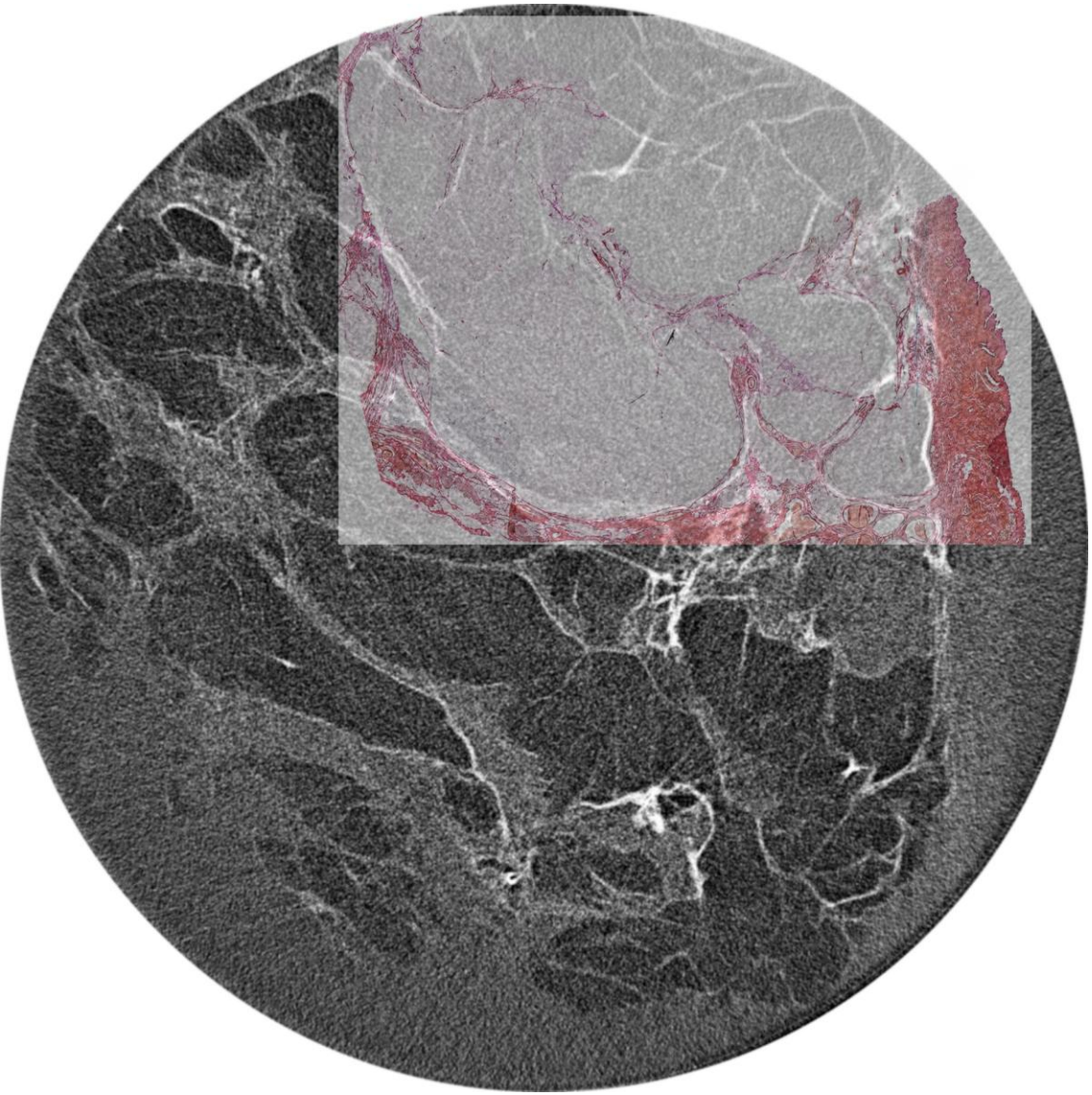

Top

Si(333)

33 keV

720 projections

Voxel: 50^3 μm^3

MGD=1.9 mGy

J. Keyriläinen et al. Radiology (2008) 249 (1) 321

Low dose breast CT inaging: new developments

- The combination of PCI at high energy X-rays (> 50 keV) and a new image reconstruction method, (**equally sloped tomography**), allows to obtain 3D imaging of a whole human breast and to identify a malignant cancer at a radiation dose less than that of dual-view mammography. The method has been implemented first by Miao et al., then applied to breast tissue imaging by Zhao et al.
- PCI in ABI modality was used with E = 60 keV
- This method reduces the radiation dose by ~74% relative to conventional (i.e. with FBP CT reconstruction algorithms maintaining high image resolution and image contrast.

3D visualization of a tumor bearing breast tissue from the PCI-CT reconstruction performed with the Equally Sloped Tomography algorithm. (A) A segmented tumor in an axial slice, in which the yellow contour line indicates the tumor boundary. (B) Volume renderings of the tumor (in red)

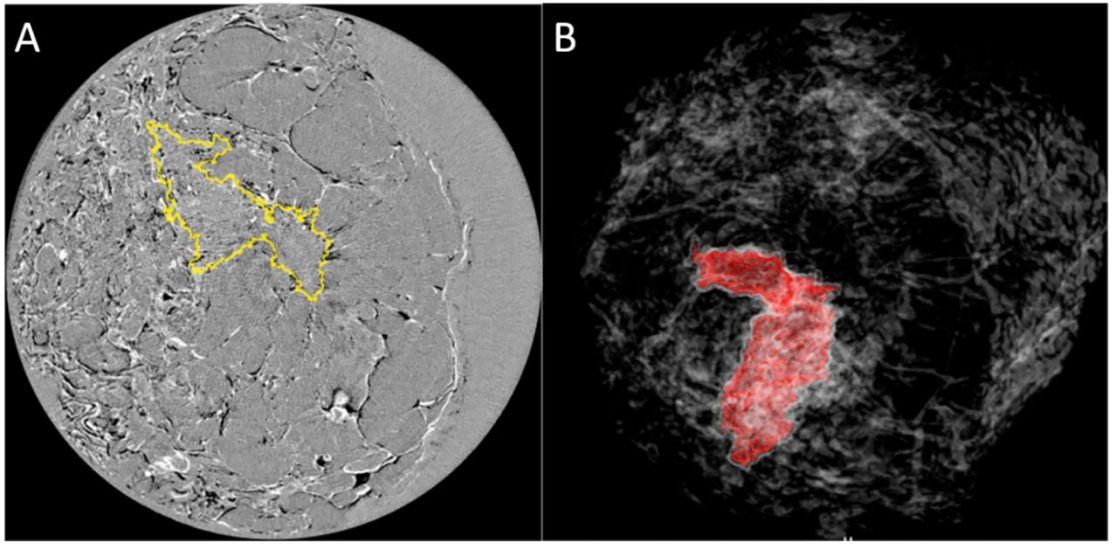

J.Miao, et al., Phys Rev. B 72, 2005, B. P Fahimian et al., Phys. Med. Biol. 55, 2010, Zhao Y et al., Proc. Natl Acad. Sci. USA 109, 2012

Tomo-mammography project (SYRMA-CT) at Elettra

Goal: Design a new clinical protocol combining **planar projection mammography** and a **CT scan** (inline PHC) on a limited breast portion

Diagnostic aim: contribute to solve the cases of lesions overlap, improve the lesions characterization and visualize better their infiltration in the healthy tissue

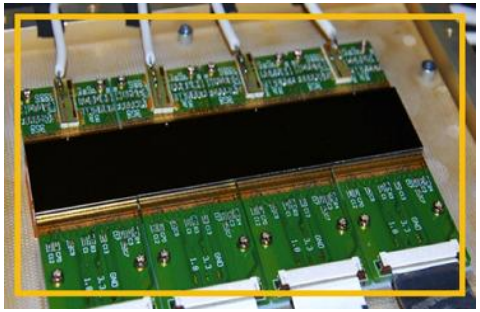

Key element: CdTe single photon counting detector, 60 µm pixel size, 25 × 2.5 cm² active area by PiXirad

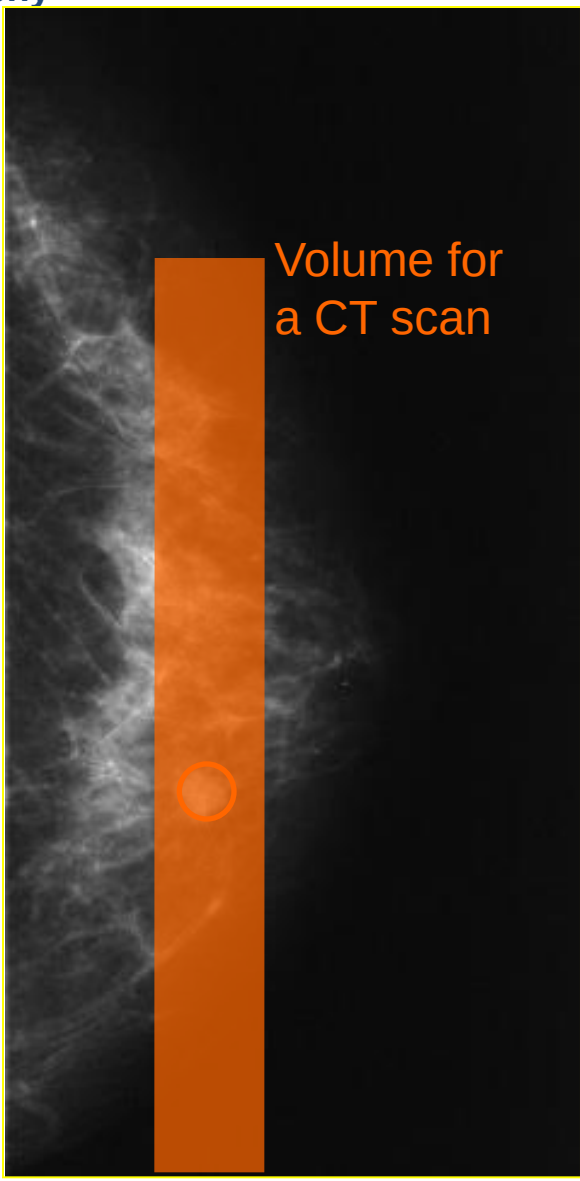

Project financed by **Istituto Nazionale di Fisica Nucleare** (INFN), Sections of: Trieste, Ferrara, Pisa, Napoli, Sassari

Approval by ethic committee is needed

First images obtained using Pixirad

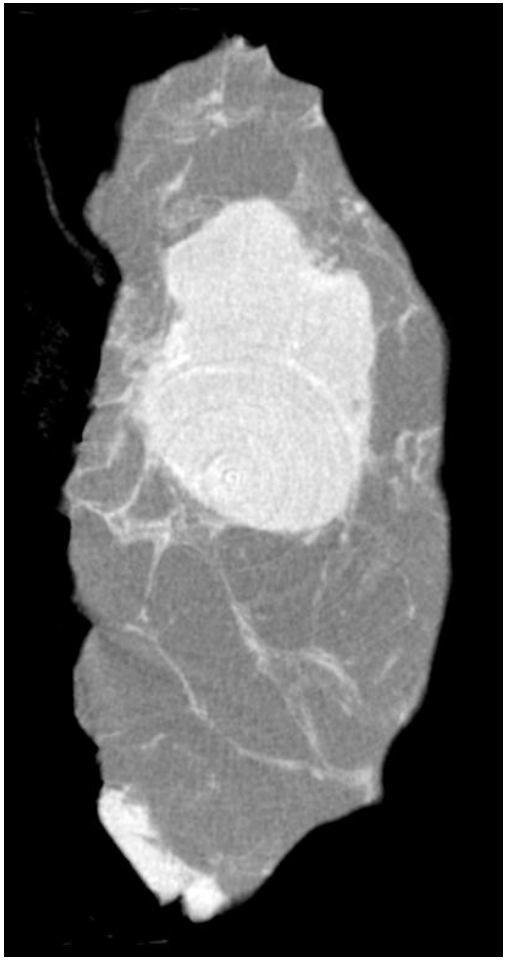

FBP reconstruction of 1200 phase-retrieved projections (MGD ~20 mGy)

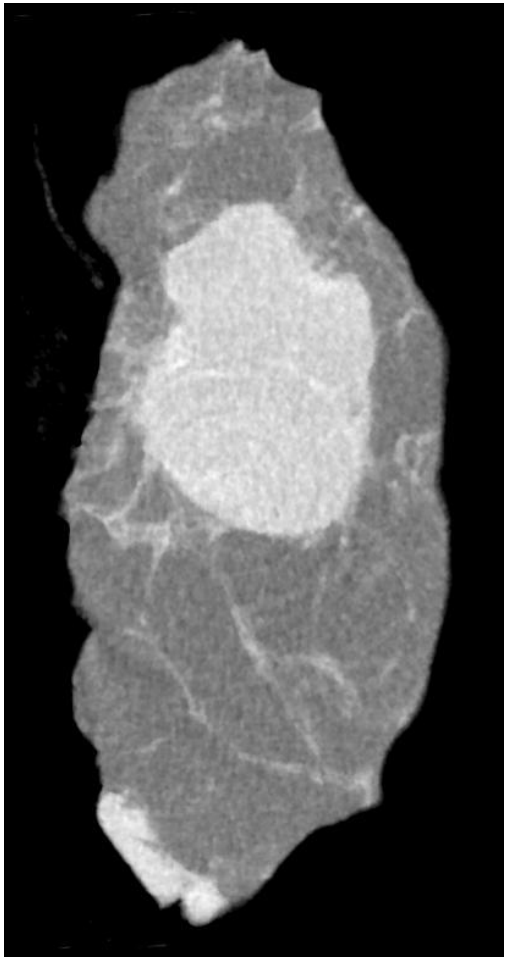

SART reconstruction of 300 phase-retrieved projections (MGD ~5 mGy)

*Longo R. et al. 2016 Phys. Med. Biol. **61** 1634-1649.*

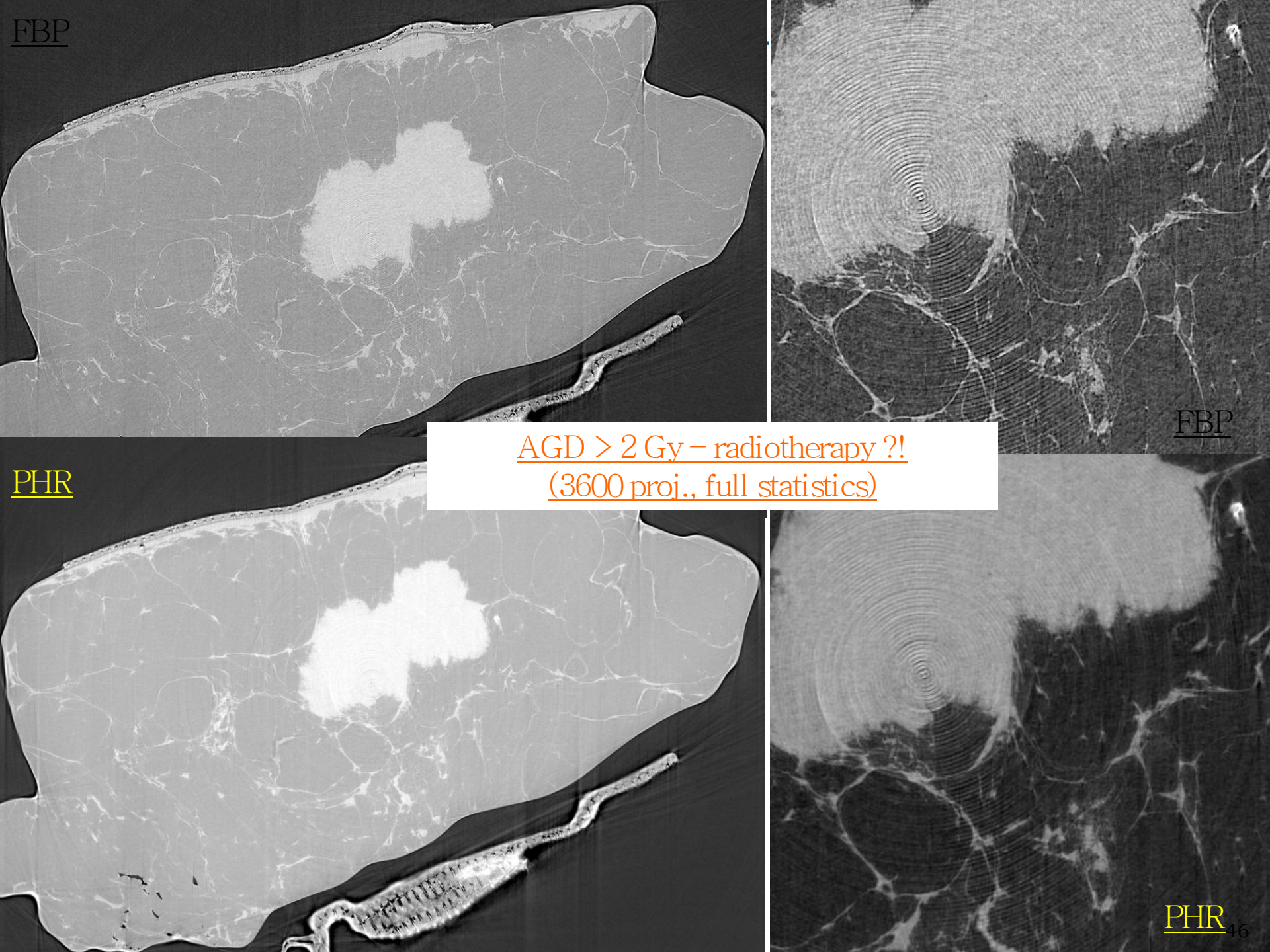

AGD > 2 Gy – radiotherapy ?!
(3600 proj., full statistics)

Low dose phase contrast breast tomography: optimization of reconstruction workflow

Geometrical test object and tissue specimens

CT in PB mode @ diagnostic dose (2.5 mGy AGD)

Reconstruction workflows
Pre-processing, reconstruction, post-processing

Definition of image quality indexes & functions for comparison

Radiological Assessment

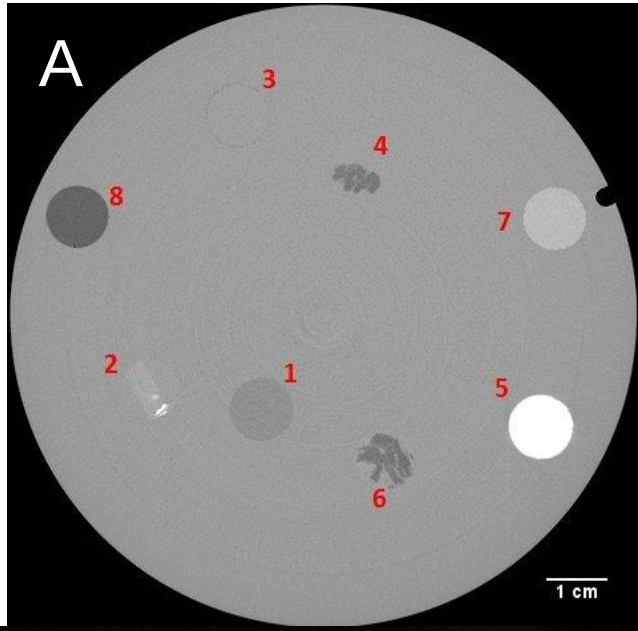

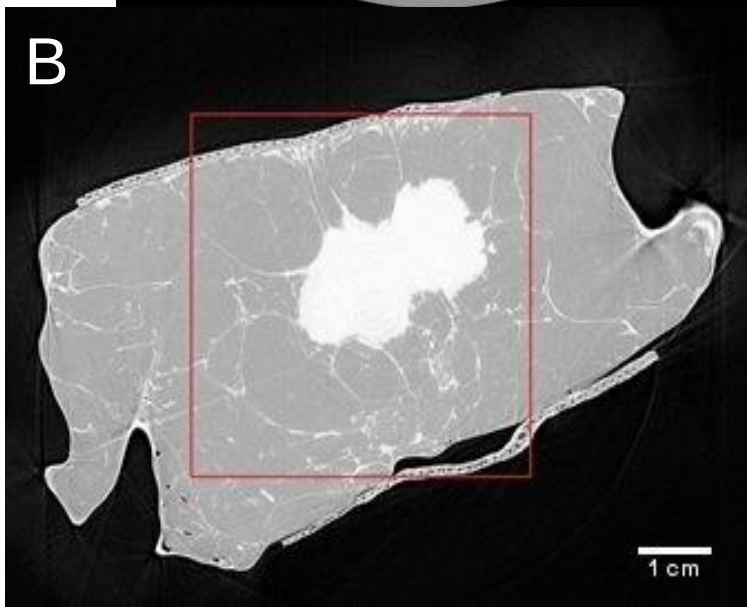

A) Polycarbonate phantom where 1 = Glycerol (C3H8O3), 2 = Unknown tissue (Malignant), 3 = Water (H2O), 4 = Fibrous tissue, 5 = Calcium Chloride (CaCl2), 6 = Adipose tissue, 7 = Paraffin wax, 8 = Ethanol (EtOH).

B) Reference image for the mastectomy sample reconstructed with FBP algorithm and considering 3600 high statistic projections. The red square indicates the region-of-interest used for the image quality assessment.

S. Pacilè, et al: Biomed. Opt. Express 6 (2015)

Elettra Sincrotrone Trieste

Reconstruction workflows

Abbreviation	Phase retrieval	Reconstruction	Post-proc.
FBP	no	FBP	
FBP-ITER	no	FBP-ITER	
SIRT	no	SIRT	
SART	no	SART	
CGLS	no	CGLS	
EST	no	EST	
phr FBP	yes	FBP	
phr FBP-ITER	yes	FBP-ITER	
phr FBP-ITER Epan17	yes	FBP-ITER	Epanechikov (w = 17)
phr FBP-ITER Susan5	yes	FBP-ITER	Susan (w = 5)
phr TV-MIN	yes	TV	
phr SIRT	yes	SIRT	
phr SART	yes	SART	
phr CGLS	yes	CGLS	
phr EST	yes	EST	

Image quality indexes & functions

Full-reference indexes

(require a ref. image)

MSE – Mean Squared Error
SNR – Signal-to-Noise Ratio
UQI – Universal Quality Index
NQM – Noise Quality Measure
SSIM – Structural Similarity Index

No-reference indexes

CNR – Contrast to Noise ratio
FWHM – Full width half maximum
Qs – Image quality characteristic(*)

$$CNR = A_{feature}^{1/2} \frac{|\langle \beta_{lesion} \rangle - \langle \beta_{adipose} \rangle|}{[(\sigma_{lesion}^2 + \sigma_{adipose}^2)/2]^{1/2}}$$

$$Q_s = \frac{SNR_{out}}{F_{in}^{1/2} \Delta x}$$

F_{in} = incident photon fluence
Δx = spatial resolution of the imaging system
SNRout = output signal-to-noise ration

(*) T. Gureyev et al, Opt. Express 22, (2014)

Radiological Assessment

From 0 (worst case) to 4 (best image)

- No-diagnostic power (0 – 2)
- Poor diagnostic power (2 – 3)
- Full diagnostic power (> 3)

S. Pacilè, et al: Biomed. Opt. Express 6 (2015)

Elettra Sincrotrone Trieste

NO-DIAGNOSTIC POWER

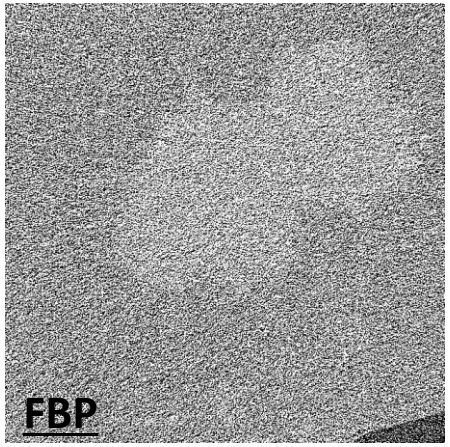

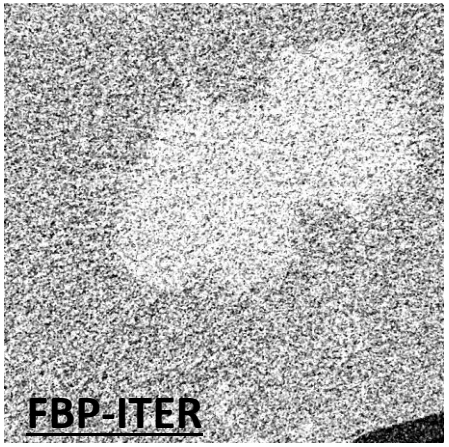

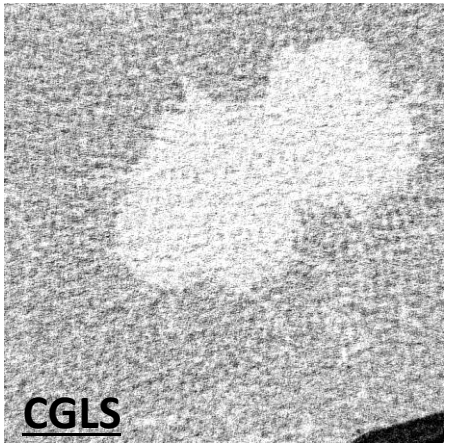

POOR-DIAGNOSTIC POWER

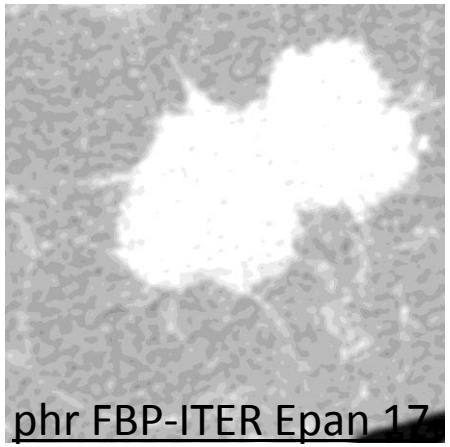

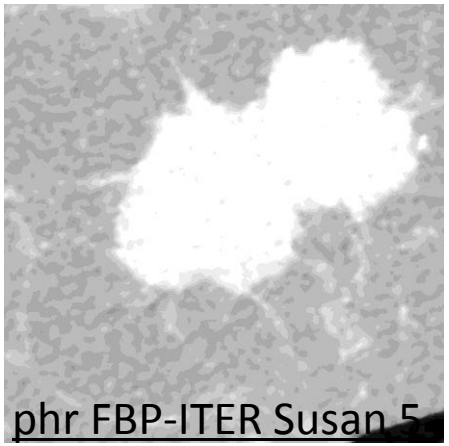

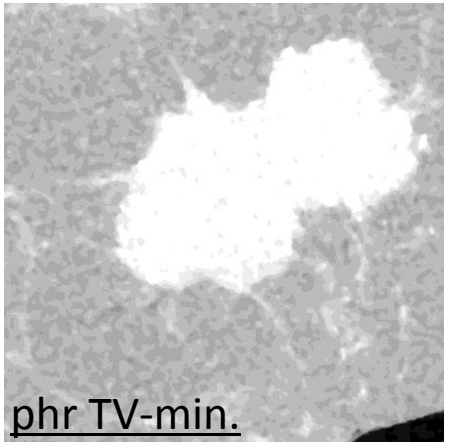

FULL-DIAGNOSTIC POWER

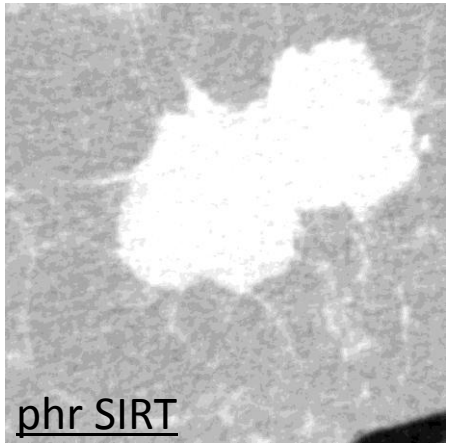

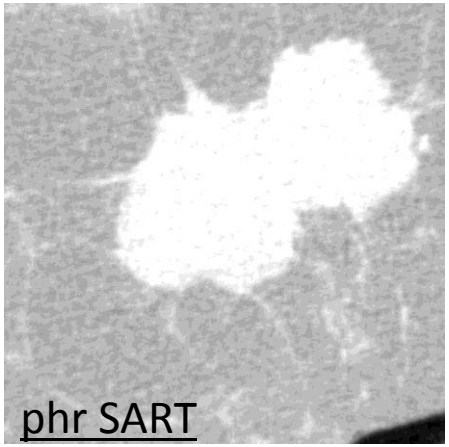

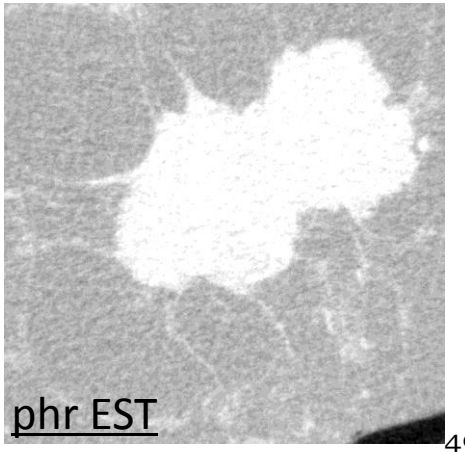

S. Pacilè, et al: Biomed. Opt. Express 6 (2015)

Contrast-to-noise ratio and image *blurring*

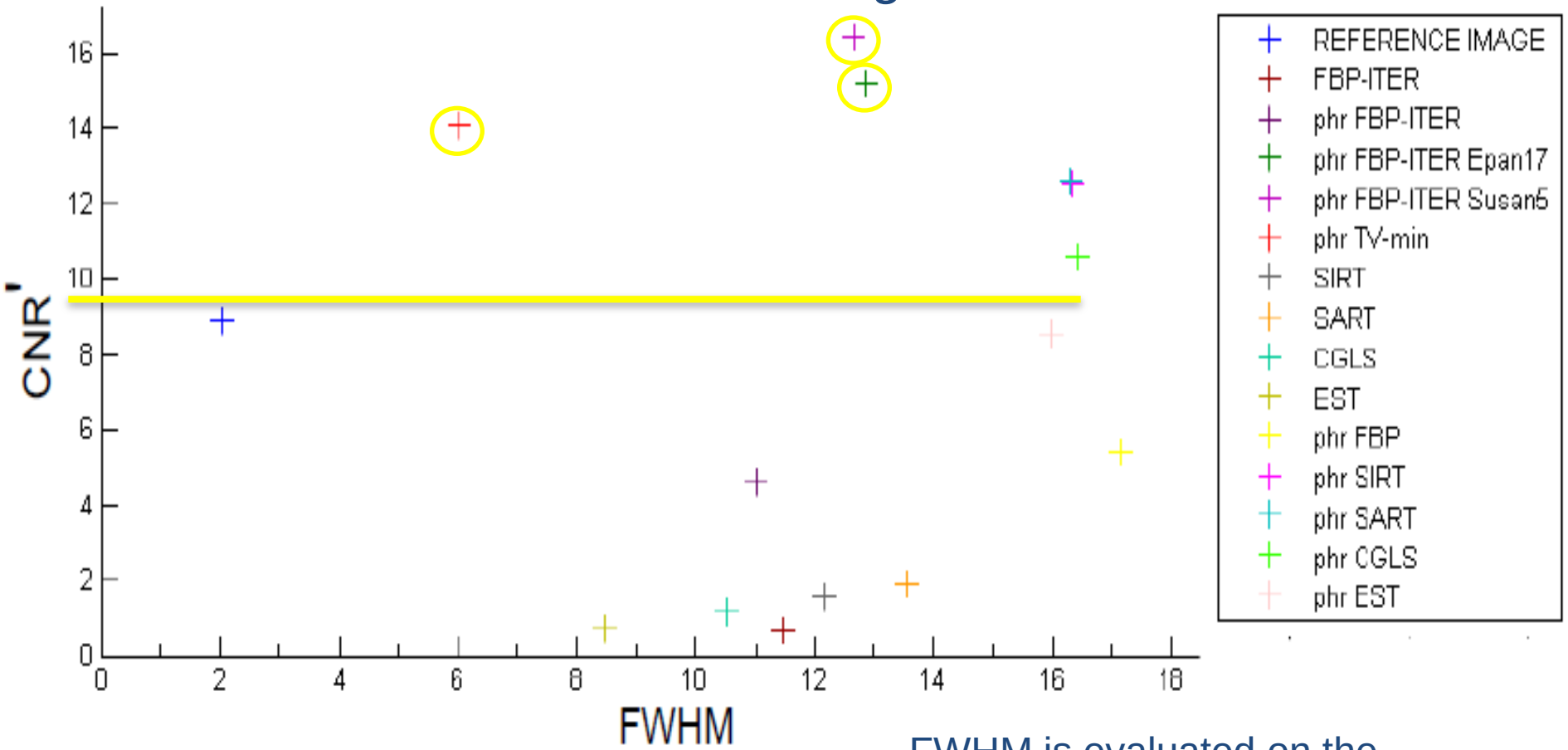

Full statistics ref image recontructed with phr and FBP: CNR' = 30.5, FWHM = 5.8

FWHM is evaluated on the phantom images)

S. Pacilè, et al: Biomed. Opt. Express 6 (2015)

Feasibility study @ the Australian source: mastectomy specimen

DIAGNOSTIC CONTEXT: Excised breast tissue containing a multifocal invasive papillar n invasion. The tumor is composed of multiple nodules through the scar tissue.

EXPERIMENTAL PARAMETERS:

Energies = 38 keV, Distance = 5,7 m

Detector pixel size = 100 μm

MGD ~ 5 mGy

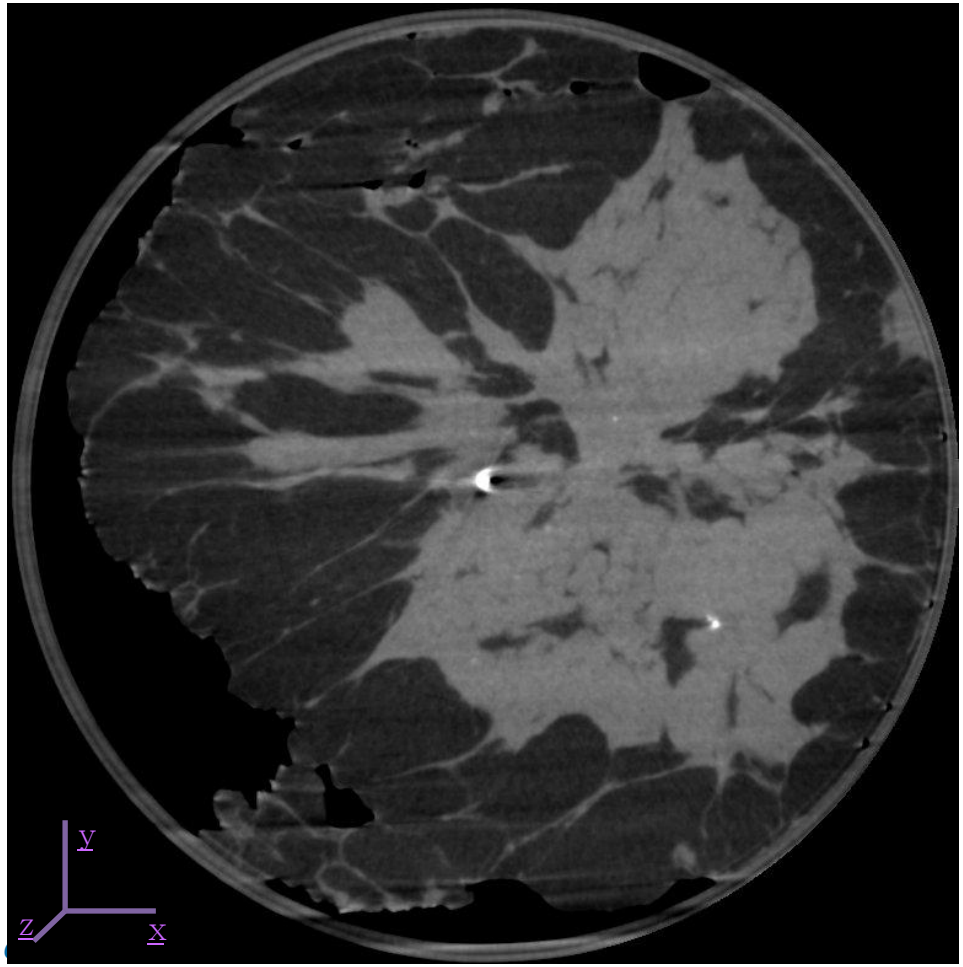

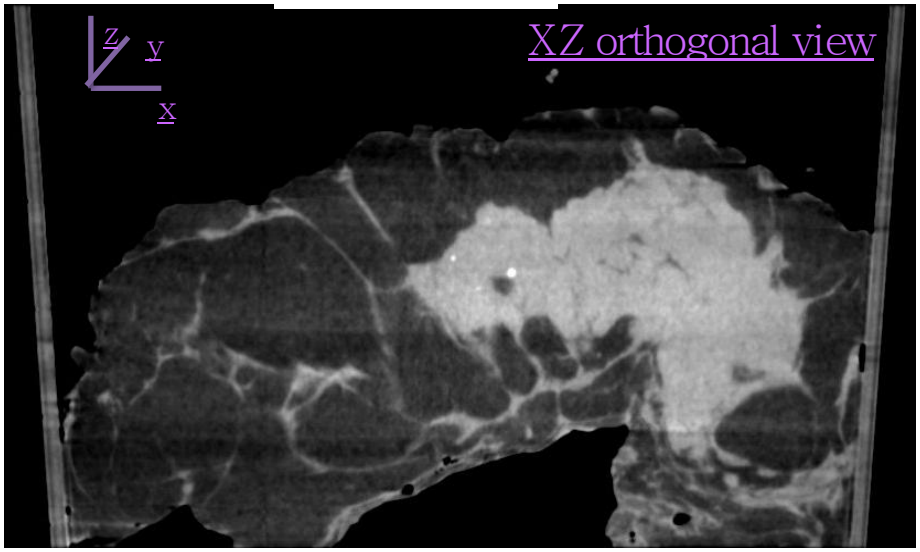

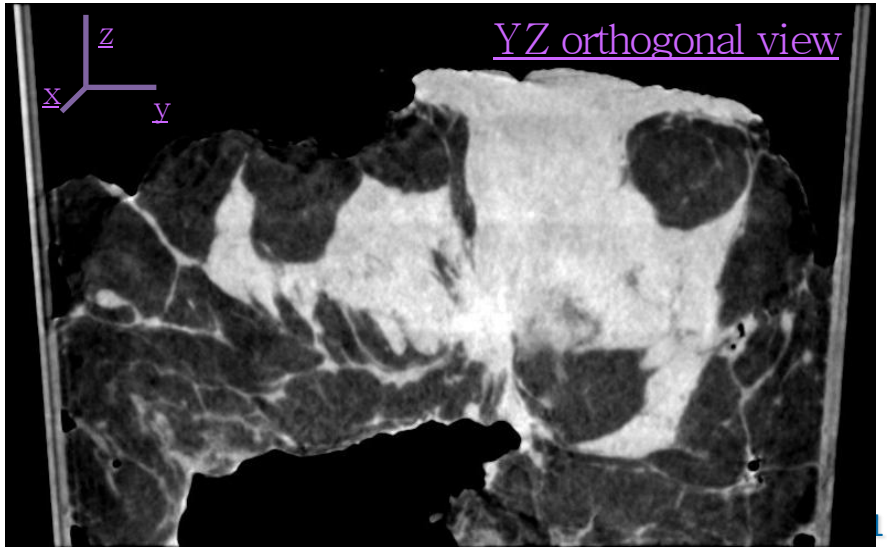

Phase-contrast data collected at Elettra, Nov 2015. Comparison with histology (1)
E = 38 keV, d= 2m, Dalsa Argus detector (54um pixel)

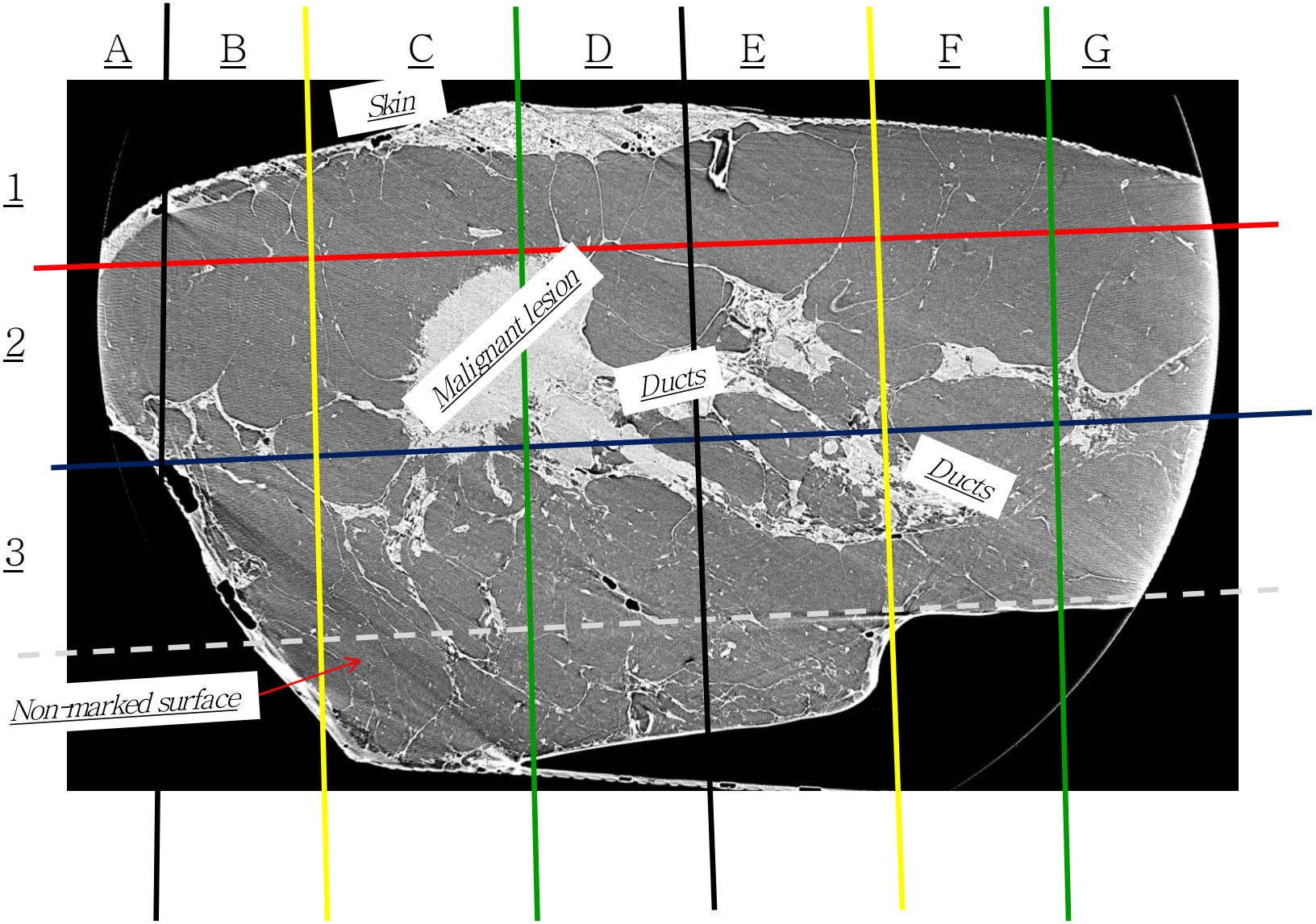

Phase-contrast data collected at Elettra, Nov 2015. Comparison with histology (2)

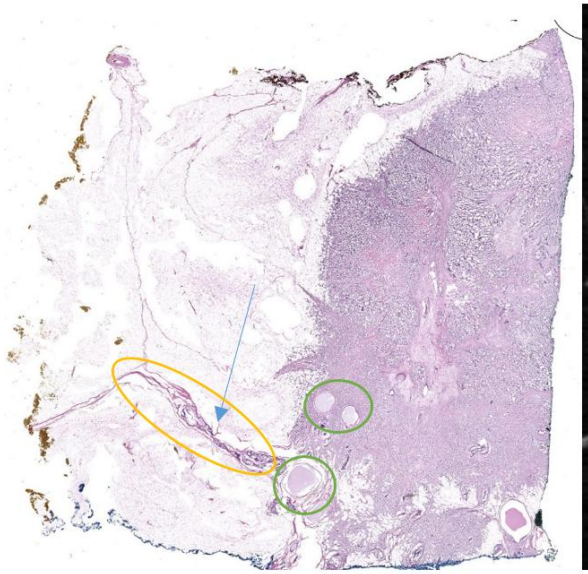

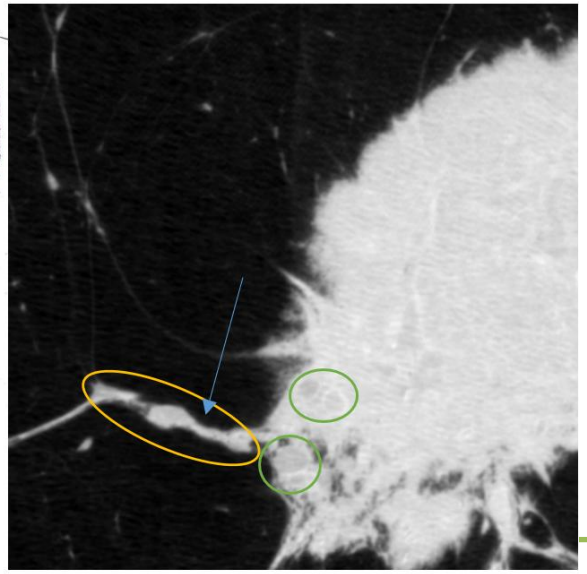

Area C2-4

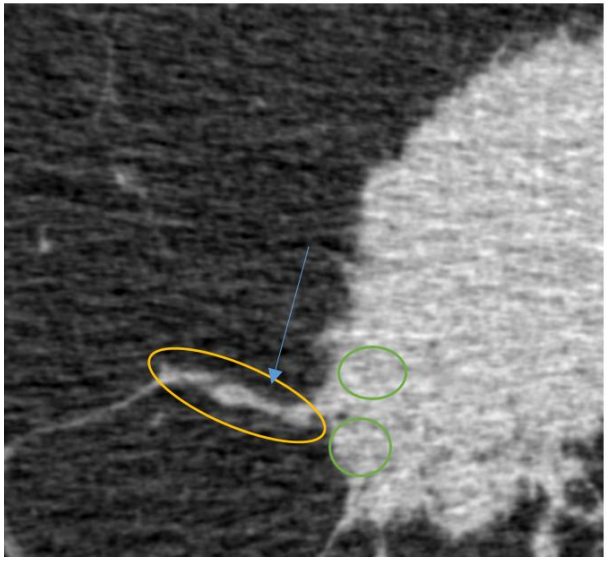

1. Clearly visible contour of the tumour with typical spiculations (which are also visible in the low-dose X-ray image).
2. In the middle of the tumour, the grey scale variation is well visible in the high-dose X-ray image.
3. Green ovals contain cysts, which are poorly visible in the low-dose image.
4. Yellow oval contains stroma with a possible satellite cancer: to be investigated in a subsequent high-res histology.

Phase-contrast data collected at Elettra, Nov 2015. Comparison with histology (3)

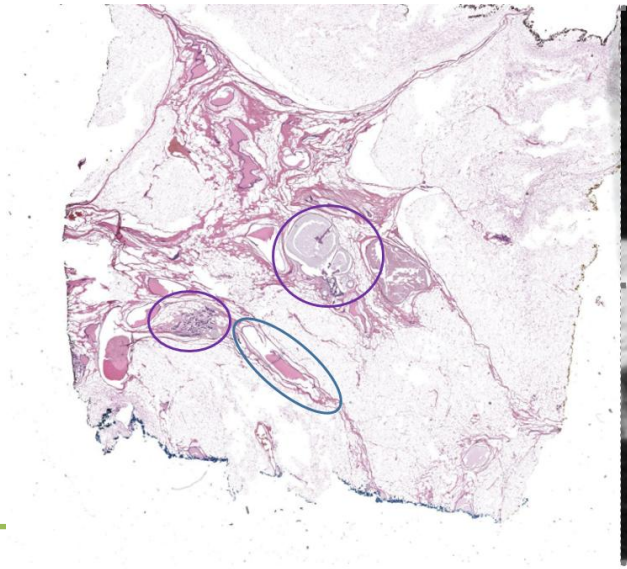

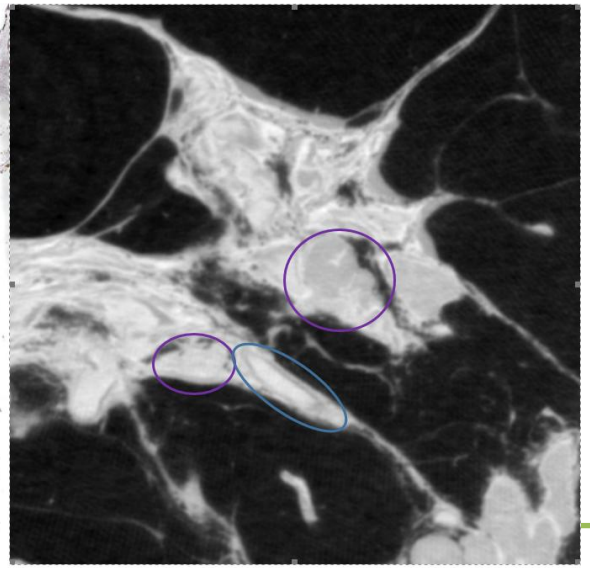

Area E2

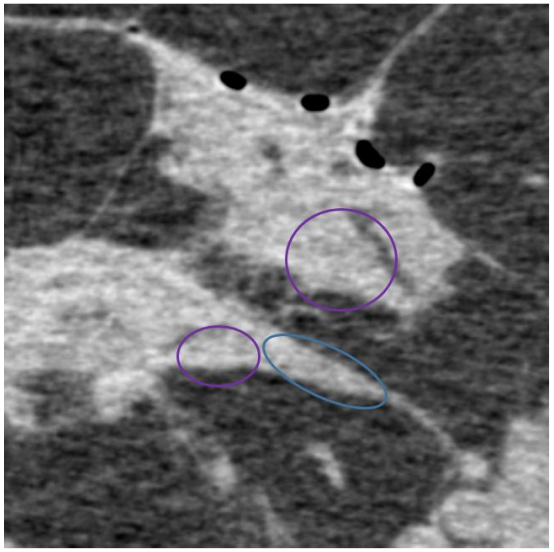

1. X-ray image not ideally matched.

2. Blue oval contains a blood vessel.

3. Purple ovals contain ducts/cysts that may have been invaded by cancer cells (this is to be verified by subsequent high-resolution histology).

4. Low-dose level shows good outline of the main tissue structures, but not the cysts.

Additional high-res histology to be done at Trieste Uni or TissuPath

Potentials of ABI

In vitro feasibility tests:

- Studies of cartilages and bones interfaces

- Imaging of finger joints

ABI studies of Cartilage and bone interface

Osteoarthrosis (OA) is a disease characterized by the progressive degeneration of articular cartilage and the development of altered joint congruency. It has a high incidence in the adult population. Affecting mainly the elderly population, it is one of the main causes of disability worldwide. Conventional radiography detects only **important osseous changes**, at advanced OA or RA stages, when therapeutic strategies are less effective. **Early changes** in the **cartilage** and other **articular tissues** are **not** directly visible. MRI imaging works better but the maximum achievable spatial resolution is not always adequate.

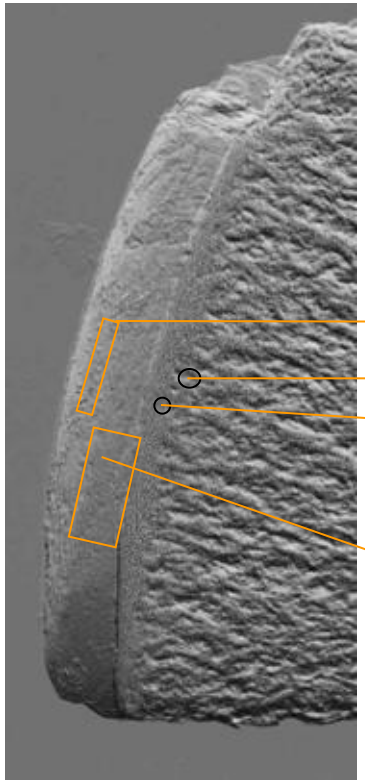

Need to study:

- cartilage
- cartilage-bone interfaces
- changes in the bone structure

Superficial Layer (Zone of horizontal collagen fibers with flat cells)

Subchondral Bone Plate (**Important for diagnostic purposes in OA**)

Tidemark (Border between normal and mineralized cartilage)

Transitional and Deep Layer (round cells, collagen fiber switches from horizontal to vertical orientation, increasing stiffness and material density)

Aim: detect the architectural arrangement of collagen within cartilage and evaluate how the cartilage degeneration affects the underlying subchondral and trabecular bone.

Femur head core cuts: collagen arcades structure

- The ABI technique allows to visualize the discontinuities in the sample and the inner structures invisibles by means of conventional X-Ray imaging.
- The transition bone-cartilage is emphasized.
- The articular cartilage striations are well visible due to X-ray diffraction at edges of fibers

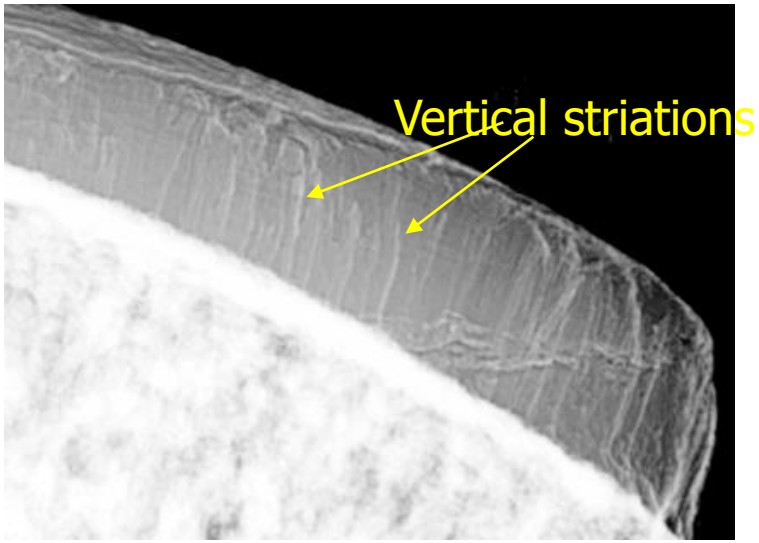

Refraction image

Apparent absorption image

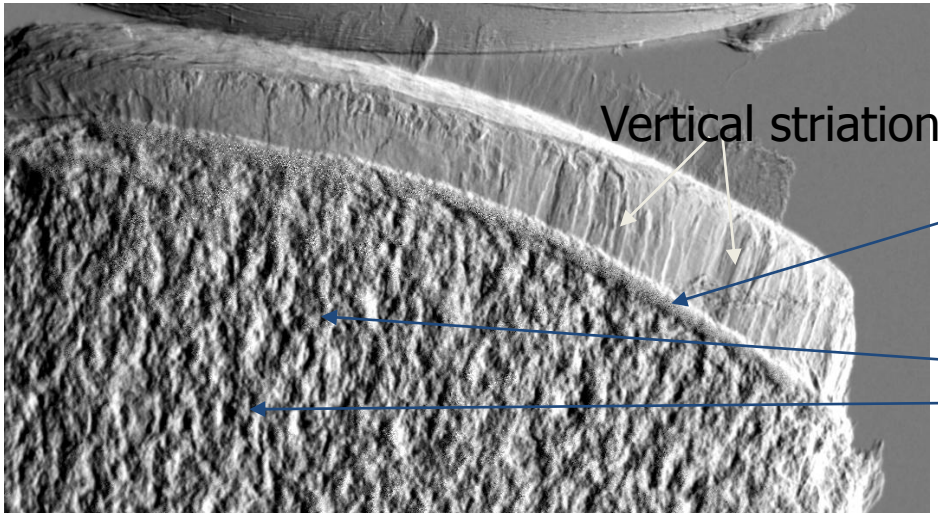

Subchondral bone

Trabecular bone

Elettra
25 keV

Muehleman C, Majumdar S, Issever AS, Arfelli F, Menk RH, Rigon L, Heitner G, Reime B, Metge J, Wagner A, Kuettner KE, Mollenhauer J, Osteoarthritis and Cartilage 12 (2): 97-105 FEB 2004

Femur head core cuts: comparison with MRI

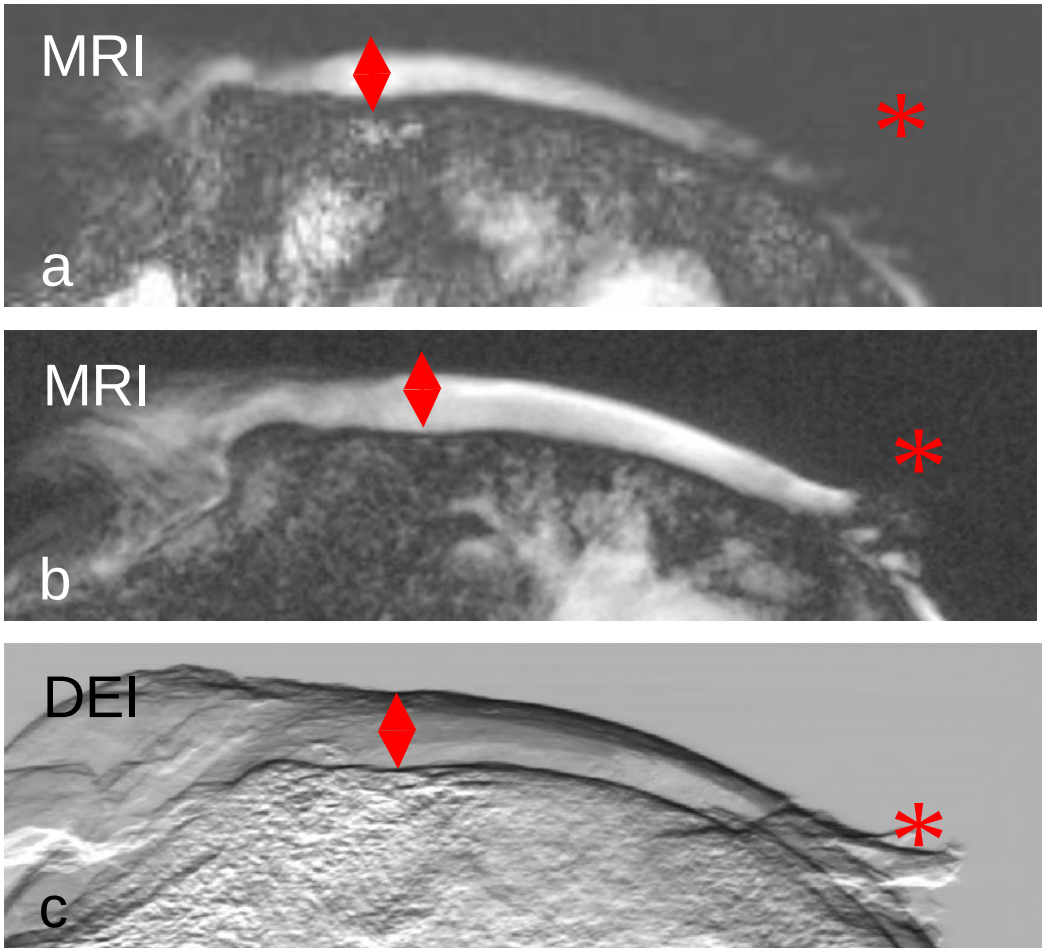

5 sec

150 sec

A Wagner, M Aurich, N Sieber, M Stoessel, WD Wetzel, K Schmuck , M Lohmann, B Reime, J Metge, P Coan, A Bravin, F Arfelli, L Rigon, RH Menk, G Heitner, T Irving, Z Zhong, C Muehleman, J A Mollenhauer sumbitted to NIM A

DEI studies of the finger joint

skin

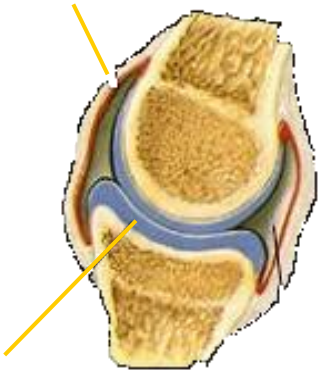

cartilage

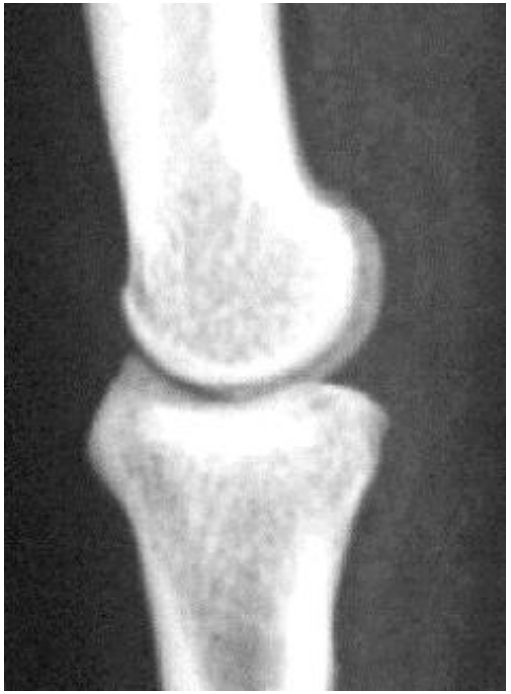

Conventional radiograph

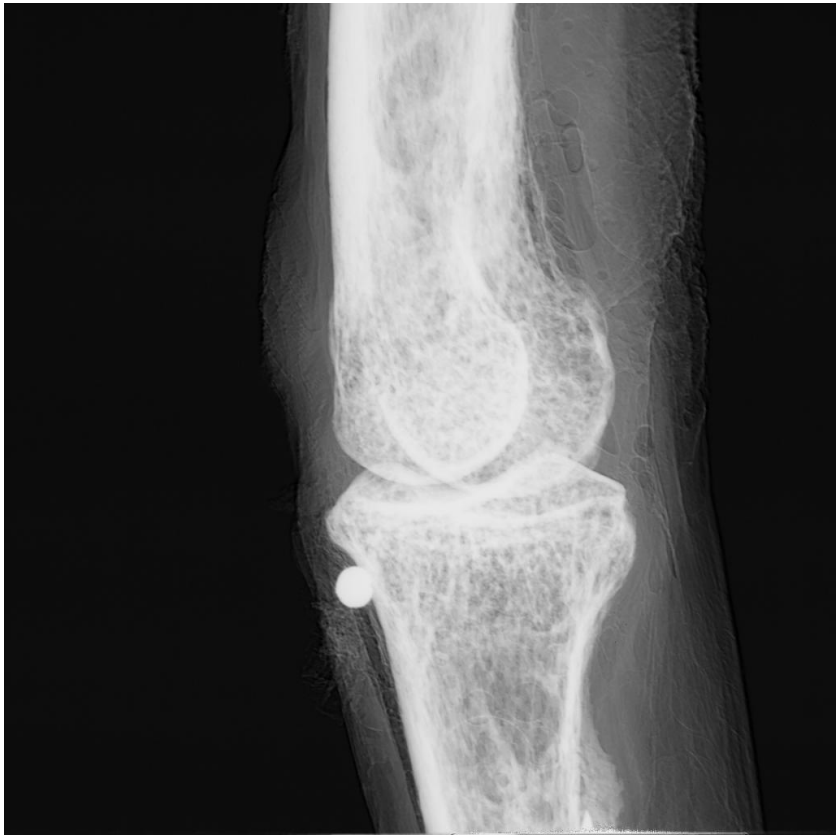

Apparent absorption image @ 20 keV
at ELETTRA

Daresbury, Elettra, University of Trieste Collaboration within PHASY project: R. Lewis et al.

Index finger proximal interphalangeal joint

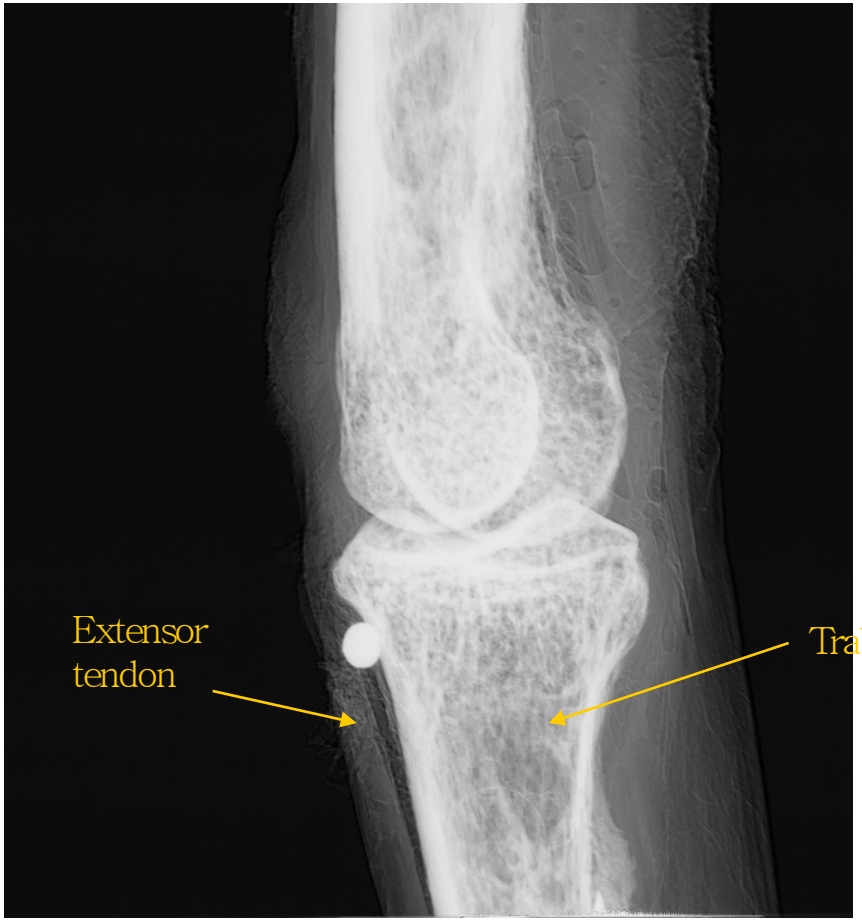

Apparent absorption Image

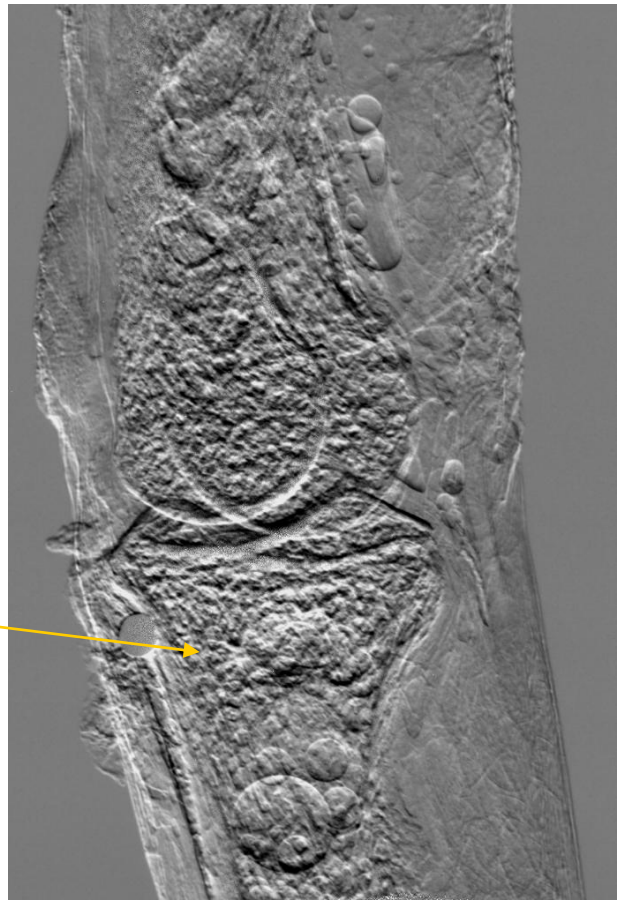

Refraction Image

Index finger proximal interphalangeal joint

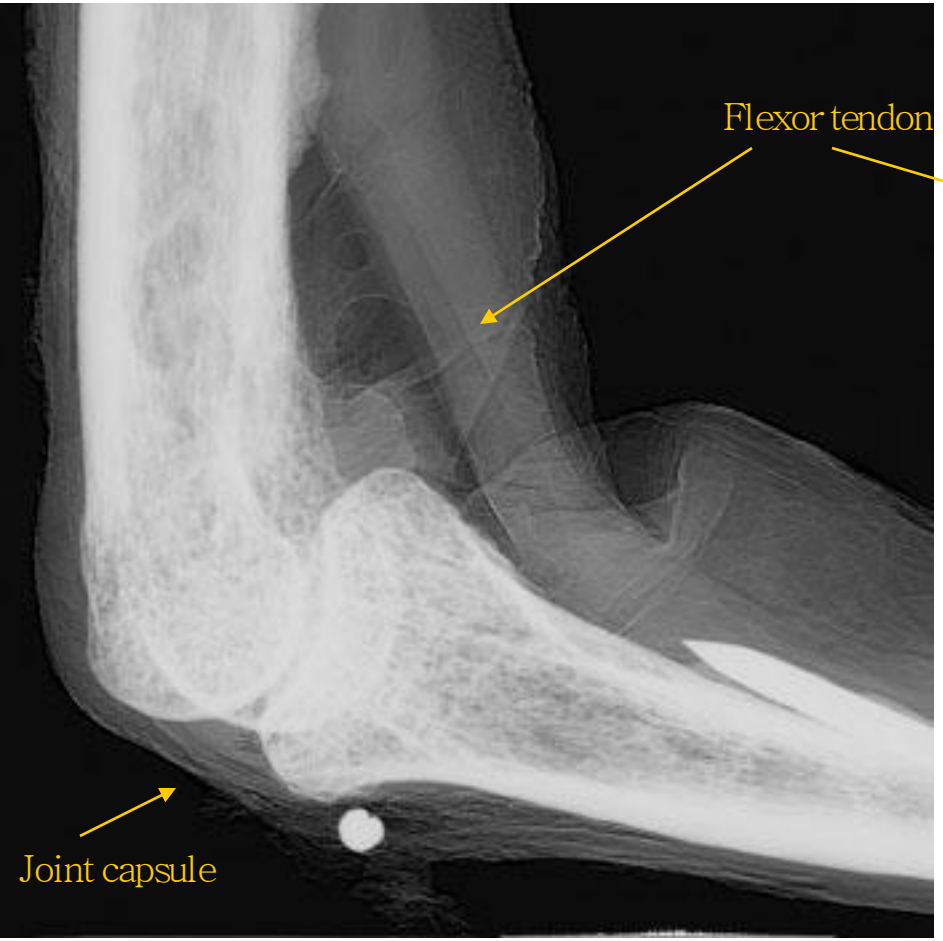

Apparent absorption Image

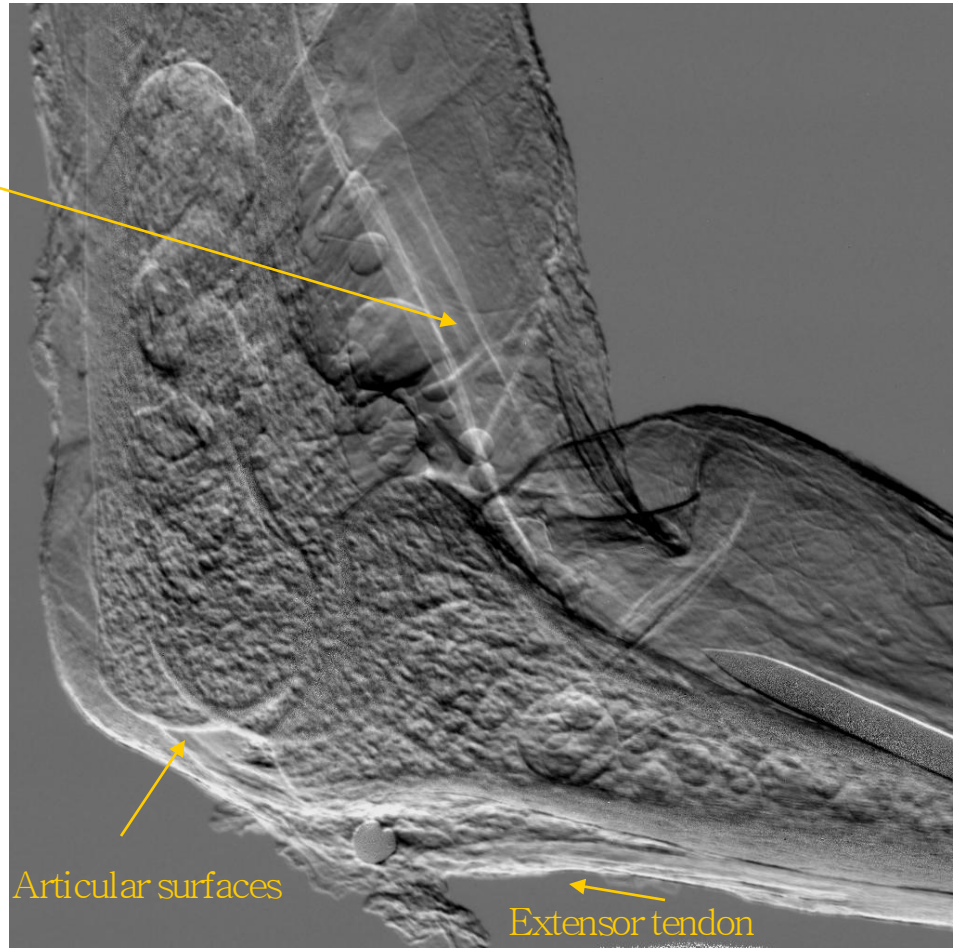

Refraction Image

Lungs imaging I

Techniques: PHC

Modalities: planar for *in-vivo* images on rabbits

Effects of Ventilation on Lung Liquid Clearance at Birth visualized by PHC

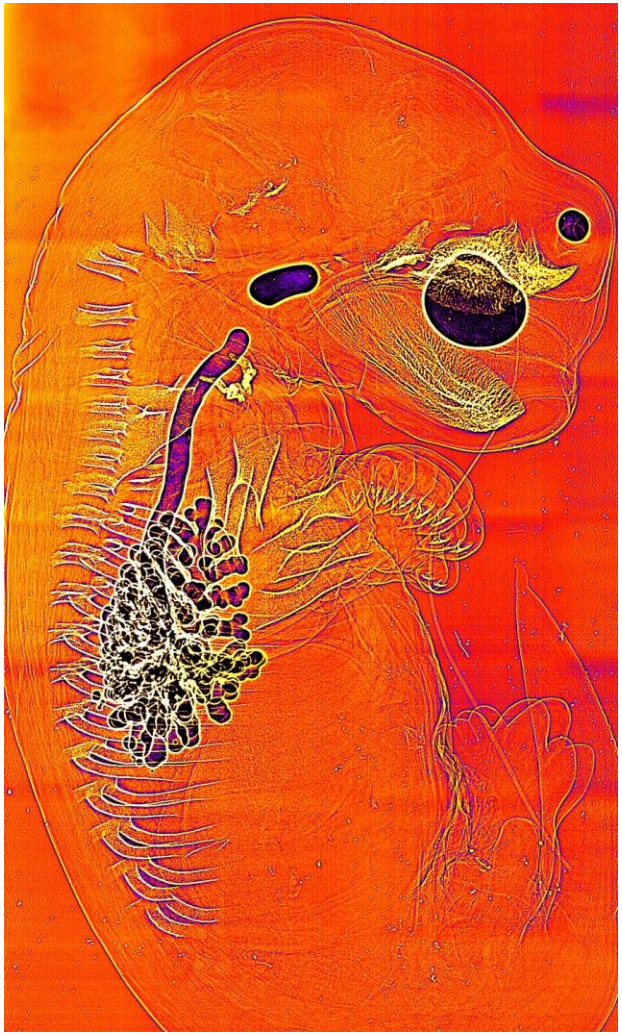

Aeration of the lung and the transition to air-breathing at birth is fundamental to mammalian life.

It initiates major changes in cardiopulmonary physiology.

The dynamics of this process and the factors involved are largely unknown, because it has not been possible to observe or measure lung aeration on a breath-by-breath basis.

Birth: a major physiological challenge

- ✓ Clear the airways of liquid
- ✓ Entry of air generates surface tension
- ✓ Separation of the pulmonary and systemic circulations
- ✓ 10 fold increase in pulmonary blood flow
- ✓ Large increase in blood oxygenation

Courtesy of Marcus Kitchen, School of Physics

Lung Aeration in Preterm infants:

Can suffer from:

- ✓ Airway liquid retention → respiratory insufficiency
- ✓ Non-uniform ventilation → lung injury
- ✓ Delayed/blunted physiological transformation

It has not been possible to observe or measure lung aeration

- Enter Phase Contrast X-ray Imaging!

Imaging lung aeration from birth

- Animal model: rabbit pups
- Imaged pups with PHC at SPring-8, Japan (Beamline 20B2).
  - Either before the first breath (fetus) or at fixed intervals after birth (up to 2h)

Courtesy of Marcus Kitchen, School of Physics

X-ray imaging of the lung

Absorption Contrast

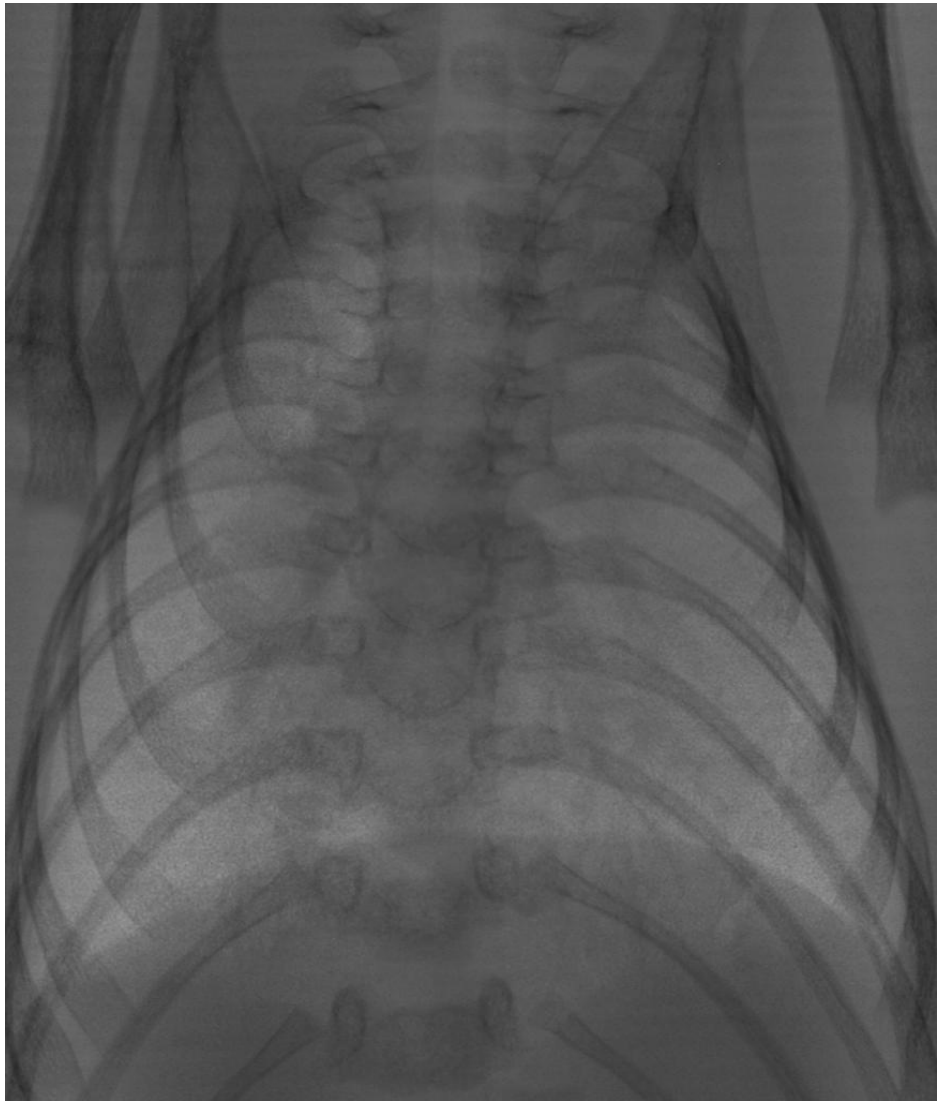

Phase Contrast, 25 keV, z=2 m

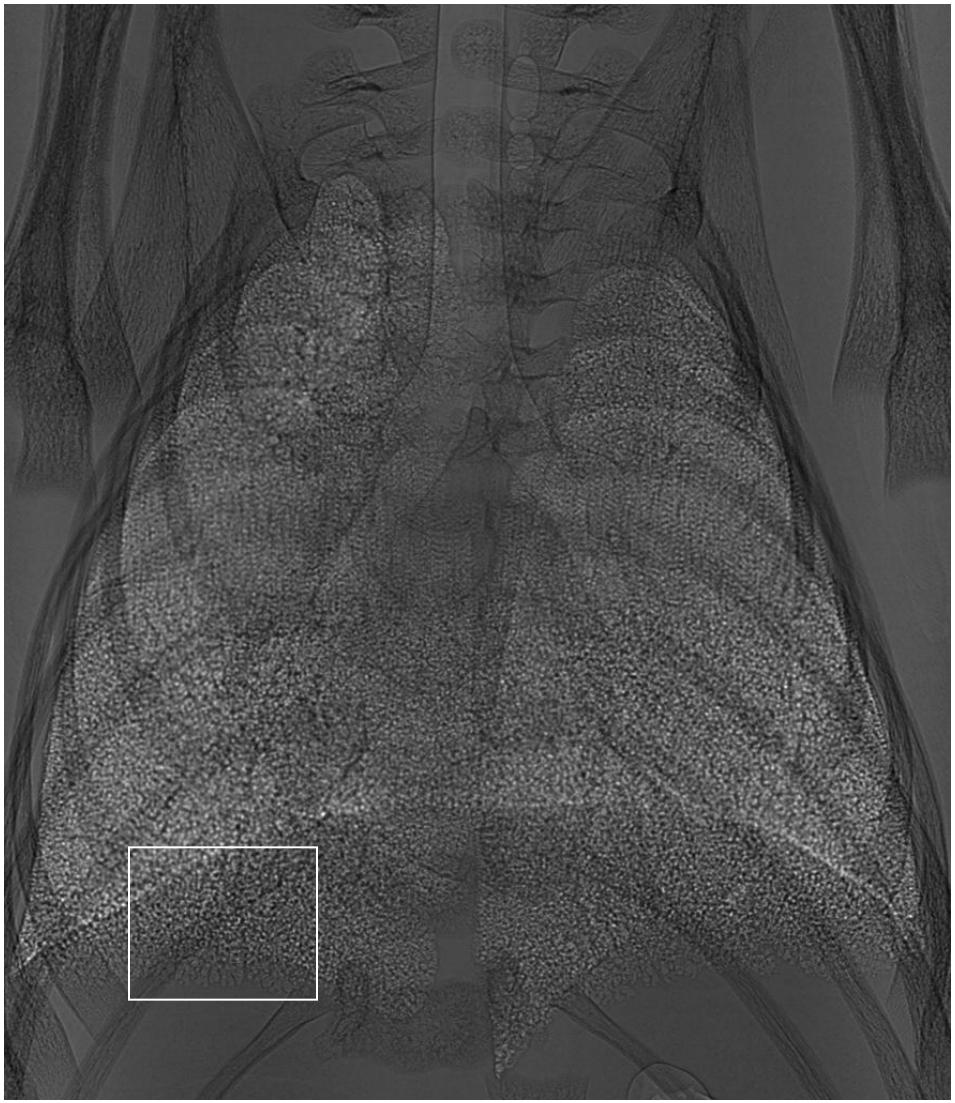

Courtesy of Marcus Kitchen, School of Physics

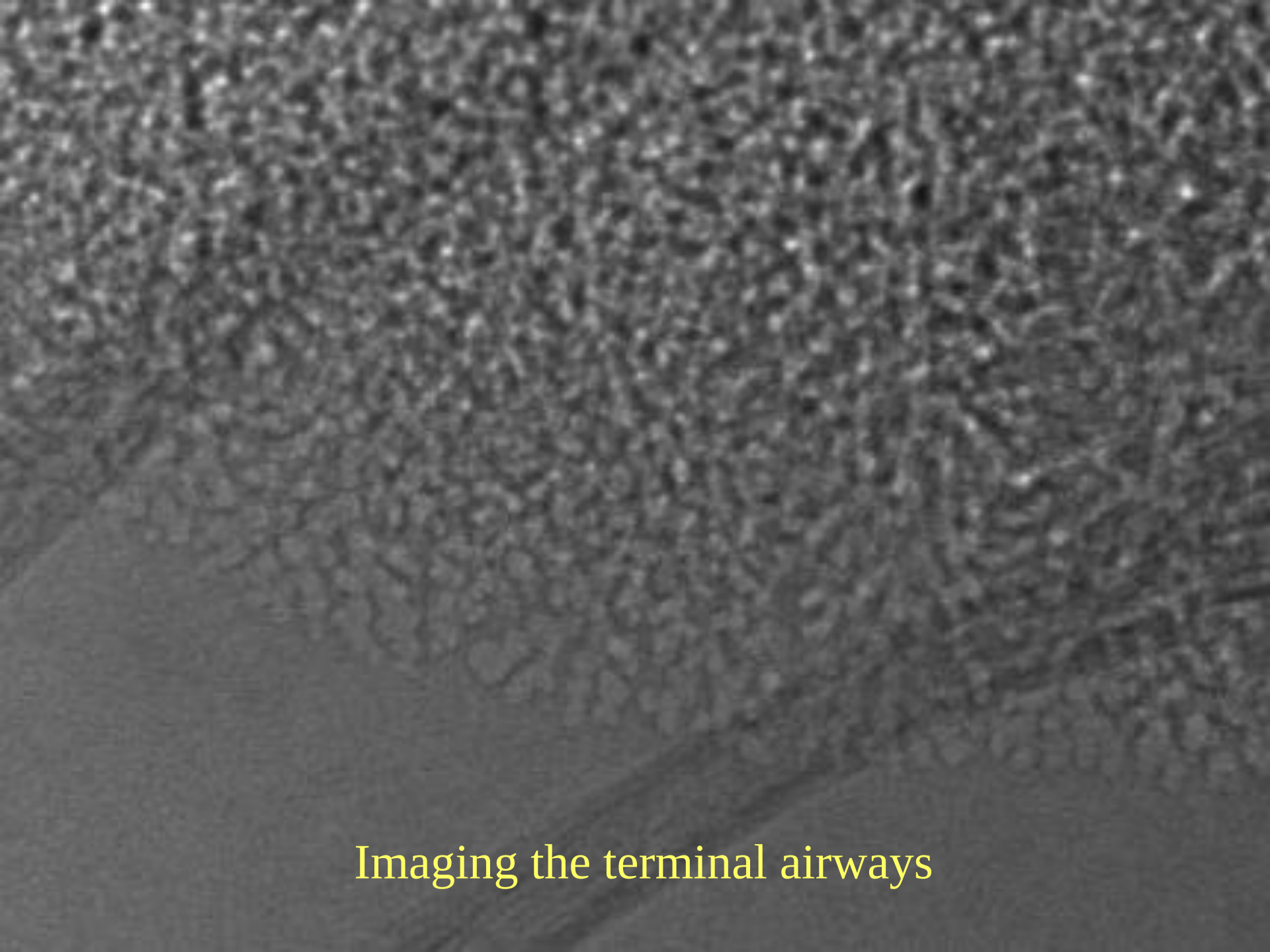
Imaging the terminal airways

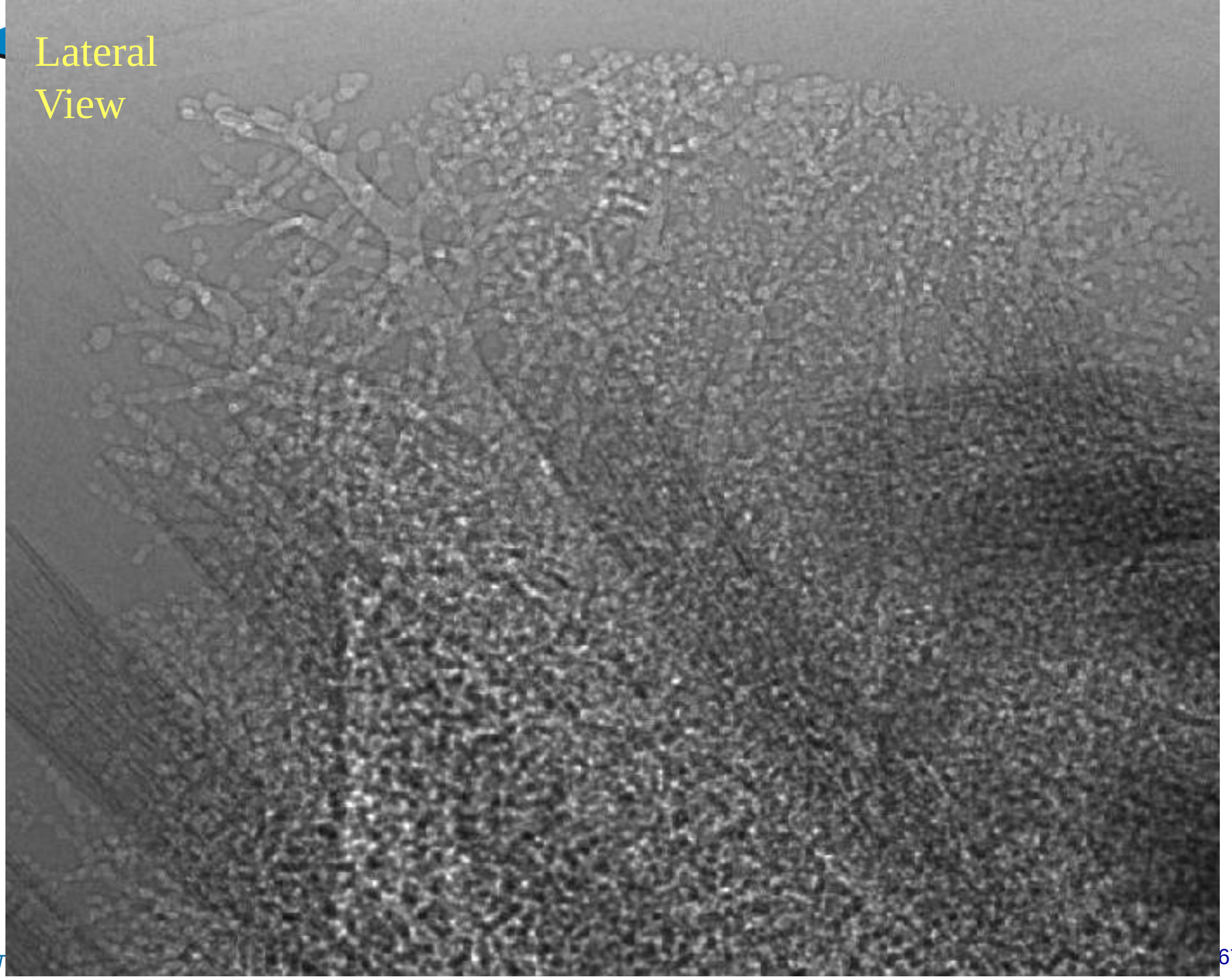
Lateral
View

Elettra Sincrotrone Trieste

MONASH University Science

Exp. time:
80 ms

Interval:
0.8 s

Skin Dose:
~ 0.15 mGy
per frame

Pixel Size:
22.5 μm

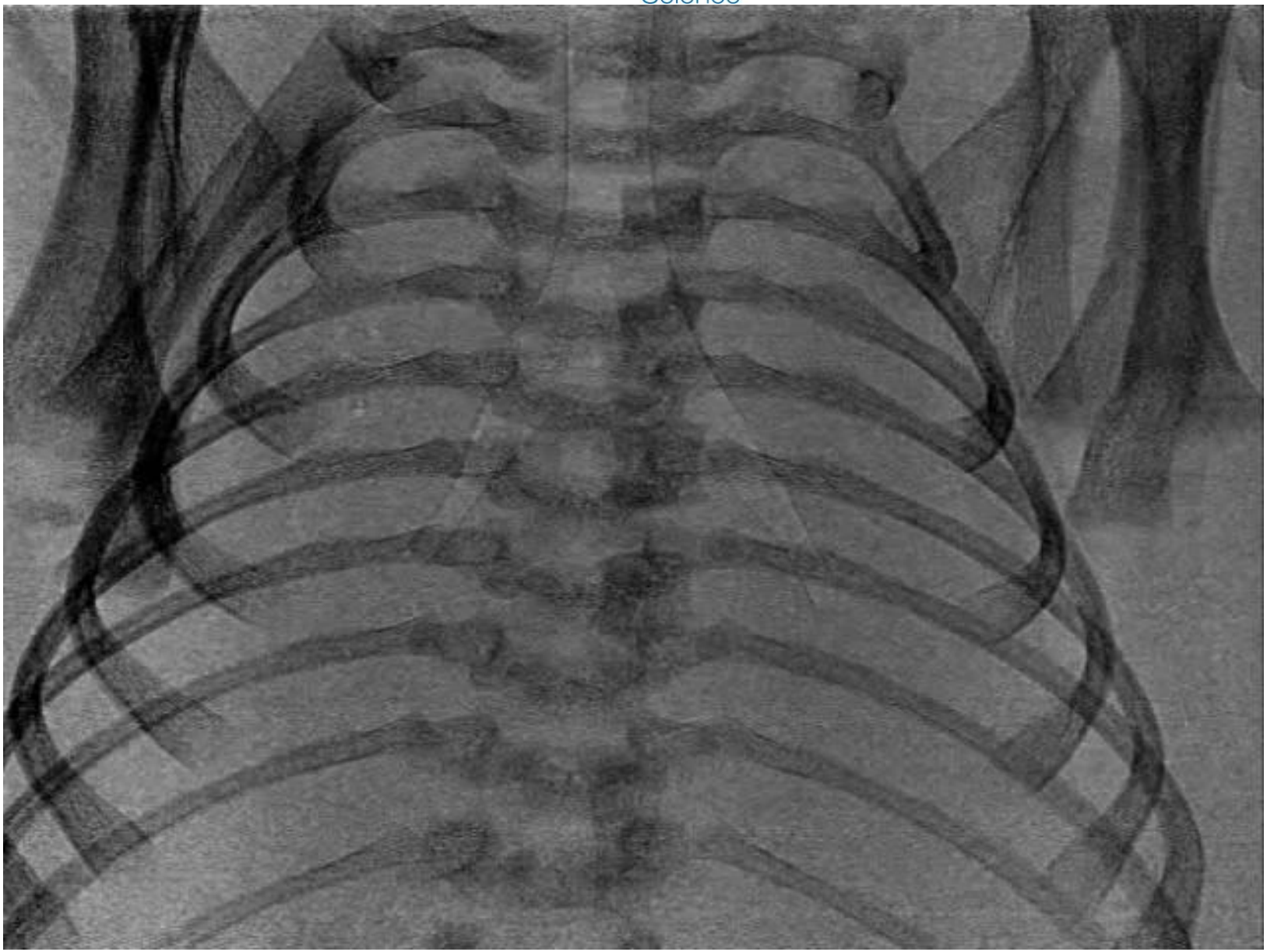

Courtesy of Marcus Kitchen, School of Physics

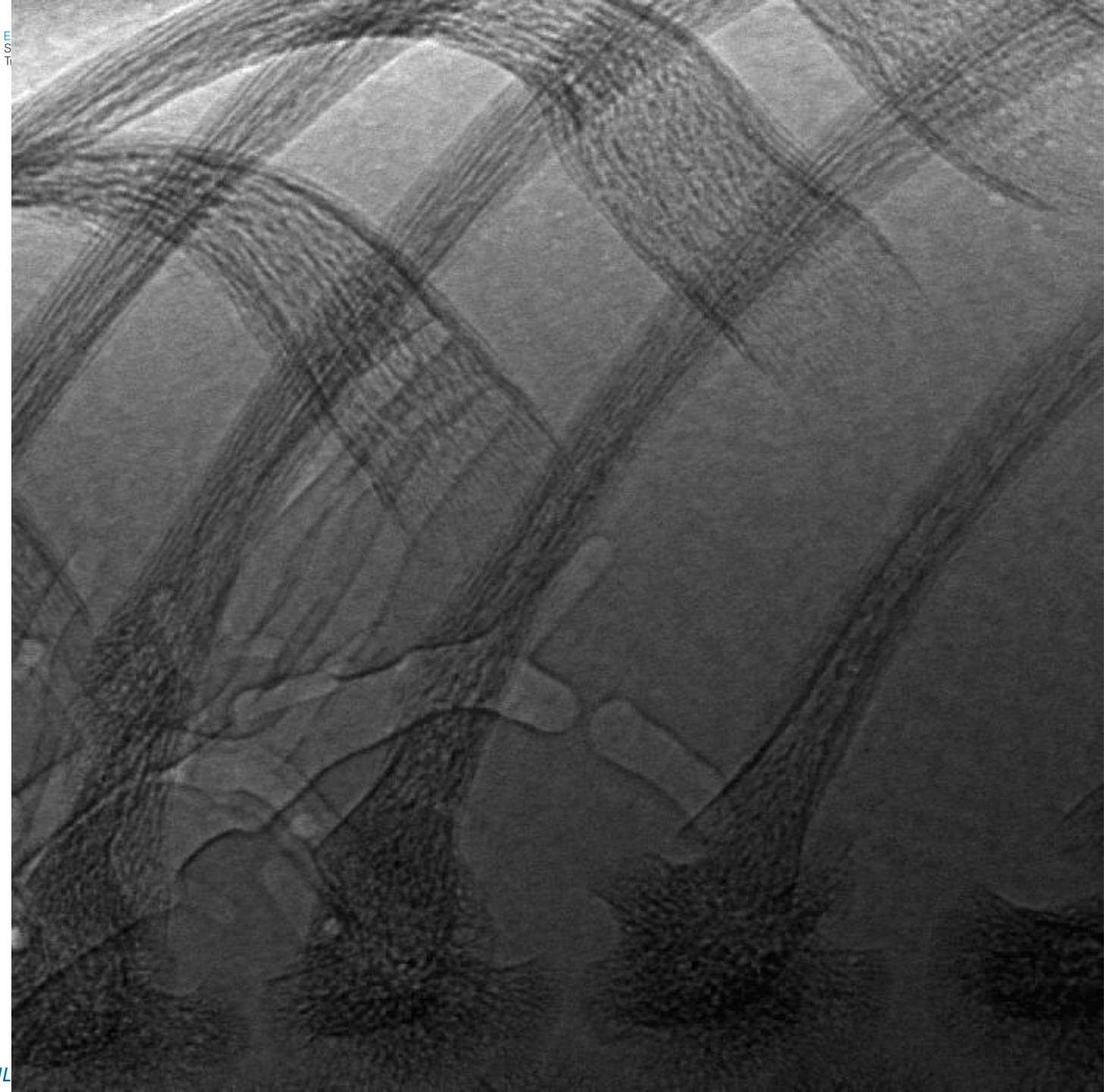

Ongoing research:
Analyzer-Based Imaging: *in vivo studies on mice*

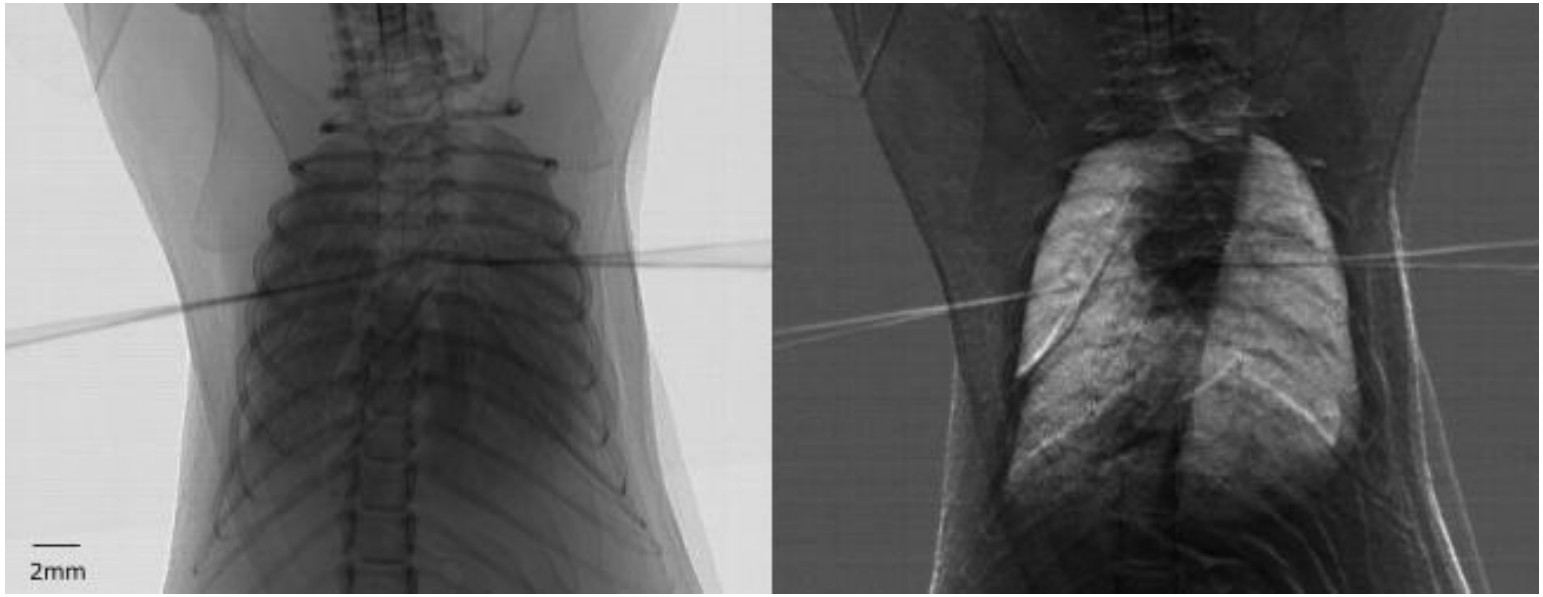

Rejection of refracted radiation (extinction contrast)

Rejection of direct beam (refraction contrast).

Courtesy of S.Bayat

Lungs imaging II

Technique: PHC + contrast agent (Barium)

Modality: micro-CT *ex-vivo* images on mice

Imaging of asthmatic mice – feasibility study

- Animal model of allergic asthma induced by ovalbumin based on balb/c mice developed by CBM in collaboration with the University of Wien.
- Aim: evaluate the potential of SR-based technique for **functional** and **morphologic** imaging of mice lungs
- Available techniques: optical imaging and PHC micro-CT

cbm cluster in biomedicine

UNIVERSITÄTSMEDIZIN GÖTTINGEN UMG

P³AGI Public Private Partnership for Asthma Imaging and Genomics

SEVENTH FRAMEWORK PROGRAMME

MEDIZINISCHE UNIVERSITÄT WIEN

Linköping University

Programme on Scientific and Technological Cooperation between Italy and Sweden financed by Ministero degli Esteri

Imaging protocol: use of macrophages with double staining

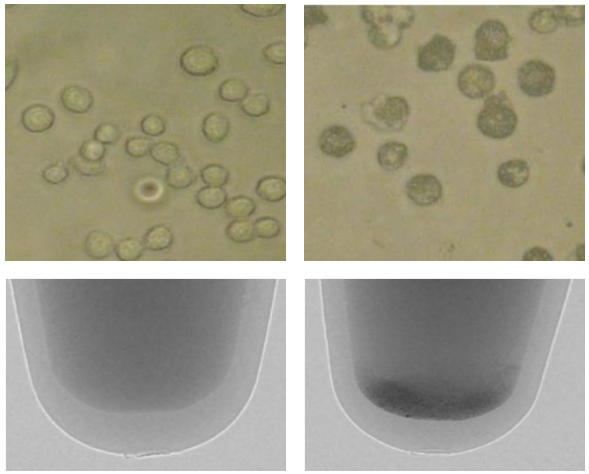

Unlabeled macrophages

Macrophages labeled with Ba

Use of immortalized Murine Alveolar Macrophage Cell line with double staining:
- Barium sulfate (clinical contrast agent Micropaque CT (Guerbet, F))
-DiD fluorescent dye to be used for cells localization inside the lungs using fluorescence microscopy.

Macrophages were adminstered intra tracheally 48 hours after asthma induction

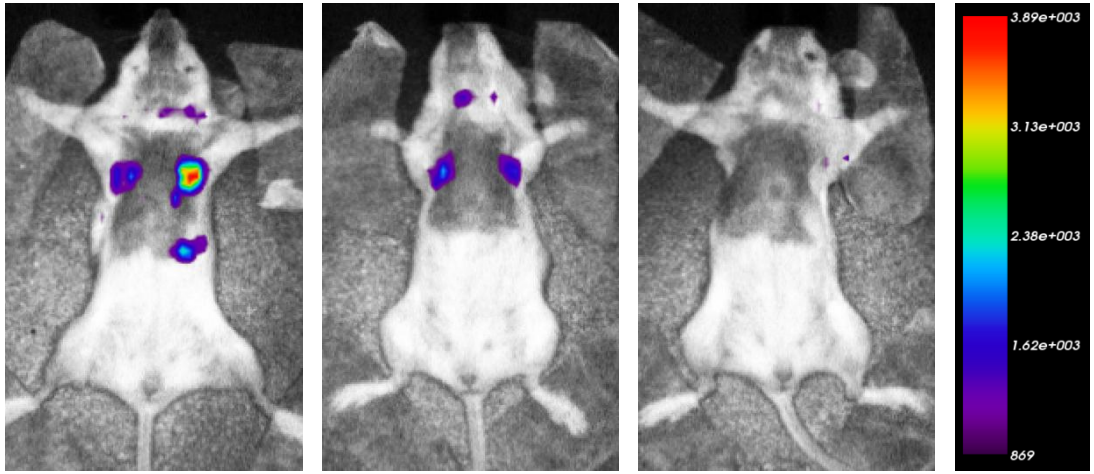

In vivo validation of homing of the macrophages to inflammation sites.
Images performed 24 hours after macrophages administration.

Asthmatic mouse treated with macrophages

Normal mouse treated with macrophages

Native mouse untreated

S.Biffi, C.Dullin et al.

Reconstructed slice - FBP

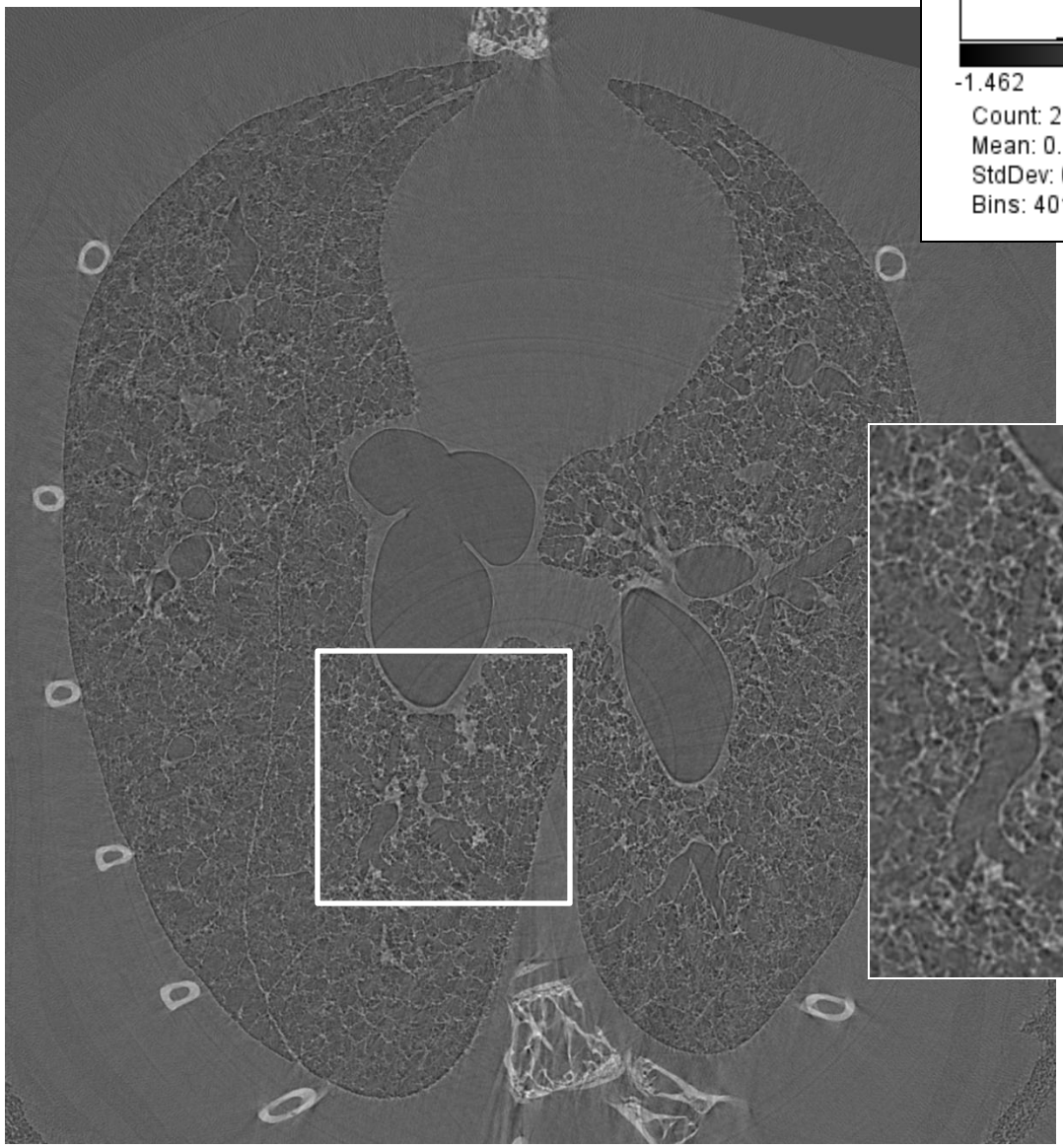

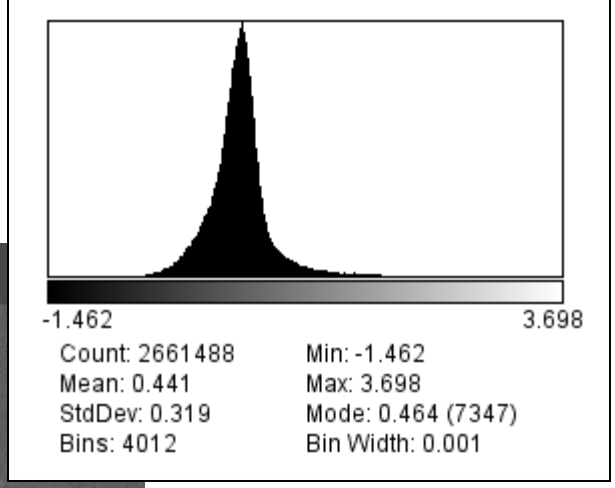

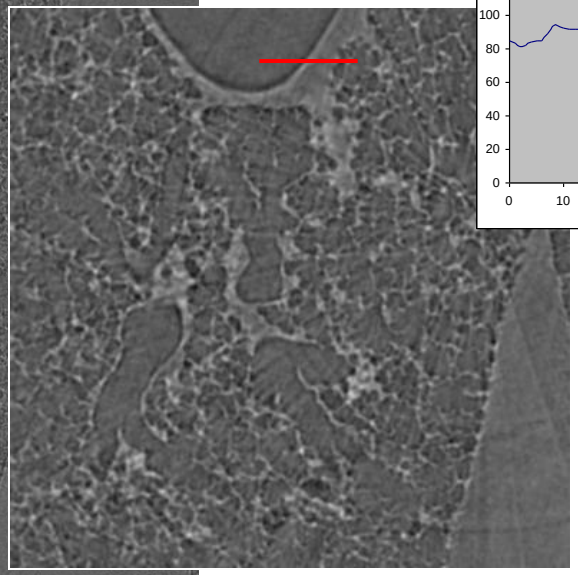

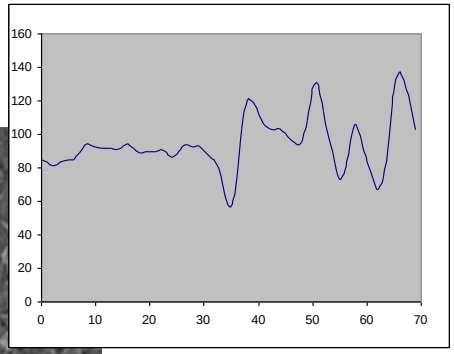

Use of Phase Retrieval for visualizing Barium

Sample: acute asthma mouse treated with macrophages labeled by Ba

E=22 keV
PHC dist=30 cm

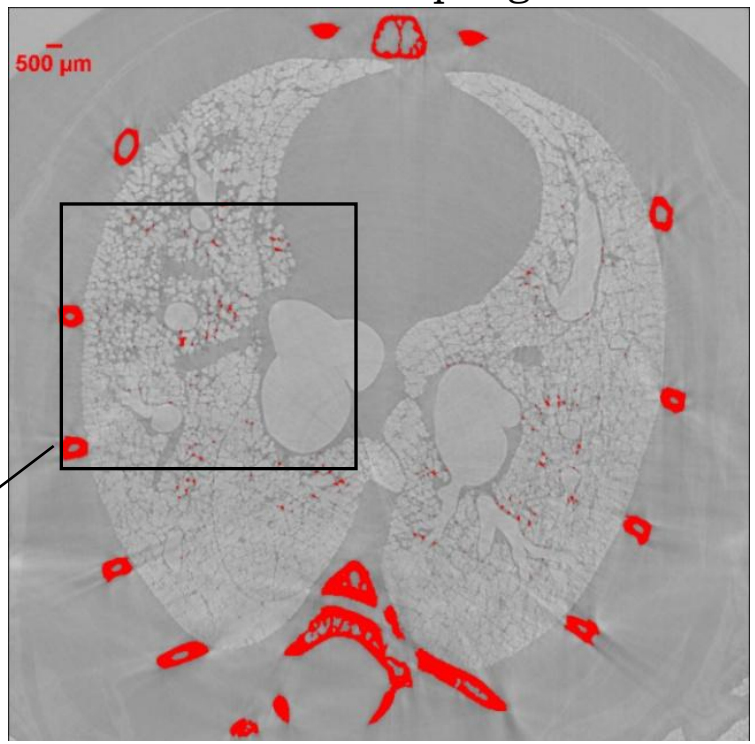

Bones
Barium

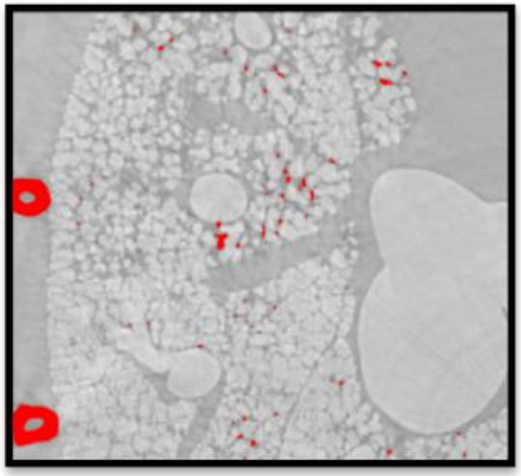

Application of Phase Retrieval for:

- Reducing the artefacts due to PHC effects around the tissue edges
- Reducing the noise
- Enhancing the phases separation

Thresholding results & macrophages visualization

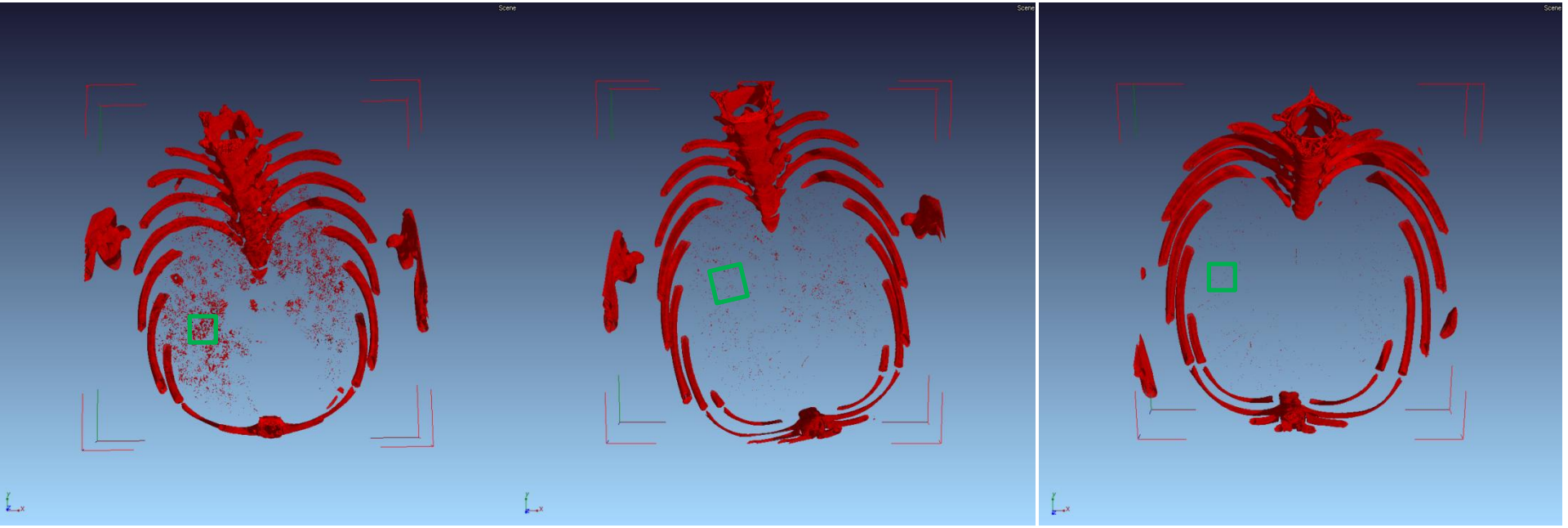

Selection of a Volume of Interest (VOI) for Quantitative analysis

The choice proposed for the visualization threshold of macrophages is adequate for the suppression of the signal due to the lung tissue. Quantitative analysis can be performed

VOI of soft lung tissue

Soft Tissue (green), Macrophages with barium (red), Medial axis/skeleton (blue)

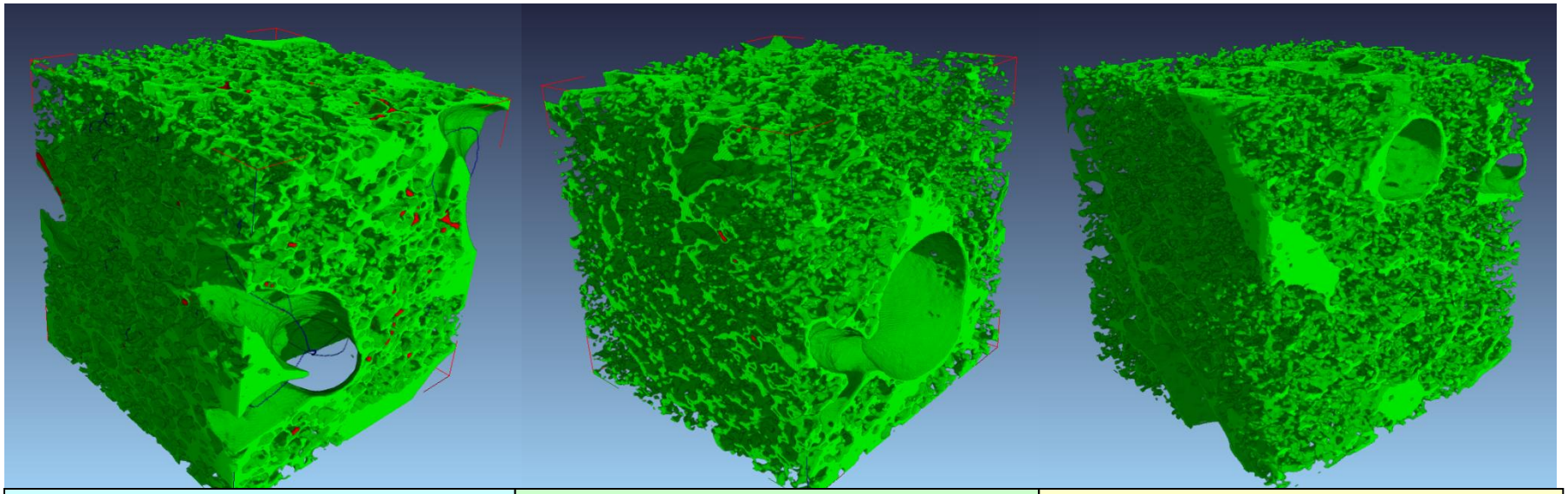

a) asthmatic mouse treated with macrophages labeled by Barium	b) healthy mouse treated with macrophages labeled by Barium	c) control: healthy mouse untreated (no Barium)

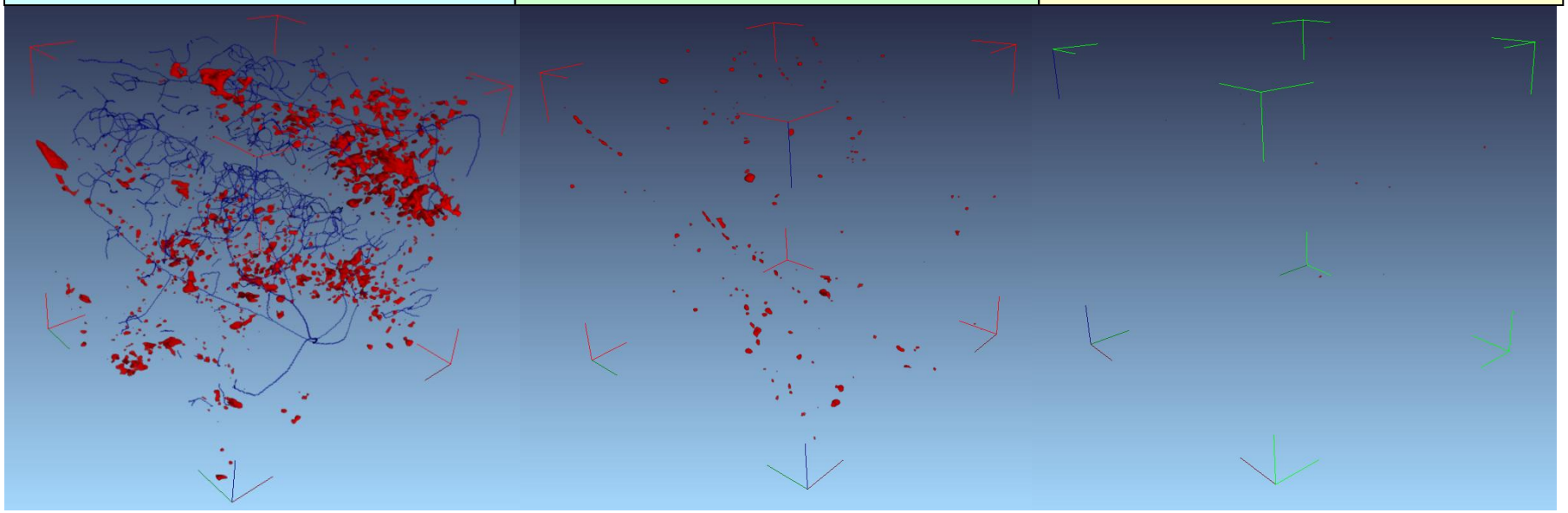

Brain studies

Technique:	FPI + contrast agent (Au nano particles)
Purpose:	tracking tumor development
Modality:	micro-CT *ex-vivo* imaging on mice
	(recent development: first *in-vivo* experiment)

Technique:	GI
Purpose:	animal model of Alzheimer disease
Modality:	micro-CT *in vitro* imaging of mice brains

Cell tracking studies for imaging of brain tumors in rats

Glioblastoma multiforme (GBM) is the most common and most aggressive primary brain tumor in humans.

An animal model based on Wistar rats have been developed to study the behavior of the tumor and to monitor the effects of therapies.

Requirements for the cell tracking technique:

- to monitor the dynamic of tumour growth
- to follow the migration of tumour cells
- to understand the dynamic of metastasis spread

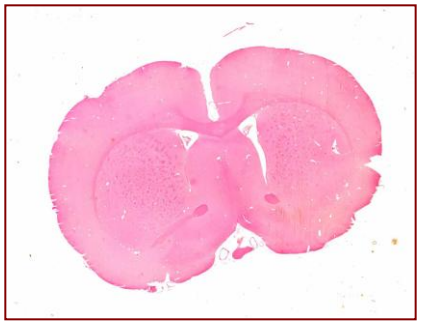

Section of healthy rat brain

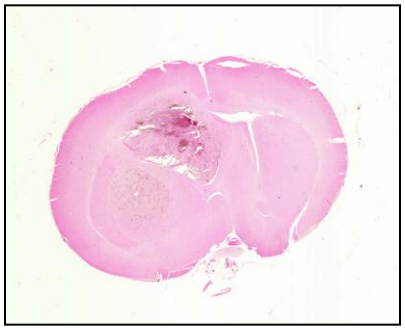

Section of rat brain with C6 glioma 2 weeks after implantation

C6 glioma cells were cultured and some of the cultures were exposed to colloidal Gold Nano Particles (GNP) for 22 hrs before harvest.

C6 glioma cells were implanted into the brain of adult male Wistar rats. The implantation was performed with the animals under general anesthesia. The animals were allowed to recover after the end of the implantation and were sacrificed two weeks later.

The detection of labeled cells is enhanced by the higher absorption of gold with respect to tissue and by PHC effects.

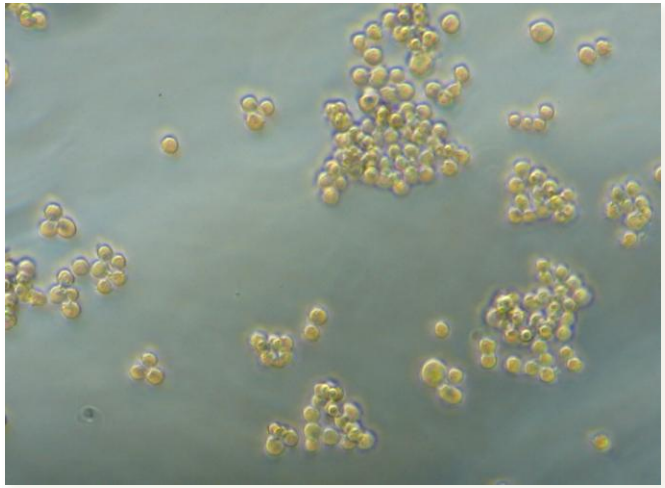

Gold Nano particles (GNP)

Our biological approach: Label tumor cells with sufficient Au nano particles (Ø ~ 50 nm)

Inert GNP bond to serum proteins

GNP are taken up by phagocytosis stored in lysosomes and are not released by exocytosis

Courtesy of E. Schultke, R.H.Menk et al.

Elettra Sincrotrone Trieste

A 1 and A 2: Tumor without colloidal gold

3D rendering of a 4 mm thick volume

E = 24 keV
Num. proj. = 720
Pixel size =14μm

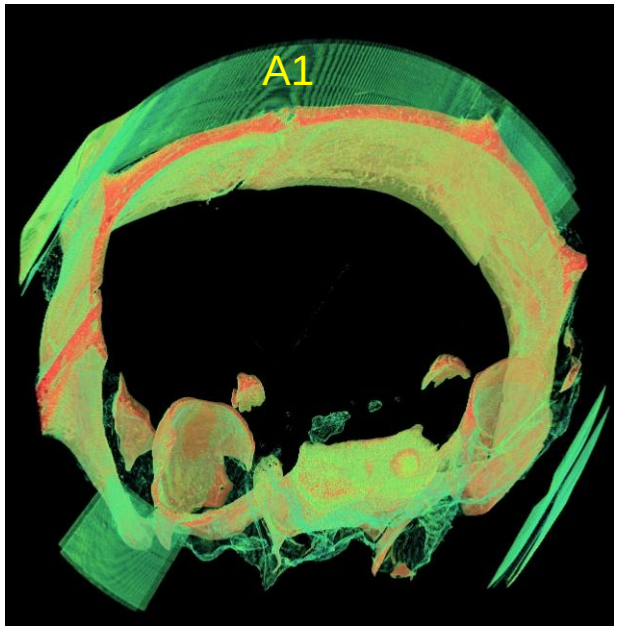

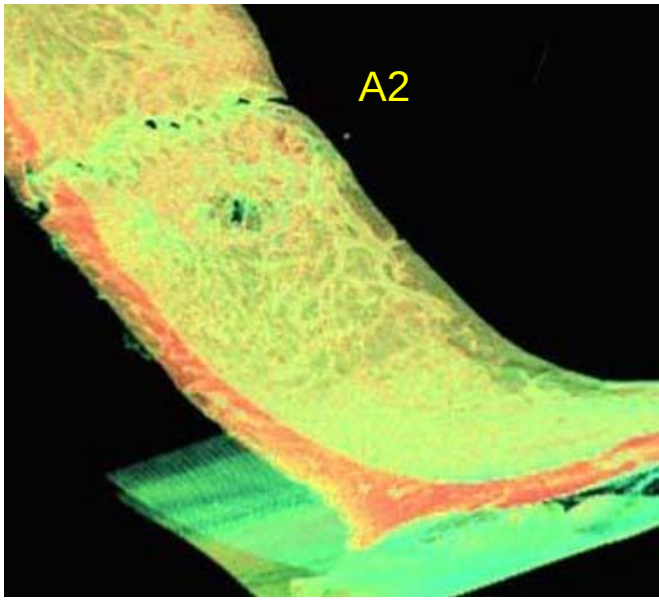

B 1 and B 2: Tumor with 300,000 colloidal gold-loaded cells

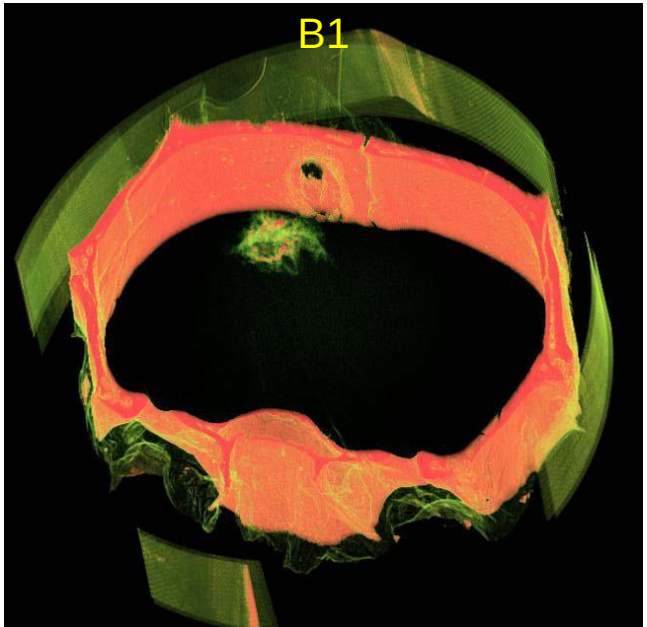

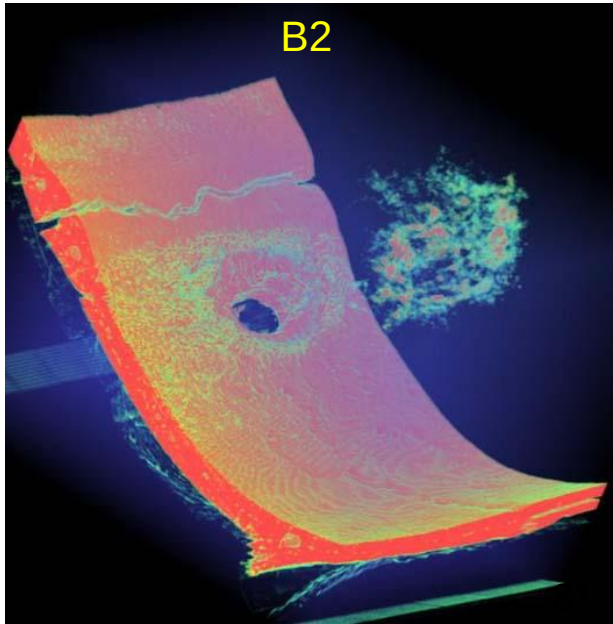

Courtesy of E. Schultke, R.H.Menk et al.

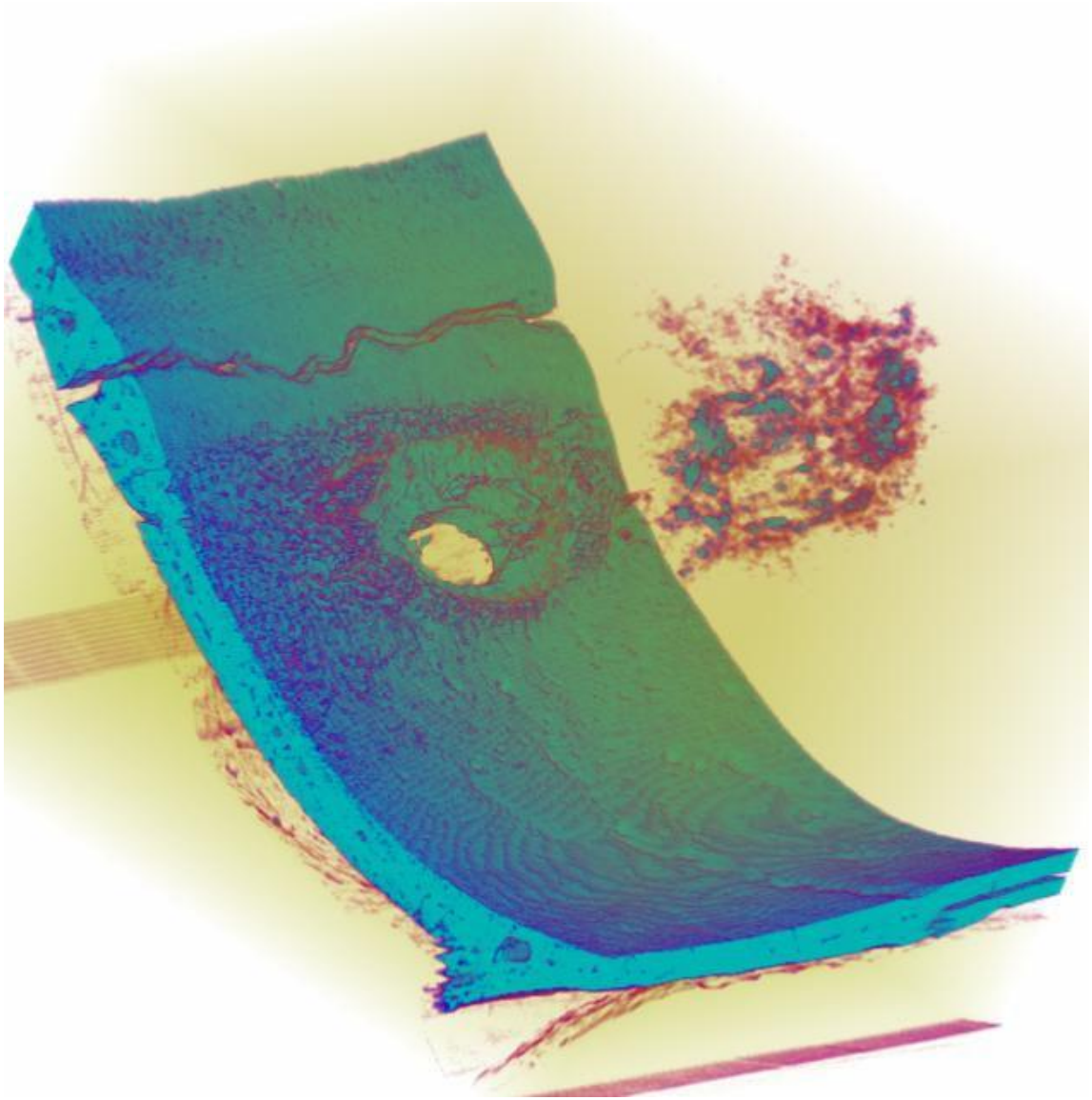

Rat 7, 100000 gold loaded C6 cells, 14 days incubation

Rat 706: Metastasis spread in the spine

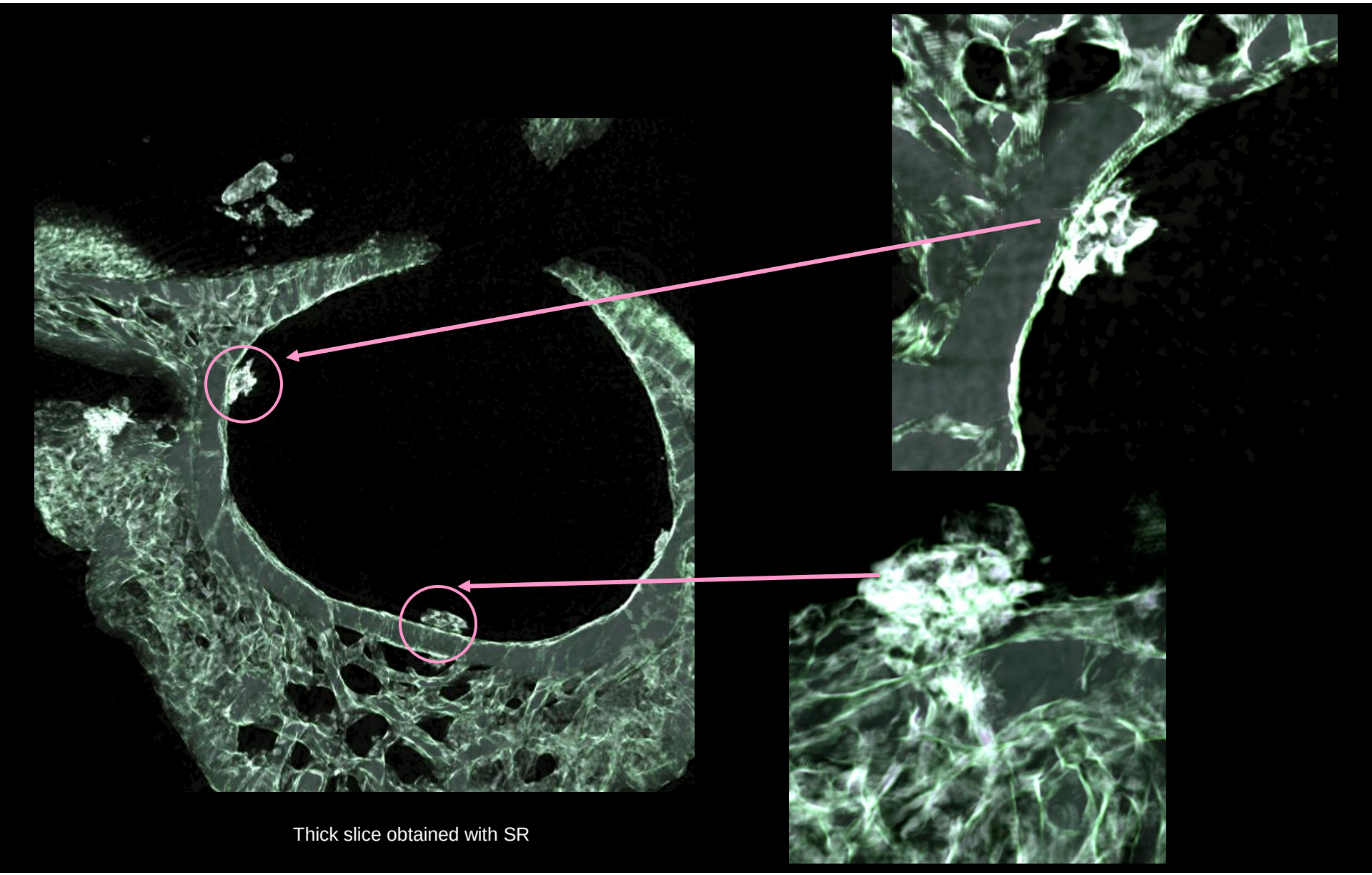

Courtesy of E. Stuultke, R.H.Menk et al.

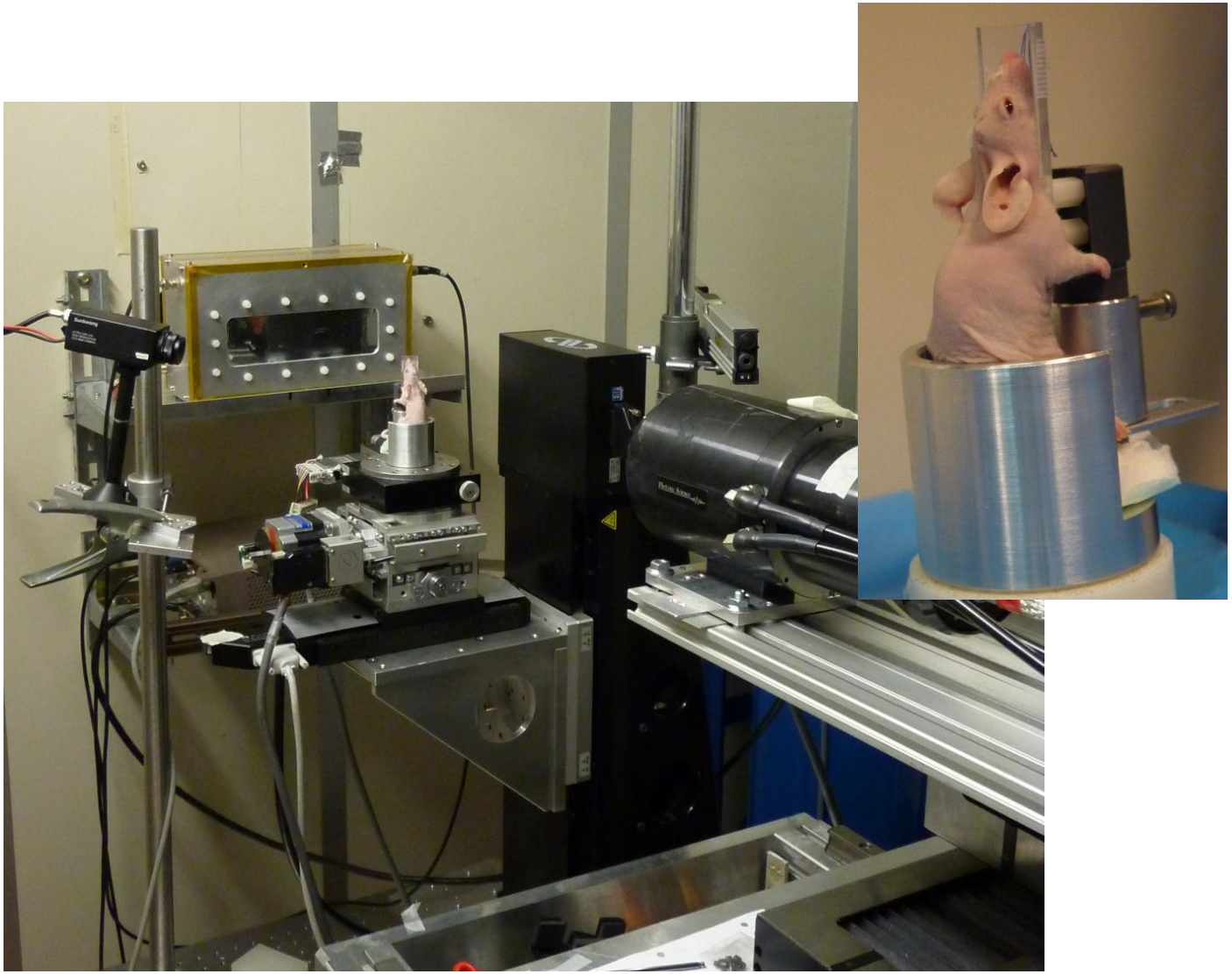

First experiment *in vivo* performed in Nov. 2010: lesions are visible also a low doses

Courtesy of A.Astolfo

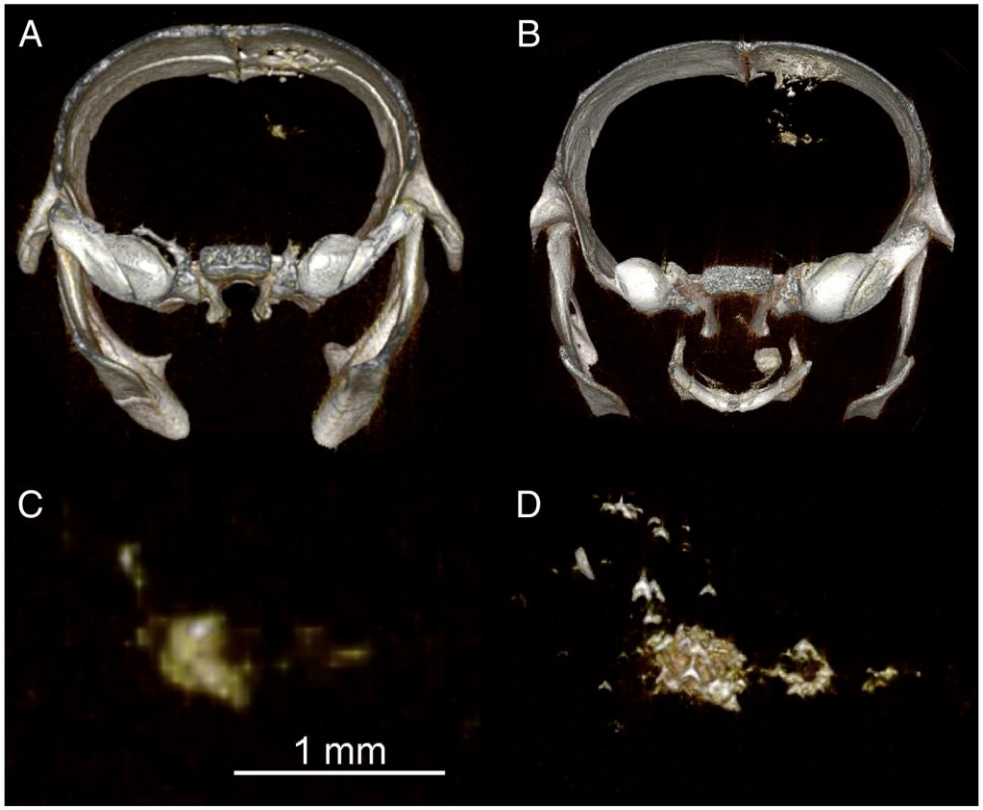

- ✓ Comparison of two 3D renderings of a CT of a mouse injected with 100,000 GNP-loaded F98 cells depicts (A–C) the low x-ray dose in vivo data and (B–D) the high x-ray dose ex vivo data. The images in panels C and D are enlargements at full system resolution of the developed tumor depicted in panels A and B, respectively.

A. Astolfo et al., Nanomedicine: Nanotechnology, Biology and Medicine, Vol. 9, Issue,2013

Alzheimer's disease

- ✓ One of the core pathological features of Alzheimer's disease (AD) is the **accumulation of amyloid plaques** in the brain. Current efforts of medical imaging research aim at visualizing amyloid plaques in living patients to evaluate the progression of the pathology, but also to facilitate the diagnosis of AD.
- ✓ GI has the capability to image amyloid plaques in the brain of a transgenic mouse model of AD. The method provides high contrast and high resolution images. Quantitative analysis can also be performed.
- ✓ GI may facilitate the development of other imaging methods such as positron emission tomography (PET) by providing convenient high-resolution 3D data of the plaque distribution for multimodal comparison.
- ✓ The study was conducted on a model of AD mouse

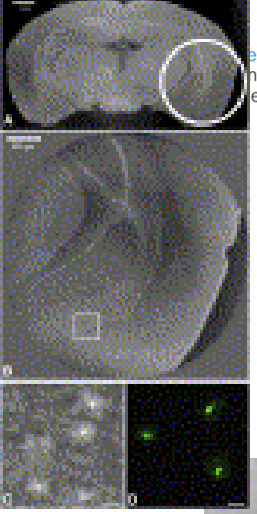

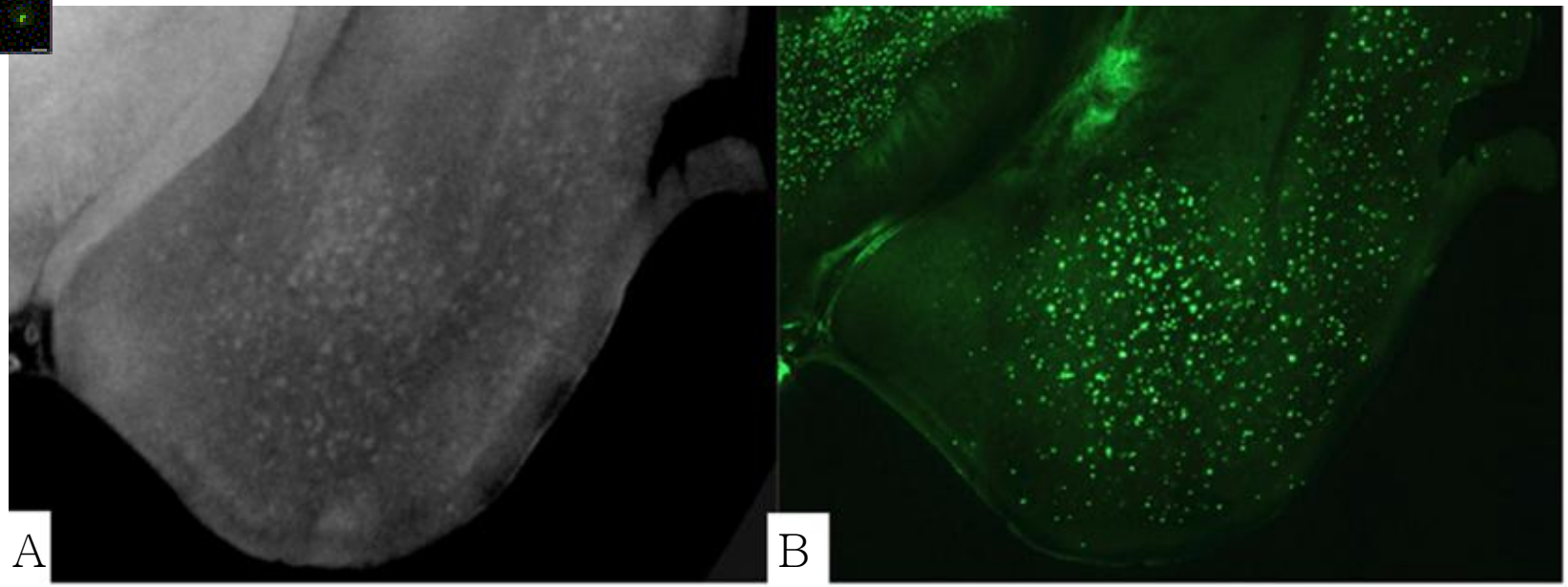

(A) - Magnified unfiltered GI tomograms of a AD transgenic mouse brain at 13 months. The brain was extracted, fixed in paraformaldehyde and scanned by GI based tomography (isotropic voxel size of 7.4 μm). **(B)** - The brain was next sliced at 400 μm and stained with Thioflavin S to reveal amyloid deposits

Pinzer et al ., Neuroimage ***61*** *1336–46, 2012*

Atherosclerotic plaque imaging

Technique: GI

Modality: micro-CT *in-vitro* imaging of mice aortas

Atherosclerotic plaque imaging using GI

- Reliable, noninvasive imaging modalities to characterize plaque components are clinically desirable for detecting **unstable coronary atherosclerotic (ATH) plaques**, which cause acute coronary syndrome.
- Although recent clinical developments in CT have enabled the visualization of luminal narrowing and calcified plaques in coronary arteries, the identification of **noncalcified plaque components** remains difficult.
- Clinical evidence suggests that ATH plaque components are important predictors of plaque stability and clinical events. The risk of plaque rupture appears to depend on the plaque components rather than the severity of stenosis.
- The study was conducted on a model of Apolipoprotein E -deficient [knockout] mice (ApoE-KO mice) developing ATH in a short time. They were fed with a normal diet or a high cholesterol diet.
- GI based micro-CT studies were conducted on excised aorta samples.

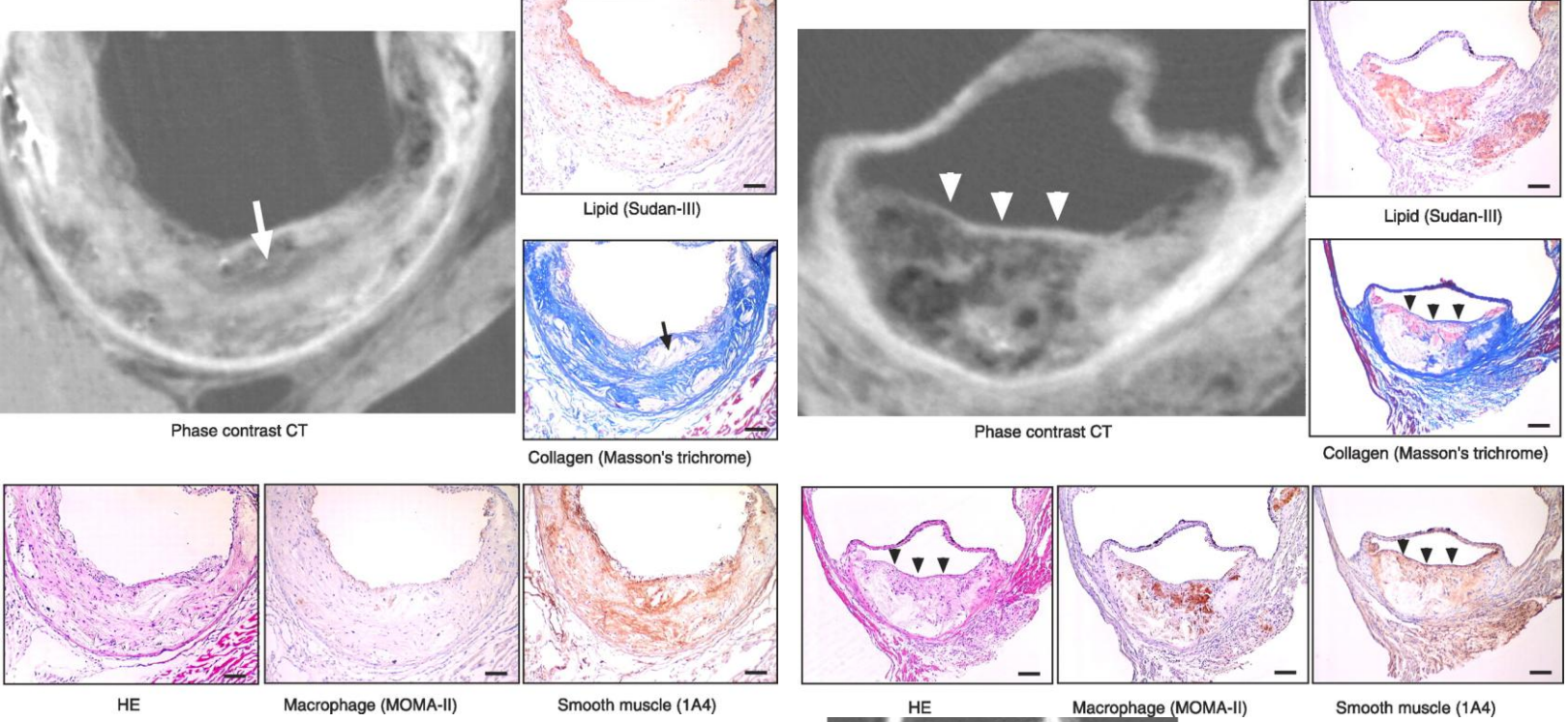

ATH lesion in the aortic sinus of a ApoE-KO mouse, **12 wk of age**, **fed with a high-cholesterol diet for 8 wk.**

ATH lesion in the aortic sinus of ApoE-KO mouse, **36 wk of age**, **fed with a normal diet.**

Scale bar = 100 µm

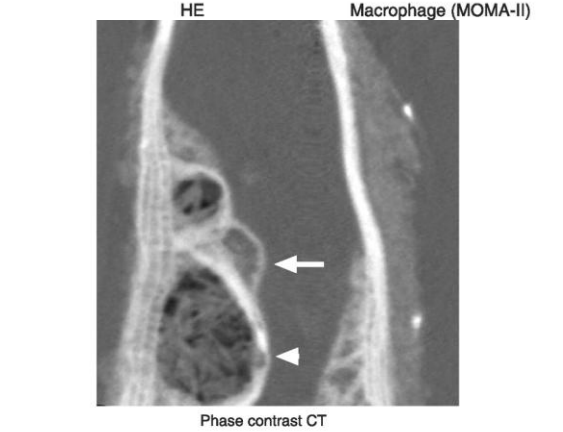

ATH lesion in the right common carotid artery of a ApoE-KO mouse, **12 wk of age, fed with a high-cholesterol diet for 8 wk.**

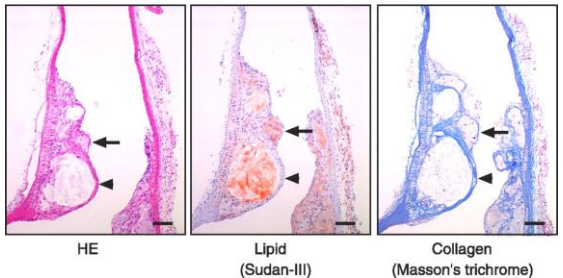

Shinohara M et al. Am J Physiol Heart Circ Physiol;294:, 2008

Elettra Sincrotrone Trieste

- The different plaques components have been recognized in the GI CT studies as it was demonstrated in the comparison with histological data.
- Quantitative measurements of refraction indexes have been provided.

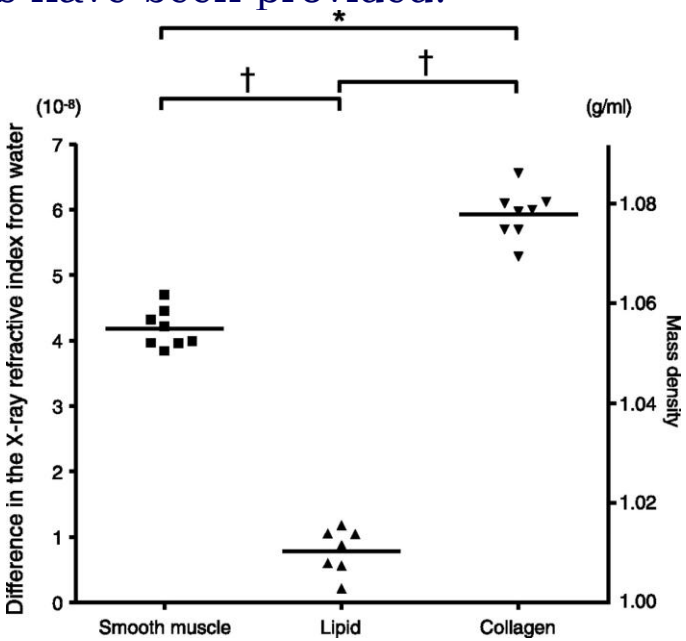

Mean dδ values and specific mass densities of the various components of plaques. The lipid area shows a low dδ ($0.79 \pm 0.13 \times 10^{-8}$) and mass density ($1.011 \pm 0.001766$ g/ml). The smooth muscle and collagen areas show high dδ (4.18 ± 0.10 and $5.93 \pm 0.13 \times 10^{-8}$, respectively) and mass density (1.057 ± 0.001407 and 1.08 ± 0.001794 g/ml, respectively). *$*P < .05$; †$P < .01$.*

Shinohara M et al. Am J Physiol Heart Circ Physiol;294:, 2008

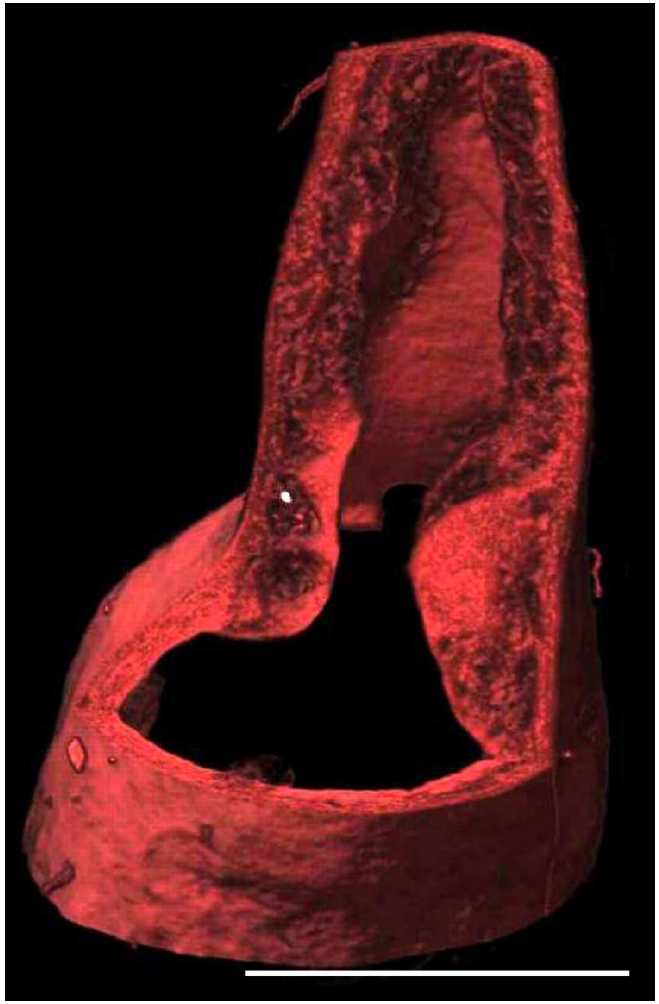

3D rendering of the right common carotid artery of the ApoE-KO mouse fed a high-cholesterol diet.

Scale bar = 1 mm.

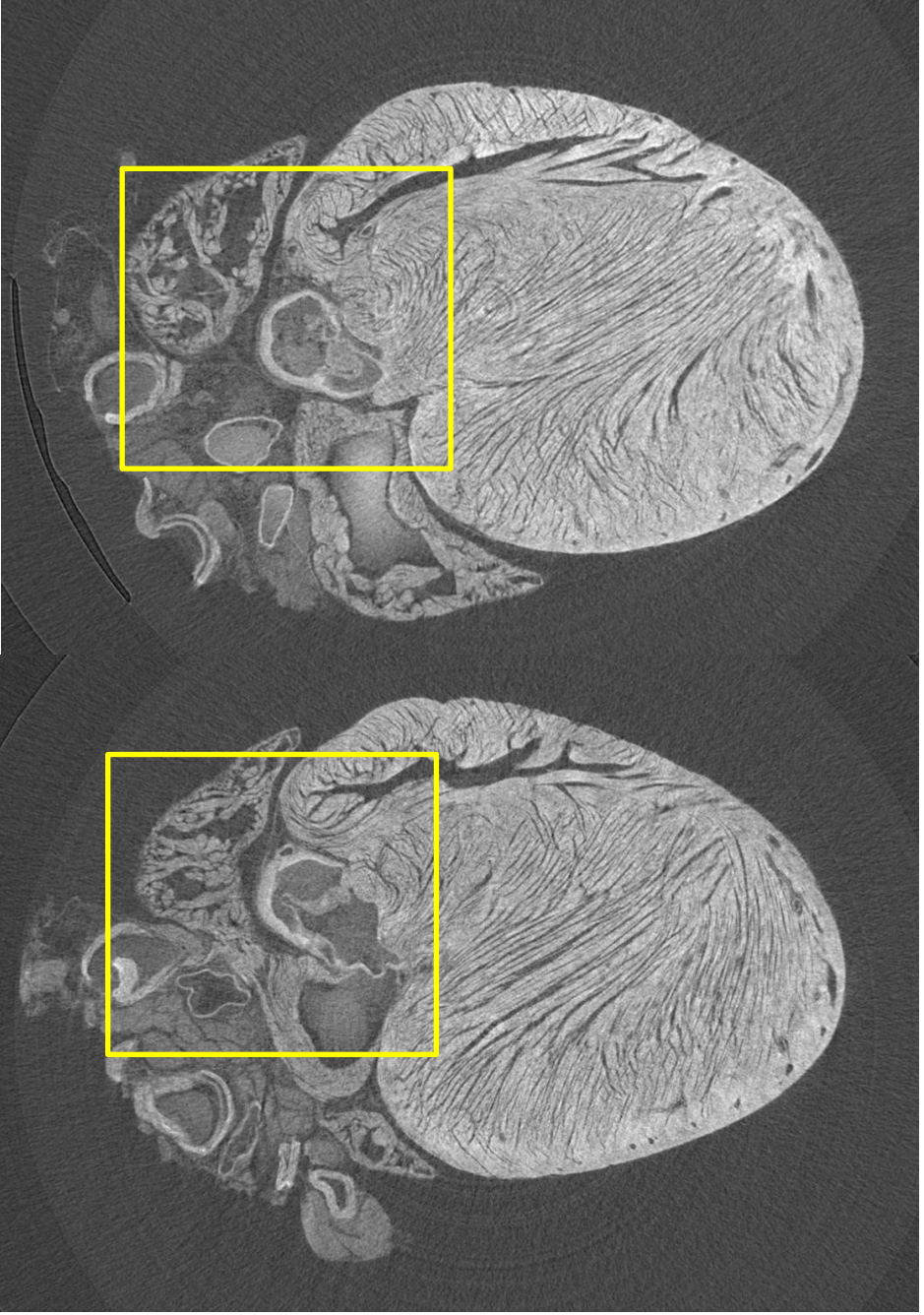

Imaging of atherosclerotic plaques

Animal model: atherosclerotic mouse
Apolipoprotein E-deficient (apoE−/−) mouse

Deficient transgenic mice demonstrates a strong tendency to develop hyper-cholesterolemia

Aim: evaluate the capability of μ–CT to highlight the formation of atherosclerotic plaques in normal and Apo mice
All mice were fed with a high fat diet for 70 days
Imaging procedures:
E = 27 keV, PHC dist = 30 cm
Staining procedure based on PTA (Phosphotungstic acid)

UNIVERSITÄTSMEDIZIN GÖTTINGEN UMG

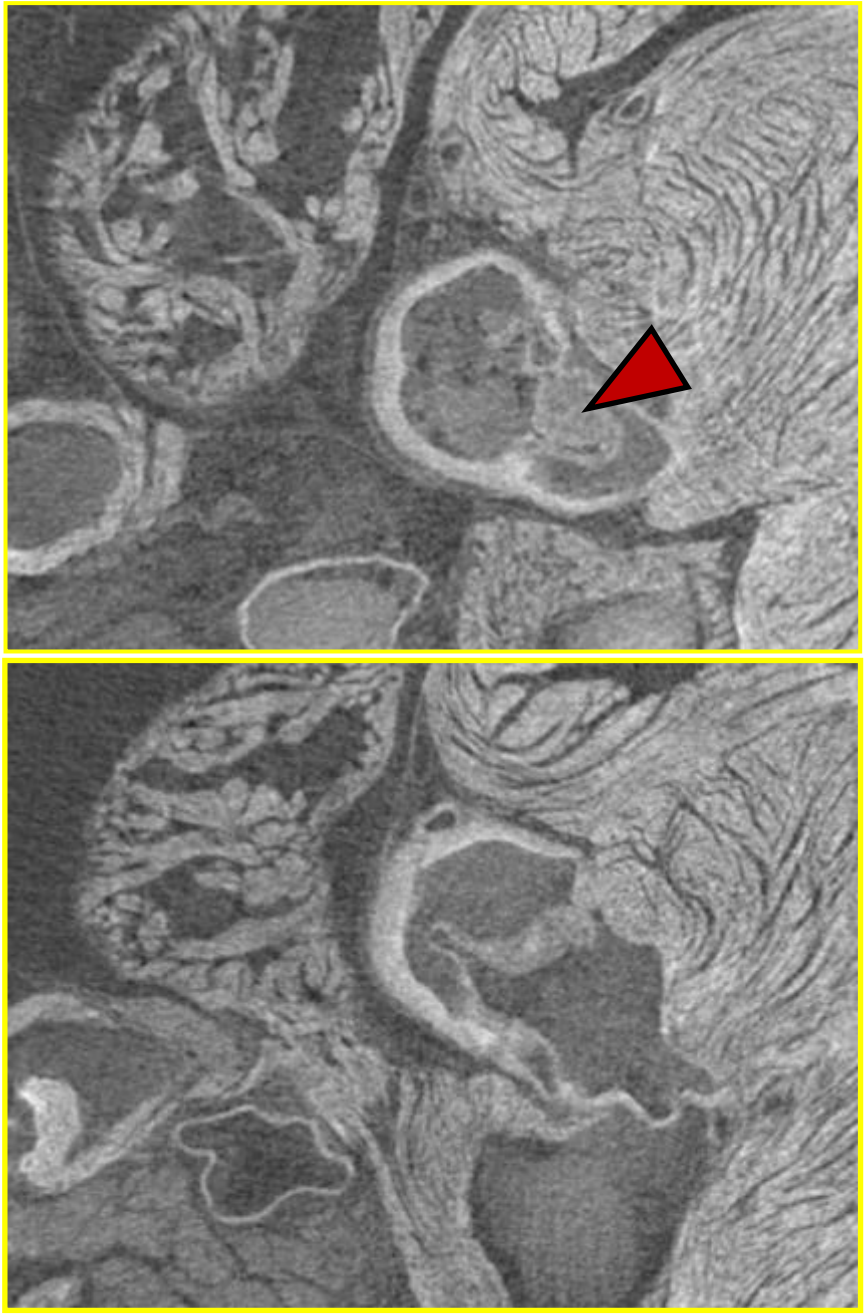

Comparing CT slice with histology

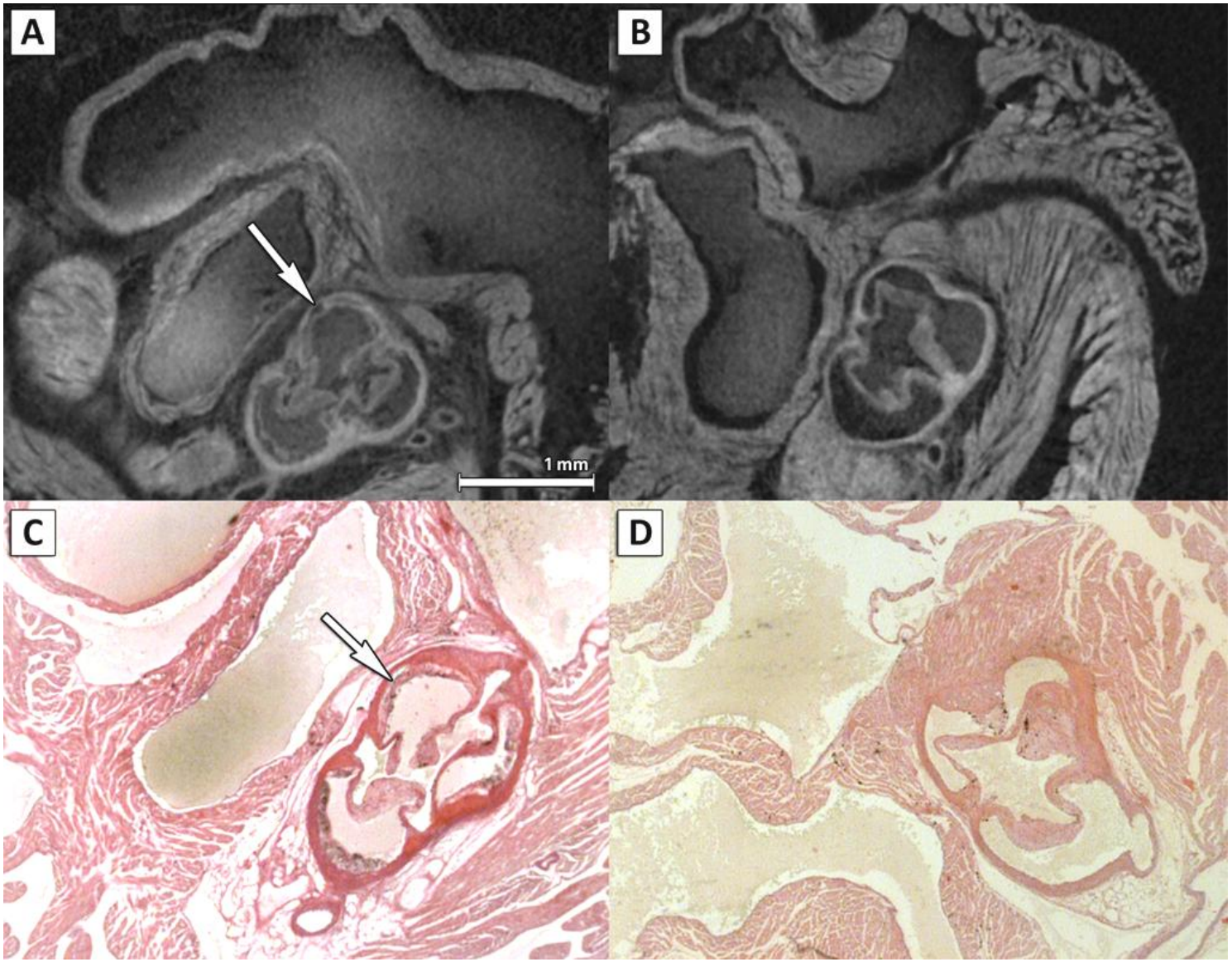

New challenges: dynamic studies and multiscale micro-CT

- Dynamic CT studies (4DCT): repeated series of scans performed at sequential time lapses, to provide information about the microstructure evolution.
  - Application in entomology
  - Lung imaging

- Multiscale micro-CT combines different resolution modalities on the same sample
  - Visualization of vascular and neuronal network

4D *in vivo* X-ray microscopy with projection-guided gating

- ✓ Visualizing fast micrometer scale internal movements of small animals
- ✓ Application of phase contrast microCT (~ 3.3 μm voxel size) with retrospective, projection-based gating
- ✓ 20 CT scans selected through the 150 Hz oscillations of the blowfly flight

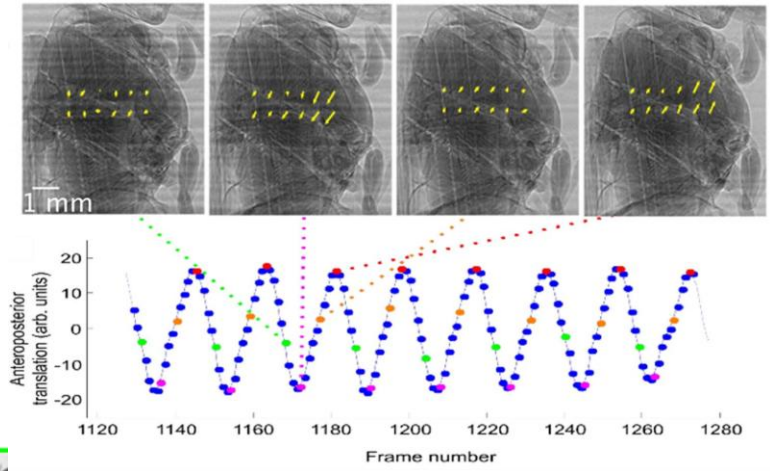

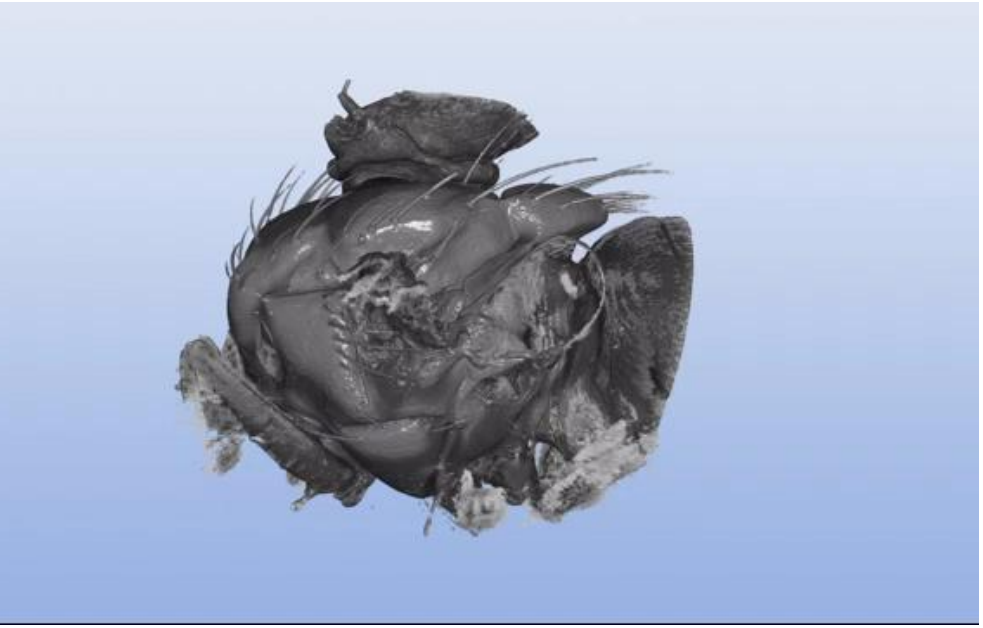

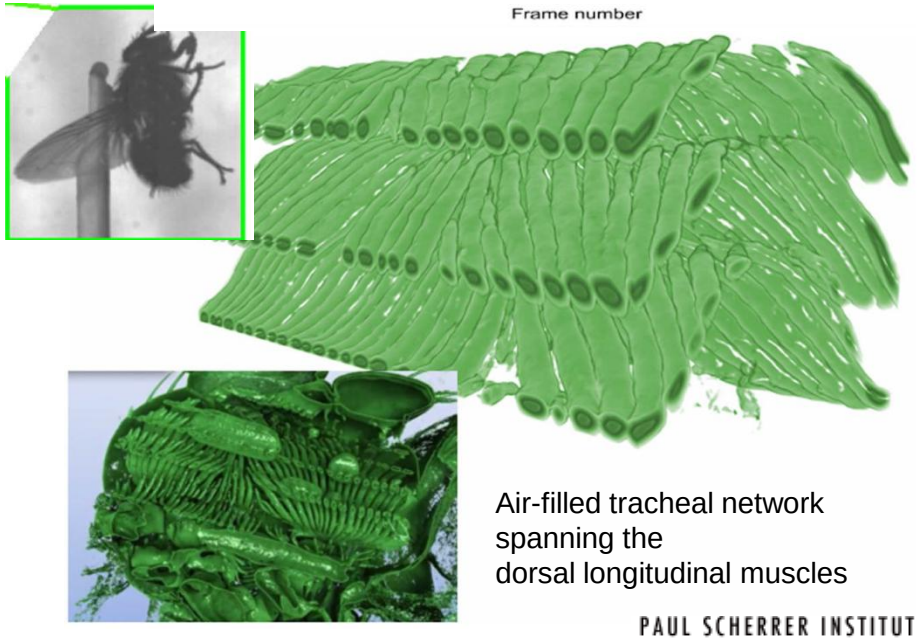

Air-filled tracheal network spanning the dorsal longitudinal muscles

Rajmund Mokso et al.: Sci. Rep. | 5 : 8727 | (2015)

Elettra Sincrotrone Trieste

Dynamic measure of **X-ray Absorption function** (Xaf) XAFs of a healthy control mouse (**blue**), an asthmatic mouse (**red**) and a dexamethasone treated mouse (**green**).

UNIVERSITÄTSMEDIZIN GÖTTINGEN UMG

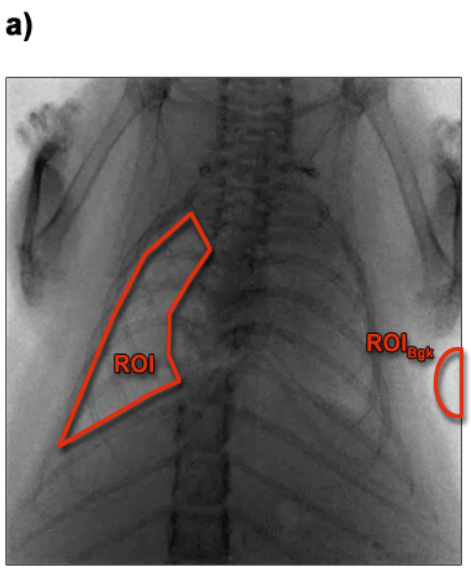

radiograph of the mouse chest

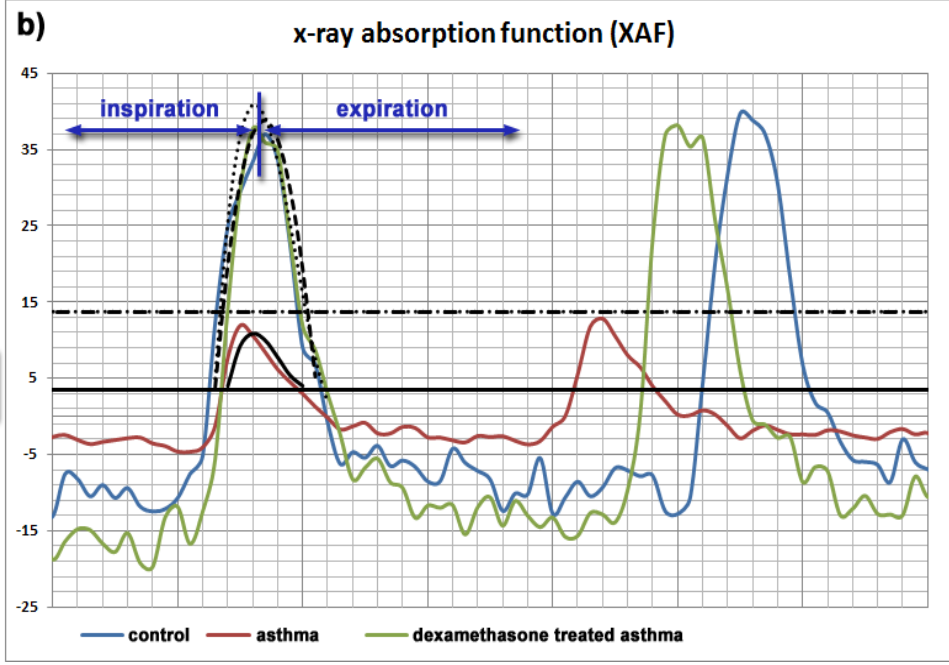

C. Dullin, et al.:, Scientific Reports | 6:36297 | 2016

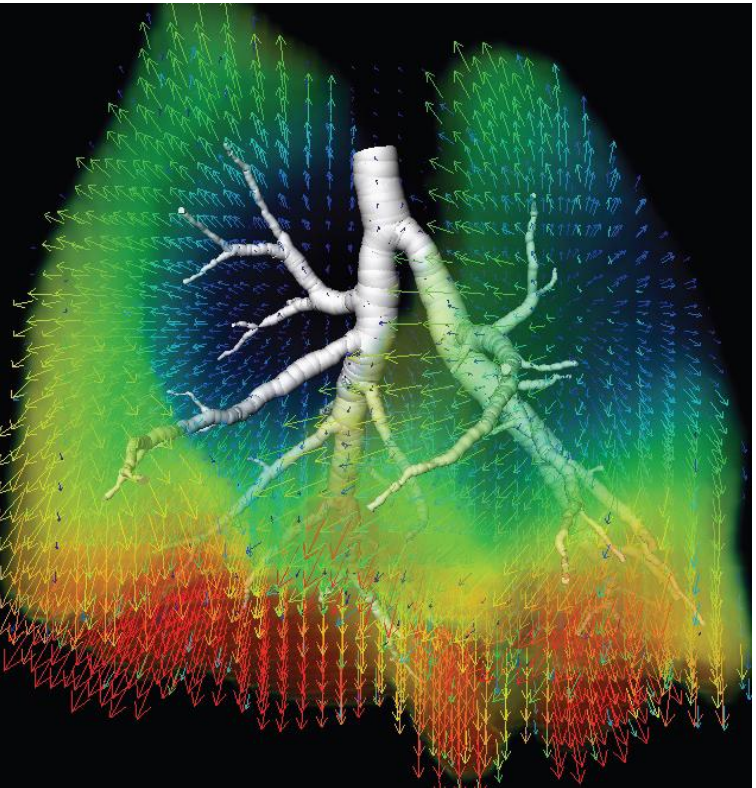

Measure of Lung function

X-ray velocimetry - 3D map of mouse lung tissue velocity during inspiration. The vectors represent tissue velocity direction, and the colours represent velocity magnitude.

S. Dubsky, A. Fouras, Advanced Drug Delivery Reviews 85 (2015)

SPring-8

Phase contrast multiscale-microCT

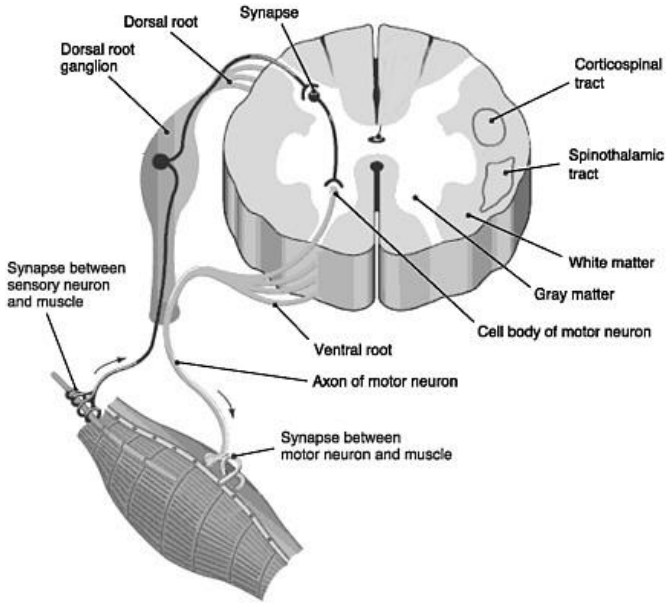

Aim:

Simultaneous 3D visualization of the vascular network (VN) and neuronal network (NN) of *ex-vivo* mouse spinal cord.

Motivation:

Pre-clinical investigation of neuro-degenerative pathologies

Reveal relationship between VN and NN

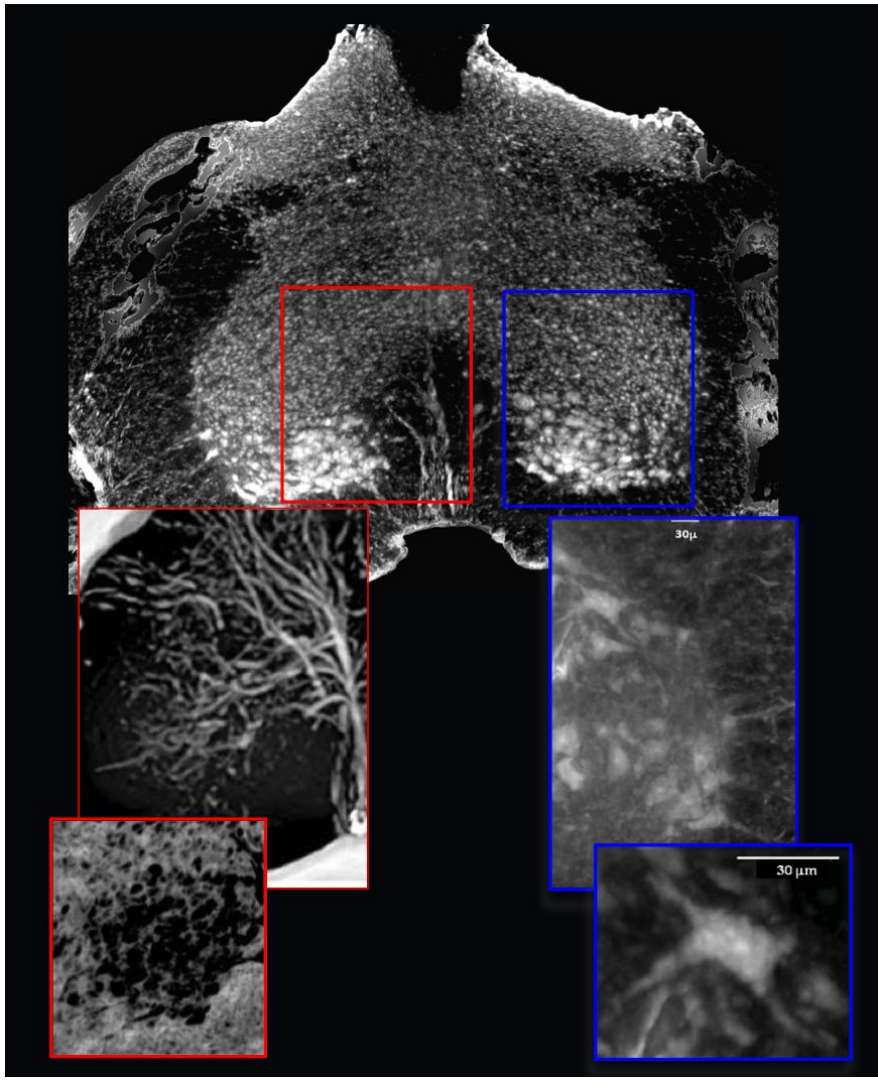

Vascular network

Neuronal network

Fratini, M. et al. (2014) Sci. Rep., | 5 : 8514 | (2014)

Micro-CT aplications: quantitative analysis

- Pore3D: A software package developed by the SYRMEP team for analysis of CT reconstructed data
- Some applications

Pore3D: a software tool for **3D image processing** and **analysis**

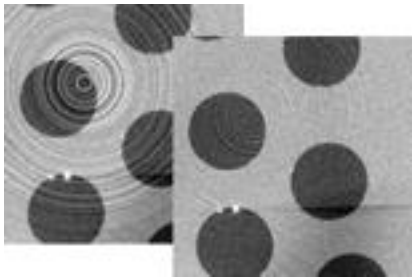

Filters
Basic (mean, median, gaussian, ...)
Anisotropic diffusion
Bilateral
Ring artifacts reduction
Binary (median, clear border, ...)

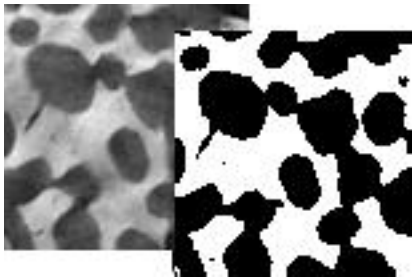

Segmentation
Automatic thresholding (Otsu, Kittler, ...)
Adaptive thresholding
Region growing
Multiphase thresholding
Clustering (*k*-means, *k*-medians, ...)

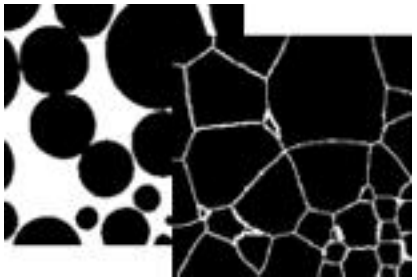

Morphological processing
Dilation and erosion
Morphological reconstruction
Watershed segmentation
Distance transform
H-Minima filter

Skeleton extraction
Thinning
Medial axis (LKC)
DOHT
Gradient Vector Flow
Skeleton pruning
Skeleton labeling

Analysis
Minkowski functionals
Morphometric analysis
Anisotropy analysis
Blob analysis
Skeleton analysis
Textural analysis (fractal dimension, ...)

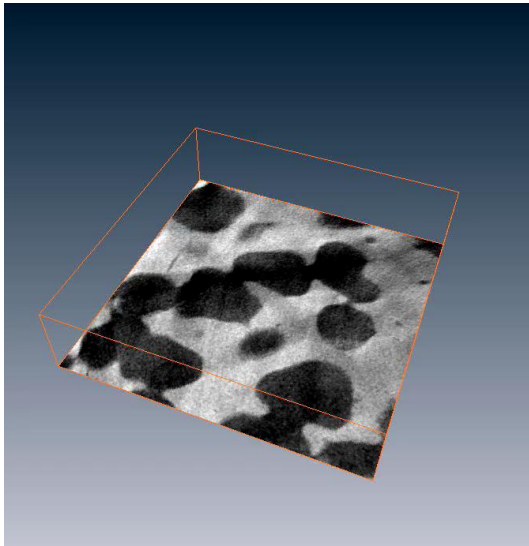

http://www.elettra.eu/pore3d/

F. Brun et al., NIM A, 615 (2010) 326–332

Characterization of urinary stones

Aim: determination of texture, microstructure and mineralogical composition of kidney stones.

Mineralized tissues and bio-mineral structures i.e. bones, teeth, kidney stones are considered as “archives” related to living habits, nutrition and exposure to changing environmental conditions.

Identification of calculi components is useful to evaluate the chance of their new development as well as to choose the terapeutic approach.

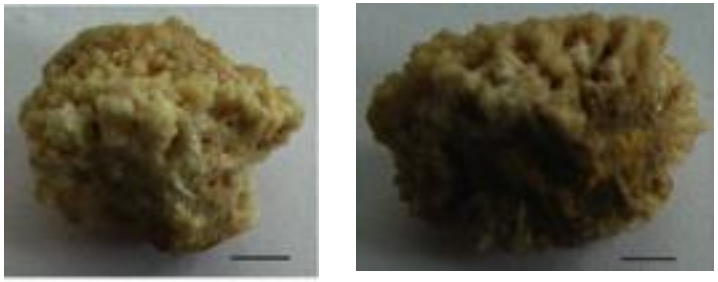

Analyzed urinary calculi fragments no.: 11847 and 11684. The bars have a length of 2 mm.

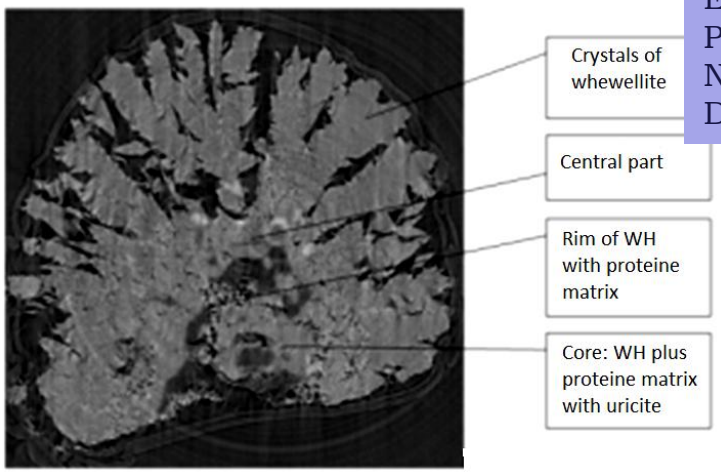

E = 30 keV
Pixel size = 9 μm
N. Proj = 900
Dist. sample-ccd = 50 cm

Texture of urinary calculi - slice n.50 of the sample 11684 situated near the core.

Courtesy of J.Kaiser, M.Hola

Analysis of human kidney stones

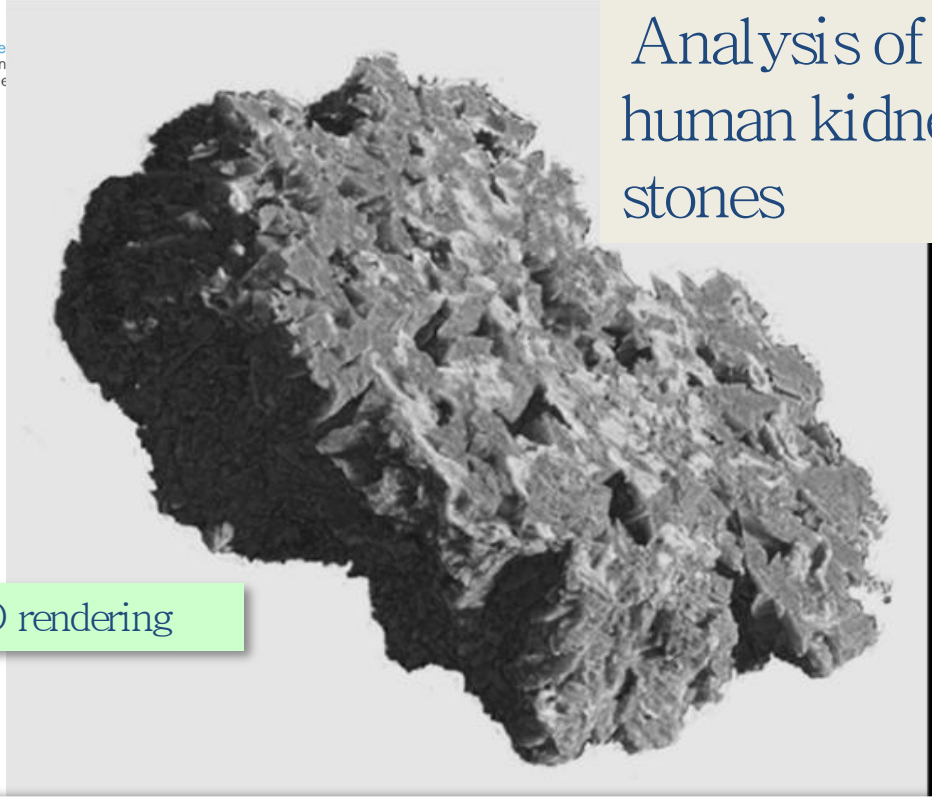

3D rendering

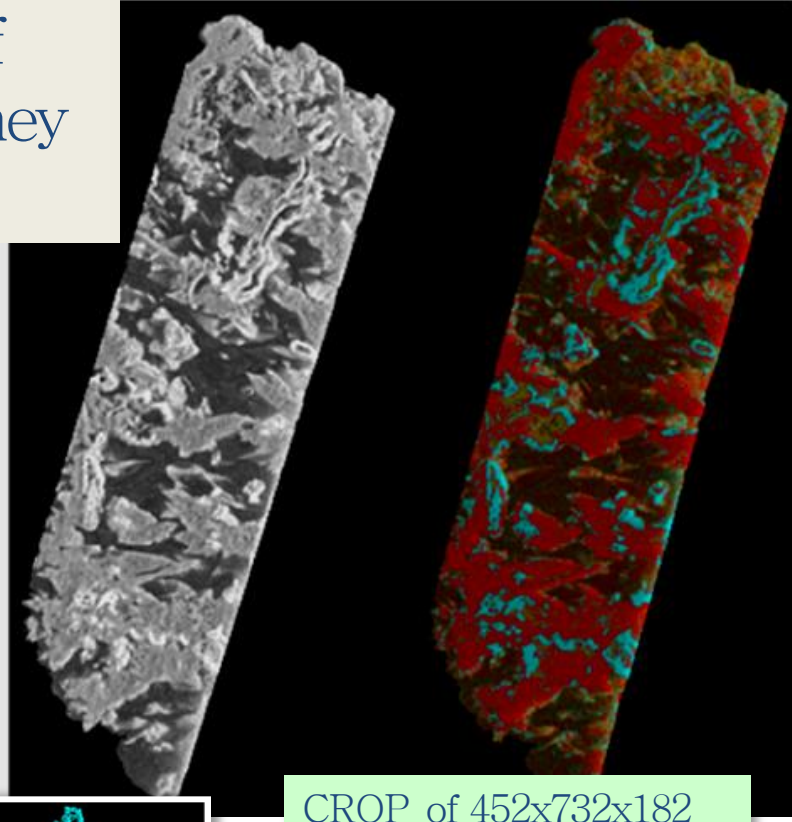

CROP of 452x732x182 pixels of the sample

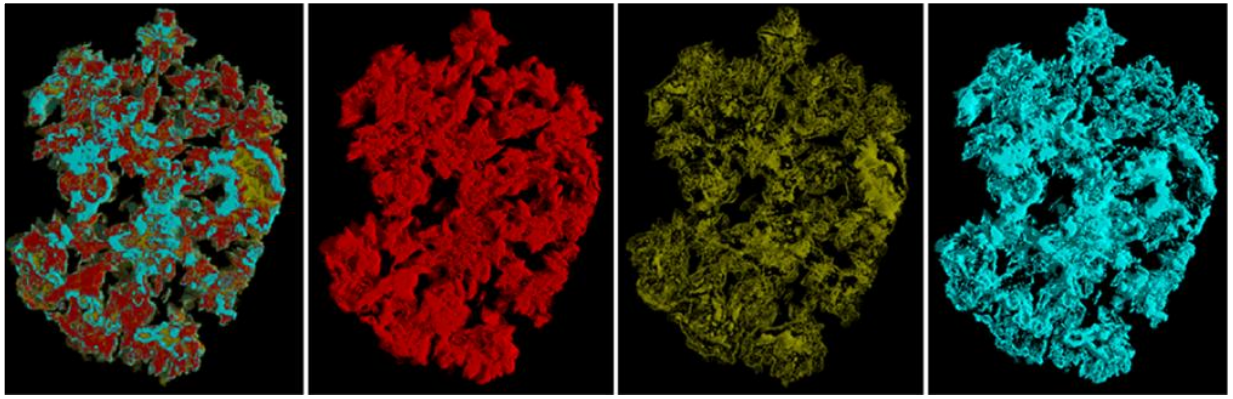

3D rendering of a stack of 20 slices showing the 3 phases segmentation whewellite (red), weddellite (yellow) and apatite (blue)

Volumes (after normalization, taking into account the air pores): are 50.5 % v_{we}/v of **weddelite**, 15.9 % v_{whe}/v of **whewellite**, 33.6% v_{ap}/v of Ca-phosphate „**apatite**“.

J. Kaiser et al., Urological Research, 39 (2011) 259-267.

Application of Pore3D: phases separation and skeletonization

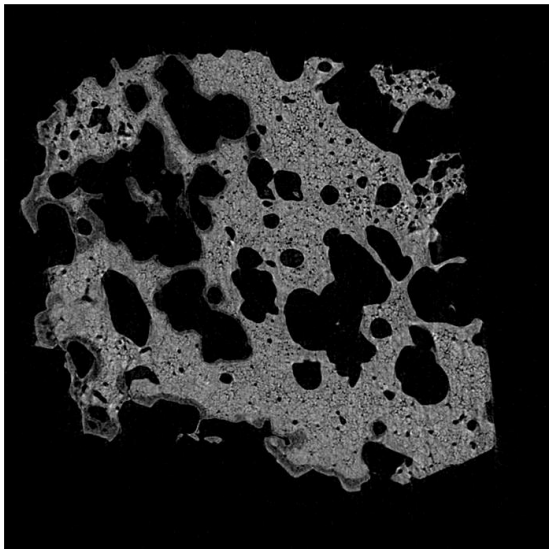

Slice of a glass-ceramic scaffold sample immersed in SBF for 4 weeks

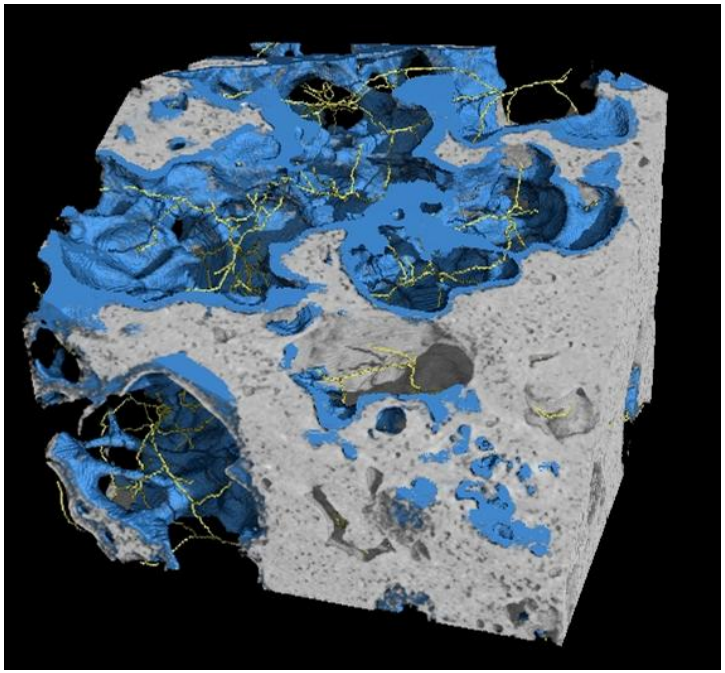

Volume segmentation highlighting the new bone formation and skeletonization

E = 19 keV
Dist. sample-ccd = 20 cm
N. proj. = 900

Other parameters used for the evalation of bio-compatibility: porosity, pore connectivity, pore volumes/total volume, trabecular thickness, etc.

C.Renghini et al., Acta Biomaterialia 5, (2009)

Imaging of scaffolds

PHC imaging and phase retrieval algorithms are essential to observe new bone formation and to visualize vascularization.

PHC slice

Phase Retrieved slice

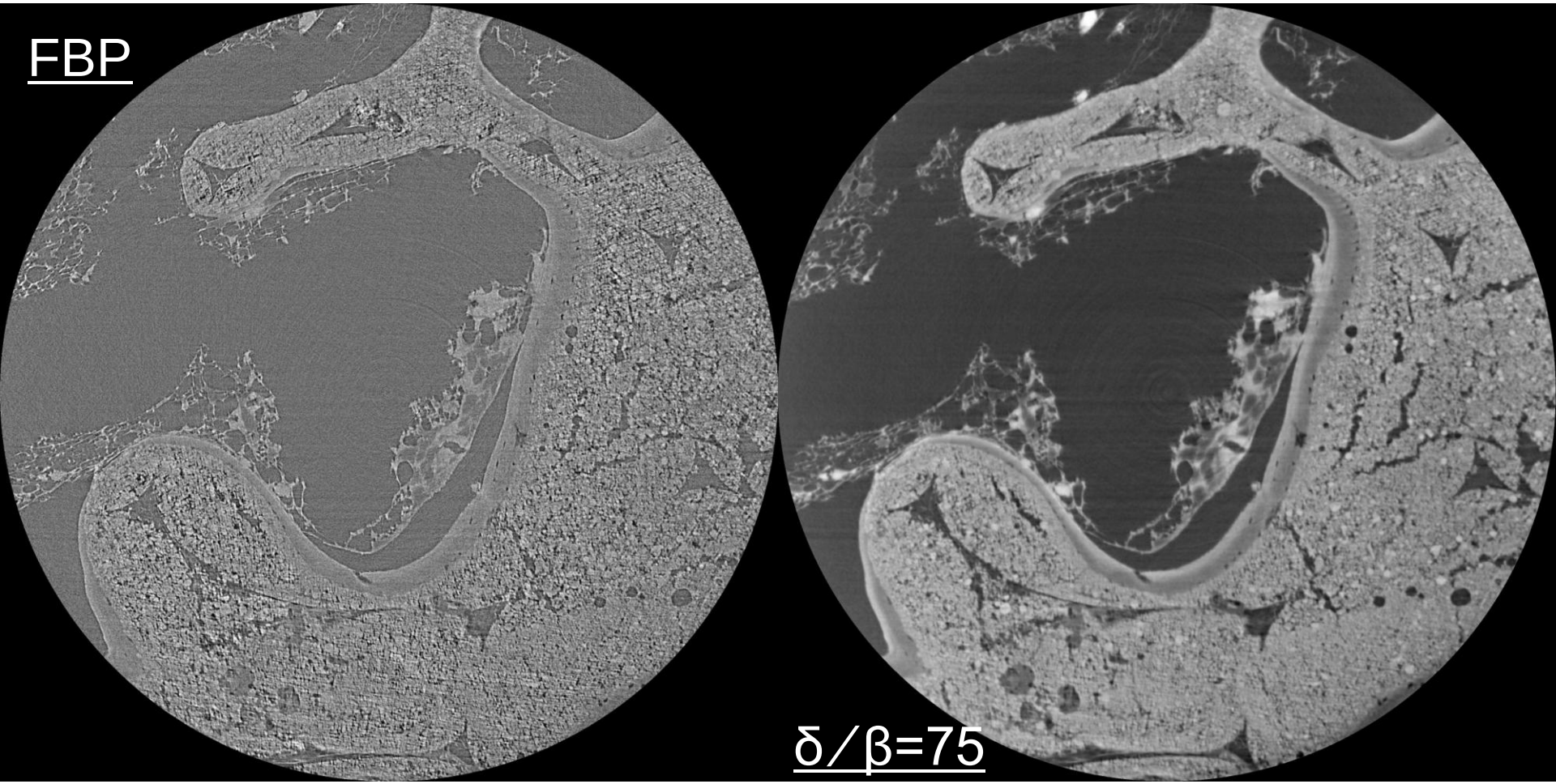

Collab: M.Mastrogiacomo, R.Cancedda (Uni Genova), A.Cedola, G. Campi, M.Fratini et al. (CNR – Roma)

Bone turnover in mice exposed to micro-gravity conditions

- 3 wild type (WT) mice and 3 pleiotrophin-transgenic (PTN-Tg) mice in a special payload (MDS - Mice Drawer System). The transgenic mouse strain over-expressing pleiotrophin (PTN) in bone was selected because of the PTN positive effects on bone turnover.
- **91 days in the International Space Station (ISS) by NASA: Aug. - Nov. 2009.**
- Controls:
  - mice on Earth in the same special payload MDS (*ground* mice)
  - mice in common cages (*vivarium* mice)
- SR μ-CT experiments were performed on femurs and spines
- Being non-destructive, μ-CT is very attractive for these rare specimens

University of Genova

Università Politecnica delle Marche

University of Trieste – Dept. of Engineering

http://www.nasa.gov/mission_pages/station/research/experiments/MDS.html

Analysis of the microarchitecture of the trabecular bone in femurs

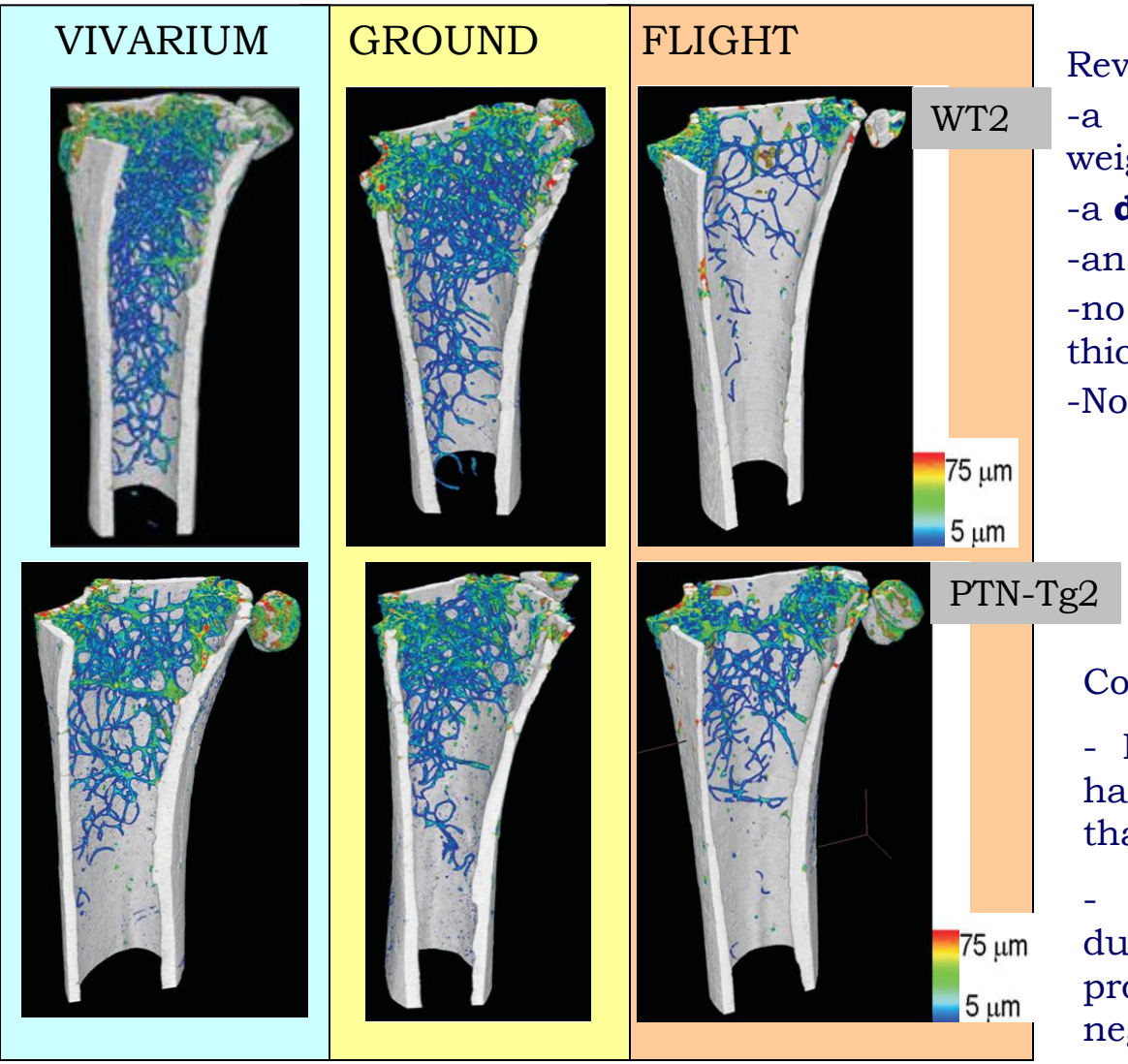

Revealed:

-a **bone loss** during spaceflight in the weight-bearing bones

-a **decrease** of the trabecular number

-an **increased** mean trabecular separation

-no significant change in trabecular thickness.

-No effects on not weight-bearing bones.

E = 19 keV
Pixel size = 9 mm
N. Proj = 900
Distance sample-ccd= 3 cm

Comparison WT vs.PTN-Tg2:

- PTN-Tg exposed to normal gravity has a poorer trabecular organization than WT mice

- the expression of the PTN gene during the flight resulted in some protection against microgravity ' s negative effects.

Color map represents bone trabecular thickness distribution in the femur (red = 75 µm, blue = 5 µm)

S. Tavella et al "*Bone Turnover in Wild Type and Pleiotrophin-Transgenic Mice Housed for Three Months in the International Space Station (ISS)*", PlosONE, March 2012

Acknowledgements

SYRMA and SYRMEP teams:

A.Abrami, K.Casarin, D.Dreossi, L.Mancini, R.H. Menk, A.Vascotto, F.Zanini - Sincrotrone Trieste
A.Accardo, F.Brun, E.Larsson, S.Pacilè - Dept of Engineering – Univ. of Trieste
F.Arfelli, C.Fedon, R.Longo, L.Rigon - Dept of Physics – Univ. of Trieste and INFN
P.Bregant, M.A.Cova, E.Quaia, M.Tonutti, F.Zanconati - Dept of Radiology & Hospital, Trieste

Beamline users & Collaborators

J.Kaiser – Brno University of Techn., Brno (Cz)
R. Cancedda, M.Mastrogiacomo – Univ Genova (I)
S.Biffi, C.Garrovo – Burlo Hospital and CBM, Trieste (I)
C.Dullin – University Hospital, Goettingen (G)
S.Mayo, Y.Nesterev – CSIRO, Melbourne (Australia)
T.Gureyev, Melbourne University (Australia)
C.Hall, M.Kitchen et al.,Monash University and Australian Synchrotron, Melburne
E.Schultke: University of Rostock (G)

I thank you for the attention

giuliana.tromba@elettra.eu

Talbot interferometry is based on the Talbot effect (1836), which is known as a self-imaging effect observed downstream a grating (object with a periodic structure), under coherent illumination.

The distances z_T between the object and self-imaging planes are determined by the light wavelength λand the period d of the structure

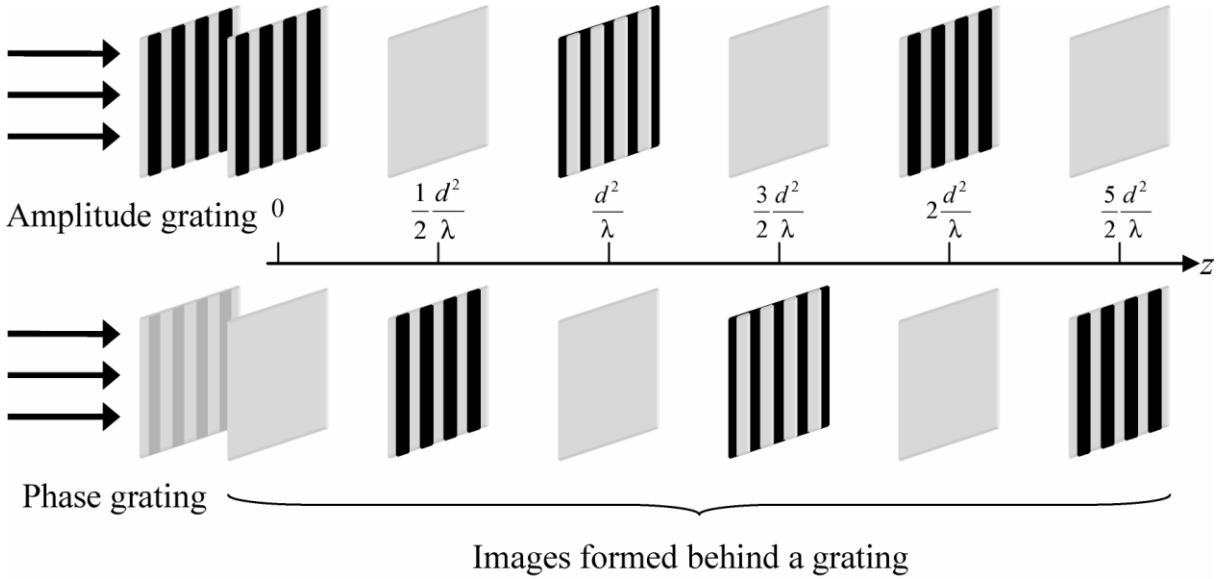

Talbot effect in the case of plane-wave illumination. For **an amplitude grating**, self-images are generated at $z_T = 0$, d^2/λ, $2d^2/\lambda$, and so on. (d is the period of the grating, λ is the wavelength). For a **phase grating**, similar patterns are observed at intermediate positions.